



The University of Sheffield

Improvements in Testing and Performance of Batteries for Automotive Applications

*A thesis submitted in partial fulfilment of the requirements for the degree of
Doctor of Philosophy*

M J SMITH

2018



The University of Sheffield

Faculty of Engineering

Department of Electronic & Electrical Engineering

Improvements in Testing and Performance of Batteries for Automotive Applications

*A thesis submitted in partial fulfilment of the requirements for the degree of
Doctor of Philosophy*

Matthew James SMITH

September 2018

Abstract

Batteries are increasingly important in modern technologies. This is particularly true in the automotive sector, with hybrid vehicles using batteries to augment the traction power traditionally provided by the internal combustion engine. In such applications, one of the most important factors is the Dynamic Charge Acceptance (DCA) performance of the battery.

This study investigates the standard method for establishing DCA performance and determines how the individual parameters of the test procedure and external factors influence the performance of lead-acid cells. This work identifies shortcomings of the standard test, which result in the true DCA performance being better than the standard test suggests. A series of modifications are proposed, which are shown to produce a more representative result.

An investigation is performed to determine the effect of cell degradation on charge acceptance. This shows that the DCA test itself is not well suited to assessing the effects of degradation on DCA, and causes the results to appear worse than reality. The work also demonstrates that the usual methods of characterising degradation do not correlate well with DCA performance, and there is very little reduction in charge acceptance over the operational life of the cell.

Investigations are undertaken into methods by which DCA performance may be improved. This shows that the application of ac ripple currents to batteries causes a significant increase in charge acceptance, and demonstrates how the frequency of the ripple is important in achieving the best results. This study also shows that the ripple currents have no detrimental effects on the health of the battery.

Finally, the work is extended to cover lithium cells. This shows that whilst the DCA performance of lithium is more consistent, maximum charge acceptance is less than lead. It is shown that, by reducing maximum charge voltage, cycle life of cells can be extended without significant loss of stored energy.

List of Publications

Parts of the work presented in this thesis have been reported in the following internationally-respected publications:

Journal Publications

1. **M. J. Smith**, D. T. Gladwin, and D. A. Stone, “Experimental analysis of Dynamic Charge Acceptance test conditions for lead-acid and lithium iron phosphate cells,” *Journal of Energy Storage*, vol. 12, pp. 55–65, 2017.
2. **M. J. Smith**, D. T. Gladwin, and D. A. Stone, “An Analysis of the Influence of High-Frequency Ripple Currents on Dynamic Charge Acceptance in Lead-Acid Batteries,” *Journal of Energy Storage*, vol. 22, pp. 27–35, 2019.

Conference Proceedings

1. **M. J. Smith**, D. T. Gladwin, and D. A. Stone, “Experimental Analysis of Dynamic Charge Acceptance Test Conditions for Lead-Acid Cells,” in *Industrial Electronics Society, IECON 2016 – 42nd Annual Conference of the IEEE*, pp. 2046–2051, Oct 2016.
2. **M. J. Smith**, D. T. Gladwin, and D. A. Stone, “Experimental Analysis of the Influence of High-Frequency Ripple Currents on Dynamic Charge Acceptance in Lead-Acid Batteries,” in *Industrial Electronics Society, IECON 2017 – 43rd Annual Conference of the IEEE Industrial Electronics Society*, pp. 7140–7145, Oct 2017.
3. **M. J. Smith**, D. T. Gladwin, and D. A. Stone, “An Experimental Analysis of the Effect of Cell Degradation on Dynamic Charge Acceptance in Lead-Acid Cells,” in *2018 IEEE 27th International Symposium on Industrial Electronics (ISIE)*, pp. 187–192, Jun 2018.

4. **M. J. Smith**, D. T. Gladwin, and D. A. Stone, “A Comparison of the Effects of Charging Strategies on Lithium-ion Cell Performance in High Temperature Environments,” in *2019 IEEE 20th International Conference on Industrial Technology (ICIT)*, Feb 2019.

Acknowledgements

Firstly, I would like to thank the Engineering and Physical Sciences Research Council (EPSRC), without whose funding, this work would not have been possible.

I would also like to express my sincere gratitude to my supervisor, Dr. Dan Gladwin, for his unwavering support, insightful suggestions and considered advice throughout the course of this work. All were given as freely as his time and vast knowledge, and have been instrumental in allowing me to see this project through to completion. Besides my supervisor, I would also like to thank the academic staff of the EEE department, in particular Prof. Dave Stone and Prof. Martin Foster, for their encouragement and assistance during the last four years.

My thanks to the organisations and people who have helped contribute to this work. Allan Cooper and the Advanced Lead Acid Battery Consortium (ALABC), who provided some of the cells used in this project. The Advanced Diesel Electric Powertrain (ADEPT) project for the opportunity to work with them on an exciting project. To Chris Longbottom and Danny Ballam from Mobile Power, who provided yet more cells, as well as the chance to help a local business improve the lives of people in developing countries.

I must also extend a heartfelt thanks to all of my colleagues at Sheffield, whose friendship and camaraderie have helped to make this far more than just a workplace. To Alex Petersen for the stimulating discussions, both highly technical and utterly inane — often both, which always add a touch of fun to the day. To Dr. Dan Rogers for his invaluable advice provided in the early years of my PhD; this time it looks like I've tried to be clever and got away with it. And to Nathan Richmond, who managed to talk me into pursuing a PhD in the first place.

Last, but by no means least, I would like to thank my parents for their limitless patience and unconditional support, not just for the last four years of my studies, but throughout my entire life. One day, soon, I will get a proper job, promise.

Contents

Abstract	i
List of Publications	ii
Acknowledgements	iv
Nomenclature	xii
1 Introduction	1
1.1 Background & Motivation	1
1.2 Thesis Contributions	5
2 Literature Review	9
2.1 Dynamic Charge Acceptance	10
2.1.1 Identification & Emergence of DCA	12
2.1.2 Developments in Charge Acceptance	13
2.2 High-Frequency Ripple Effects	15
2.2.1 Typical Converter Frequencies	15
2.2.2 Low-Frequency Ripple	17
2.2.3 Heating Effect	17
2.2.4 Ripple Charging	18
2.2.5 Mid-Frequency Ripple	19
2.2.6 Microcycling	20
2.3 Conclusions	21
3 Analysis of DCA Test Conditions for Lead-Acid Cells	23
3.1 Introduction	23
3.1.1 Battery Use in Vehicles	23
3.1.2 Charge Acceptance	26
3.2 DCA Overview	27
3.2.1 Microcycling	29
3.2.2 Standard DCA Test A3 Procedure	32

3.2.3	DCA Calculation	33
3.3	Experimental Setup	33
3.4	Test Procedure Modifications	36
3.4.1	Modified SoC Profile	36
3.4.2	Modified DCA Calculation	37
3.4.3	Increased Charge Current	38
3.4.4	Rest Period Variation	40
3.4.5	Temperature Variation	42
3.5	Comparison with Standard Lead-Acid	45
3.6	Extended Testing	47
3.6.1	High Current Testing	48
3.6.2	Extended Microcycle Testing	50
3.7	Conclusions	54
4	Analysis of the Effects of Cell Degradation on DCA in Lead-Acid Cells	55
4.1	Introduction	55
4.1.1	Lead-acid Cycle Life	55
4.1.2	DCA and Battery Degradation	56
4.2	Test Procedure	58
4.2.1	DCA Testing	58
4.2.2	Cycling	60
4.3	Results & Discussion	63
4.3.1	Degradation	63
4.3.2	DCA Performance	64
4.4	Conclusions	68
5	Analysis of the Influence of High-Frequency Ripple Currents on DCA in Lead-Acid Batteries	69
5.1	Introduction	69
5.2	Battery Analysis	72
5.2.1	Spectroscopy	72
5.2.2	Modelling	75
5.2.3	Ripple Frequency Selection	77
5.3	Test Procedure	79
5.3.1	Effect of History on DCA Performance	80
5.3.2	Test Rig	80
5.3.3	Test Description	82
5.4	Results & Discussion	83
5.4.1	Effects of 700 Hz Ripple	84
5.4.2	Effect of Varying Frequency	86

5.4.3	Effect of Ripple Current on SoC	89
5.4.4	Effect of Ripple Current on SoH	91
5.5	Effect of Ripple Currents on Cell Balancing	95
5.5.1	Cell Balancing	95
5.5.2	Test Procedure	97
5.5.3	Cycle Imbalance	98
5.5.4	Static Imbalance	101
5.6	Conclusions	102
6	Considering Lithium Chemistries	104
6.1	Introduction	104
6.2	DCA Performance of Lithium-ion	105
6.3	Lithium-ion Charging Strategies	107
6.3.1	Renewable Energy in the Developing World	108
6.3.2	Test Procedures	109
6.3.3	Impedance Testing	113
6.3.4	Results & Discussion	114
6.3.5	Conclusions	121
7	Conclusions & Further Work	122
7.1	Chapter 2	122
7.2	Chapter 3	123
7.3	Chapter 4	125
7.4	Chapter 5	126
7.5	Chapter 6	127
7.6	Further Work	128
	References	130
	Appendix: High Frequency Test Rig Schematics	138

List of Figures

1.1	UK FiT Accredited Installations, Jan 2010 – Jun 2018	2
1.2	UK Electric Vehicle Registrations, Jan 2011 – Jun 2018	3
2.1	DCA Test Microcycle Current Profile ($t_1 - t_5$)	11
2.2	Converter Switching Frequencies Data	16
3.1	DCA Test A3 Conditioning Phase SoC Profile	29
3.2	DCA Test A3 Microcycle Profile	30
3.3	DCA Performance Examples	31
3.4	DCA Test A3 SoC Profile	32
3.5	2 V, 6 Ah, VRLA Cell	34
3.6	Maccor S4000 Test System & Environmental Chambers	34
3.7	8 Cells in Environmental Chamber	35
3.8	Modified DCA Test SoC Profile & DCAPP Locations	37
3.9	DCA Analysis Result at 25 °C, Modified SoC Profile	38
3.10	DCA Analysis Result at 25 °C, Modified Microcycle Profile and Increased Charge Current	39
3.11	DCA Analysis Result, Variation with Rest Period at 25 °C	41
3.12	DCA Analysis Result, Variation with Temperature with 30 s Rest Period	43
3.13	Randles' Cell Equivalent Circuit	44
3.14	2 V, 2.5 Ah, EnerSys 'Cyclon' VRLA Cell	46
3.15	DCA Analysis Result for 2 V, 2.5 Ah Standard VRLA cell, 25 °C	47
3.16	DCA Analysis Result, Increased Current Limit	49
3.17	DCA Analysis Result, Extended DCAPP at 70 % SoC and 25 °C	52
3.18	Cell Surface Temperature for Extended DCAPP test, with Discharge History	53
4.1	DCA Test SoC Profile & DCAPP Locations	59
4.2	DCA Test Microcycle Current Profile ($t_1 - t_5$)	60

4.3	Discharge Curve for Cyclon Cells at Various Currents	62
4.4	Capacity Loss with Degradation	64
4.5	DCA Performance at Various SoC Levels with C_{exp} Normalisation	65
4.6	DCA Performance at Various SoC Levels with C_{nom} Normalisation	67
5.1	12 V, 4 Ah, RS Pro VRLA Battery	73
5.2	EIS Spectra	74
5.3	Battery Equivalent Circuit Models	75
5.4	Relative Current Flow in Hybrid Model R_1 , C_1 & C_2	78
5.5	Impedance Spectrum for Hybrid Model, Neglecting R_1 & L_1	79
5.6	Test Rig Schematic	80
5.7	Ripple Generator	81
5.8	Superposition of ac and dc Components	81
5.9	Test Procedure SoC Profile & DCAPP Locations	82
5.10	Test Procedure Details	83
5.11	DCA Analysis Result - Effect of Injected Ripple Current	84
5.12	DCA Analysis Result - Effect of Reduced Rest Period	85
5.13	Charge Acceptance Improvement with 700 Hz Applied Ripple Current	86
5.14	DCA Analysis Result - Effect of Injected Ripple Currents of Various Frequencies	87
5.15	Average Charge Acceptance Improvement with Applied Ripple Currents	88
5.16	Voltage Profiles from 5-day SoC Test	90
5.17	Discharge Curve for RS Pro Battery with 1 C_{nom} A Discharge	91
5.18	Long-term Cycle Performance for Baseline Test	93
5.19	Long-term Cycle Performance with 700 Hz Ripple	93
5.20	Long-term Cycle Performance with 30 kHz Ripple	94
5.21	Cell Imbalance Example	96
5.22	8 V, 4-cell Test Battery	98
5.23	Cycle Imbalance Profiles for Baseline Test	99
5.24	Cycle Imbalance Profiles with 30 kHz Ripple Current	100
5.25	Static Imbalance Profiles with 30 kHz Ripple Current	102
6.1	3.2 V, 3.3 Ah, Mottcell IFR26650 LFP 26650 Cell	105
6.2	DCA Analysis Result for 3.2 V, 3.3 Ah, LiFePO ₄ cell, 25 °C	106
6.3	Portable Li-ion Battery Pack	108
6.4	3.6 V, 2.6 Ah, Samsung ICR18650-26J Li-ion 18650 Cell	109
6.5	OCV Determination Test for Method 2 Charging	111

6.6	Charge Current & Voltage Profiles	112
6.7	EIS Spectra for Samsung 18650 Cell at Various SoC Levels . .	113
6.8	State of Health Profile for all Cells	117
6.9	Cell Impedance at Various SoC Levels	120
A1	MP111FD Amplifier and Ancillaries	139
A2	Signal Processing	140
A3	Power Supplies	141
A4	IO Connections	142

List of Tables

3.1	Conditioning Operation Sequence	28
3.2	Standard DCA Test A3 Microcycle Current Profile	29
5.1	Model Component Parameters	76
5.2	Average Charge Acceptance Improvement with 700 Hz Applied Ripple Current	86
5.3	Battery Impedance and Power Requirements for Various Frequencies of Ripple Current	89
5.4	Battery Start, End and ΔV Voltages from 5-day SoC Test	90
6.1	Full Test Parameters for all Methods	112
6.2	Starting Capacity for all Cells	115
6.3	Available Capacity from all Tests	115
6.4	Charge Speed Improvement	116
6.5	SoH Cost by Cell & Method	118

Nomenclature

ADEPT Advanced Diesel Electric Powertrain.

ALABC Advanced Lead Acid Battery Consortium.

BER brake energy recuperation.

BMS Battery Management System.

CCCV constant-current, constant-voltage.

CH charge history.

DCA Dynamic Charge Acceptance.

DCAPP DCA Pulse Profile.

DH discharge history.

EFR Enhanced Frequency Response.

EIS Electrochemical Impedance Spectroscopy.

EV Electric Vehicle.

FiT feed-in tariff.

HEV Hybrid Electric Vehicle.

HPPC Hybrid Pulse Power Characterisation.

HRPSoC high-rate partial state of charge.

HVAC heating, ventilation and air-conditioning.

IC internal combustion.

LFP lithium iron phosphate.

Li-ion lithium-ion.

NEDC New European Drive Cycle.

OCV open-circuit voltage.

OEM original equipment manufacturer.

PHEV plug-in Hybrid Electric Vehicle.

PLL phase-locked loop.

PRBS Pseudo-random Binary Sequence.

PV photovoltaic.

SLI starting, lighting and ignition.

SoC state of charge.

SoH State of Health.

VRLA valve-regulated lead-acid.

WLTP Worldwide harmonized Light vehicles Test Procedure.

Chapter 1

Introduction

1.1 Background & Motivation

Batteries are now becoming an increasingly important aspect of modern technologies. For many years, they have been used to provide energy in low-power portable devices, and as an auxiliary supply in vehicles. Battery technology in these areas is mature and well understood. Recently, driven by environmental and economic factors, battery technology has begun to be used far more widely, particularly in the power and automotive sectors.

With increases in the costs of electricity, together with more awareness of the environmental impact of fossil fuel usage, it is becoming increasingly popular for domestic consumers to install renewable energy systems on their homes. These systems fall into two primary categories, heat and electricity. Heat systems gather solar or geothermal heat energy, and store it for later use; of more interest to this project are the electrical systems. These systems use renewable resources to generate electricity, the major benefit with electrical systems is the flexibility of the energy source. Whereas a heat system is limited to heating the building, renewable electricity may be used to heat, cool, light and power the building, depending on the requirements and systems installed. A secondary benefit of the electrical systems is the ability to feed energy back into the grid. In many areas, such as the UK, consumers are paid a feed-in tariff (FiT) for the energy they supply; this gives an additional

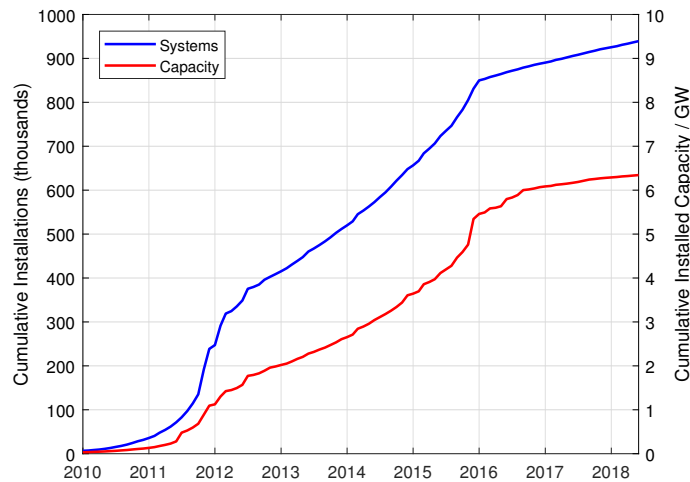


Figure 1.1: UK FIT Accredited Installations, Jan 2010 – Jun 2018 [1]

financial incentive to the installation of an electrical system. The number of installations which are accredited to receive this FiT, together with the total installed capacity is shown in figure 1.1. It may be seen from this figure that the uptake has been considerable over the period 2010 – 2018.

The energy may be generated in several ways, solar photovoltaic (PV) systems convert sunlight directly into electricity, whilst other methods such as wind turbines or hydro-electric systems use the energy from moving air or water respectively to drive a generator. Once generated the electricity must be stored until it is needed, this is particularly important for PV systems, where demand is likely to be greatest when generation is least, at night, for example. Batteries are the primary means of providing energy storage in these systems. The ability of the battery to collect and store the energy available is thus a critical factor in the overall effectiveness of the system, and therefore it is of great importance that the performance of batteries in such systems is well understood.

At a much larger scale, battery storage systems are beginning to be used as high-power, short-term energy sources to provide distributed supply and frequency balancing for mains power grids. In this application, large capacity banks of batteries are placed at strategic points within the power distribution system, they may then be used to meet short-term imbalances in demand and

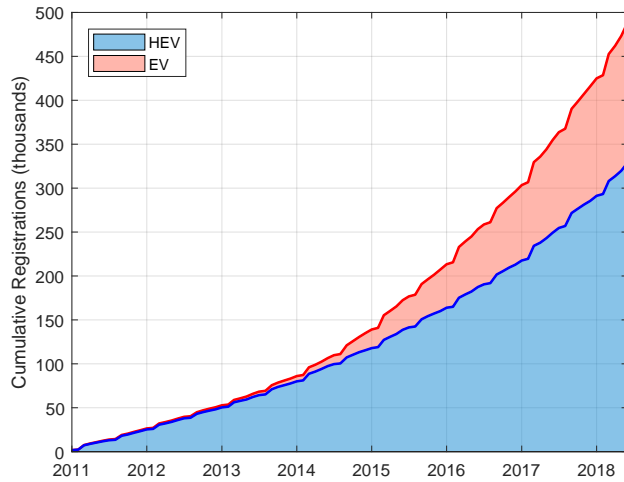


Figure 1.2: UK Electric Vehicle Registrations, Jan 2011 – Jun 2018 [2]

provide a power buffer to cover transient loads which traditional generating stations cannot react quickly enough to correct. As with the domestic systems the performance of the batteries is the major limiting factor to the overall effectiveness of the system.

Another aspect to consider with both systems is the capital cost of the battery, in both cases this is a significant proportion of the cost of the overall system. To maximise the cost efficiency of the systems it is crucial that the batteries are operated in a way that maximises their lifetime, whilst still maintaining satisfactory performance in terms of energy storage and supply.

In the automotive sector the battery has traditionally been simply an auxiliary power source, used for starting, lighting and ignition (SLI) of the vehicle, once running the internal combustion (IC) engine supplies all power. Driven by a desire to reduce emissions and fuel consumption, modern Hybrid Electric Vehicles (HEVs) are beginning to use the battery as an integral part of the traction package, or in the case of fully Electric Vehicles (EVs), as a complete replacement for the IC engine. Figure 1.2 shows the number of hybrid and fully electric vehicles registered in the period 2011 – 2018, again it may be seen that the uptake of such vehicles has been considerable.

There are many possible configurations of drive train for HEV applications but all make the battery a key part of the vehicle’s transmission system.

The increased mass and complexity of a HEV drive system, together with the required battery packs means compromises must be made to the size and performance of the IC engine fitted to the vehicle; this typically means the use of a smaller, less powerful unit. Whilst the fitting of a smaller IC engine is the main cost and environmental benefit of HEVs — a smaller engine uses less fuel and produces less emissions — the reduction in performance is a large disadvantage to consumers. To overcome this issue the HEV makes use of its battery and electrical machine to supplement the power of the IC engine when accelerating, and returning energy to the batteries by using the electric machine as a generator under braking. In this way the performance of the vehicle is maintained.

It may be seen that the use of batteries in HEV applications are subject to similar requirements to those of renewable and grid storage, that the battery is a crucial and expensive part of the system. In all cases the performance of the battery, both in terms of energy storage and longevity are critical to the overall effectiveness and attractiveness of the systems in which they are installed. The performance of batteries of various chemistries in all these applications is now the subject of much research, and the continued advancement of knowledge is necessary if these areas of technology are to continue to advance.

The use of a battery as a dynamic energy storage device places certain requirements on the system in which it is to be used. Firstly batteries are dc devices, therefore any system with ac input or output requirements, such as renewable or grid storage, will require ac-dc power conversion. Secondly, in all the systems discussed, the power flow is bi-directional; energy flows into the battery to be stored, at some later point it flows back out to perform useful work. It is therefore necessary for the power electronics to be capable of bi-directional operation. The final major consideration is the operating voltage of the battery, whilst the specific values vary with chemistry, all batteries have a defined voltage range in which they must be operated. There is a certain amount of leeway given by the configuration of the batteries, the voltage may be increased by using several in series, for instance, and practical systems often utilise many batteries in various series and parallel configurations to

achieve more desirable performance.

Clearly then, in most systems the battery cannot be used in isolation, it must come with a power converter if it is to perform effectively. The requirements discussed above also show that the power converter may need to perform multiple tasks, it must certainly be bi-directional, but may also need to be capable of inversion, rectification or transformation, or any combination thereof. Furthermore, to maximise the effectiveness and attractiveness of the system the converter must be as efficient as possible. It may be seen therefore, that the converter is as critical to the overall system performance as the battery itself.

In recent years advances in power transistor technology and microcontroller design have allowed for improvements to converter designs, of most interest to this project is the increases in switching frequency which have been achieved. Increasing the frequency of device switching in converters allows for a reduction in the value of the inductors required, thus allowing the inductor to be physically smaller. This then leads to reduced overall converter size and reduced material costs. These benefits, combined with modern high-speed switching devices and readily available, powerful microcontroller-based control systems have allowed high-frequency converters capable of meeting the needs of a battery-based energy storage system to become readily available at reasonable cost.

Any switched-mode converter will produce some ripple current on its outputs, this is a fundamental artefact of the way such converters work. The use of high-frequency converters with battery systems applies the ripple produced onto the battery. As many of these systems, particularly in renewable and grid storage applications are expected to be operating continuously for long periods of time, the battery will be subjected to extended operation in the presence of high-frequency ripple currents.

1.2 Thesis Contributions

The aim of this research is to investigate Dynamic Charge Acceptance (DCA) and its associated effects as applied to automotive applications, and linked

to this, investigate how the application of high-frequency current ripple to batteries affects their performance in terms of DCA and lifetime. Together these areas represent two important limiting factors to the increased uptake of battery technology, namely energy storage effectiveness and longevity.

Through four novel chapters, investigations are presented into the analysis of the effects of various external factors on DCA performance, and possible methodologies to improve it. Increased understanding of DCA performance of automotive batteries will lead to improvements in performance of HEVs, better battery designs and control schemes to maximise DCA performance. This should make HEVs more attractive, helping to reduce fossil fuel use and environmental damage.

Results are also presented into the effects of the operation of batteries in the presence of high-frequency ripple currents, showing the influence such currents have on the lifetime and DCA performance of batteries. By better understanding the effects of high-frequency ripple, it may be possible to design converters to maximise the benefits or minimise any negative effects, alternatively, it may be that the ripple has no detrimental effect. In this case it would be possible to reduce the output filtering of the converter, thus reducing component count, cost and complexity.

The novel results arising from this research have been the subject of two journal articles and four conference proceedings papers. A summary of the contributions presented in this thesis is given below:

Analysis of the effects of varying test and environmental conditions on DCA performance

DCA has been recognised as a critical factor influencing the performance of batteries in HEV applications. This has resulted in much research into DCA and the factors which influence it, which has culminated in the adoption of a European Standard test procedure for characterising DCA performance; this procedure however, does not address all the factors which have been shown to affect DCA performance.

Chapter 3 therefore presents a detailed sensitivity analysis to determine

how varying the conditions used within the test procedure, together with external factors, influence the results produced by the DCA test. This work shows that the standard test methodology has several shortcomings, and for HEV applications produces results which suggest significantly poorer DCA performance than is likely to be the case in reality. A modified test procedure is proposed and experimentally validated, showing the importance of using charge currents which are representative of real-world conditions and of distinguishing DCA with respect to both temperature and operational history independently.

Analysis of the effects of cell degradation on DCA performance

Chapter 4 extends the work of the previous chapter to consider the effects of cell degradation on DCA performance. This demonstrates how the methodology of the standard test procedure may again produce misleading results, suggesting that DCA performance reduces proportionally in line with cell capacity.

This is in fact not the case, and DCA performance is not closely correlated with capacity as a cell degrades. Further, this chapter demonstrates that for the typical lifetime of a cell, DCA performance does not significantly change, despite the degradation of the cell and consequent loss of capacity. This indicates that for applications where DCA performance is more important than absolute capacity, cell lifetime may be longer than would typically be expected from capacity loss alone.

Analysis of the influence of high-frequency ripple currents on DCA performance and cell lifetime

Where the previous chapters considered how to better assess DCA performance, Chapter 5 considers how DCA performance may be actively improved by the application of high-frequency ripple currents. A wide-bandwidth hybrid battery model is proposed, which indicates the likely range of frequencies over which ripple currents may be effective.

A range of ripple currents are applied to a battery using a custom-made

ripple generator. This shows that the application of ripple currents can significantly improve DCA performance, and that selection of the proper frequency is vital if the benefits are to be maximised. This work demonstrates that the battery suffers no detrimental effects as a result of being exposed to ripple currents, even for long periods. Further it is shown that the presence of ripple currents does not cause any worsening of cell imbalance issues.

DCA and charging performance of lithium-based cells

Chapter 6 extends the work of previous chapters to consider how aspects of the research described in preceding chapters may be applied to lithium based cells. Firstly, the DCA performance of lithium is considered; this shows that whilst the charge acceptance of lithium is more consistent, lead-acid is capable of much higher levels of charge acceptance than lithium.

Secondly, an investigation is performed to determine the most appropriate charging strategy for lithium cells when they are subject to a high-rate charge. This demonstrates that high-rate charging need not result in high levels of degradation, and cycle life can be significantly extended simply by a small reduction in the maximum charge voltage. Further it is shown that these benefits may be achieved without significant loss of energy storage capability.

Chapter 2

Literature Review

The work proposed for this project focusses on two separate but related areas of battery research, and therefore the review undertaken has similarly been divided into two sections. Furthermore, the objectives of the proposed project differ between the areas, thereby necessitating a different kind of review between each area.

For the DCA analysis the investigation is primarily concerned with extending the current DCA testing methodologies to better match real-world HEV operating conditions. To this end the review has concentrated on understanding the ways batteries are now being used in the automotive sector and the reasons for DCA becoming an important factor in their performance.

For high-frequency ripple effects on the other hand, the objective of the work is to investigate whether ripple may be beneficial to DCA performance, and if the application of ripple currents may have any damaging side-effects for the battery. Therefore, the review has concentrated on identifying the range of frequencies at which converters typically operate, and assessing any previous work on ripple effects on battery life or DCA performance undertaken in this area.

2.1 Dynamic Charge Acceptance

The years following the millennium have seen battery technology and performance become increasingly important in automotive applications. Driven by a desire to reduce emissions and rises in fuel costs, the function of automotive batteries has shifted from an auxiliary power source to providing significant contributions to the performance of the vehicle; particularly in the case of fully electric vehicles, where it is the only source of energy. This, coupled with increasingly power-hungry driver-aids, entertainment and heating, ventilation and air-conditioning (HVAC) systems makes it increasingly important that the behaviour of automotive batteries is well understood.

One key area which has emerged is that of the DCA performance of automotive batteries. Fundamentally, DCA is a measure of a battery's ability to accept charge under high-rate partial state of charge (HRPSoC) conditions. The DCA test procedure determines this ability by applying a current waveform as shown in figure 2.1 to the battery under test, the response to this stimulus is used to determine the DCA performance. The key aspect of this waveform, from which DCA is determined is the initial charge pulse ($t_1 - t_2$), which lasts for 10 seconds. During this period of charging the terminal voltage of the battery will rise, in the ideal case this rise will remain below the maximum voltage allowable (2.47 V per cell for lead-acid), and all of the available charge will be accepted by the cell. If, however, applied current causes the voltage rises above the maximum safe value, the current is reduced to maintain the voltage within its limits. In this case, as the current is reduced, correspondingly, charge acceptance will also be less.

The charge pulse is followed by a rest period of 30 seconds, a discharge pulse and finally another 30 second rest; together these make up one complete DCA microcycle. Microcycles are not used individually, rather they are grouped into a block of 20 to form a DCA Pulse Profile (DCAPP) which is applied to the battery under test. DCA is calculated from the average recuperation current, I_{recu} , from all the microcycles in the DCAPP. For each

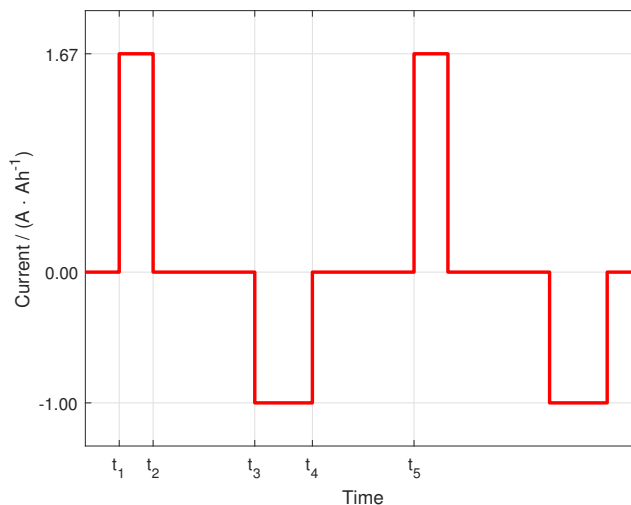


Figure 2.1: DCA Test Microcycle Current Profile ($t_1 - t_5$)

microcycle this is given by

$$I_{recu} = \frac{Ah_{recu} \cdot 3600}{t} \quad (2.1)$$

where Ah_{recu} is the charge accepted in ampere-hours and t is the length of the charge pulse in seconds. Given that the charge pulse is known to have a length of 10 seconds, the DCA for the complete 20-pulse DCAPP is given by

$$I_{recu} = \sum_{n=1}^{20} (Ah_{recu}(n)) \cdot 18 \quad (2.2)$$

A review of the literature concerning DCA has been undertaken to understand how the changes in automotive battery usage have altered the demands on the battery and how DCA has come to be an important factor. This has revealed the literature to be separated into two broad groups, one concerning the changes to battery demands over time and the emergence of DCA as a concept [3–6], and the second concerning how batteries may be designed, controlled or modelled to take account of or maximise DCA, and to develop test procedures to quantify DCA performance [7–13]

2.1.1 Identification & Emergence of DCA

Of all the literature reviewed, the first two papers provide the first indications of how the use of batteries in automotive applications has begun to change. They are amongst the first to mention DCA in literature [3,4]. These papers present the initial work on the demands to be placed on batteries by the use of hybrid technology in vehicles, they also begin to identify some key conditions under which these batteries will be expected to operate. Such conditions include HRPSoC operation, where the battery is exposed to high charge and discharge currents across a wide range of state of charge (SoC) conditions. This is presented in the context of examining the likely future requirements for batteries supplied to large automotive original equipment manufacturers (OEMs), in this case Ford. Taken together, they conclude that, whilst lead-acid batteries remain a viable option for HEV applications, it is important that the effects of these changed operating conditions be considered.

The third paper in this group, [5], identifies charging, and specifically, DCA as a key parameter which will influence the overall system performance when batteries are used in hybrid and electric vehicle applications. This is the first paper to propose specific test procedures to determine, amongst other parameters, DCA performance. It also presents the results of an analysis into some of the factors which influence DCA performance, and identifies the key role that the history of the battery, i.e whether it has previously been charged or discharged, and the rest period between this and the beginning of testing plays in affecting the charge acceptance. A key conclusion of this paper is that many testing regimes do not correlate well with the real-world operating conditions of the battery, and therefore do not produce representative results. Thus, if DCA performance is to be properly characterised, any test regime must match as closely as practical the conditions a battery would see in service. This paper also identifies that many of the factors which make DCA an important factor in automotive applications, such as HRPSoC operation and limited charge times are also found in other areas, such as static PV or other renewable energy storage systems.

The final paper examined in this area, [6], stands apart from the others so far considered, firstly its publication date is significantly later (2012 vs. 2007 – 2009), and thus has the benefit of several years' worth of real-world data from vehicles to draw upon; secondly it is primarily focussed on the underlying chemical processes responsible for the battery performance observed. The most useful feature of this paper, however, is the details it contains of the typical currents and SoC ranges to be found in real-world hybrid vehicles. The results of this work show that a typical HEV battery can expect to see charge currents of up to 30 times the 1-hour rate, across a wide range of SoC from around 50 % – 90 % SoC. This data allows comparisons to be drawn between the currents which can be expected in service and those used during the test procedures described below.

2.1.2 Developments in Charge Acceptance

The papers reviewed in this section form the second phase of research around DCA. The work reported here was performed in the years following the publication of the papers covered in the previous section (with the exception of [6], as mentioned above), once DCA had been formally identified and codified as an important phenomena affecting automotive batteries. This area can be further subdivided into two categories, those papers dealing with the design and development of batteries and systems optimised specifically for performance under HRPSoC conditions [9, 13], and those concerned with determining the factors responsible for DCA performance and the development of models and test procedures to formally quantify such performance [7, 8, 10–12].

The papers dealing with the development of batteries are useful sources of information as they provide details of the way micro-hybrid vehicles have been developed by major automotive manufacturers [9], and the challenges this has posed for battery design. They also have detailed descriptions of typical drive-cycle [9] and battery current [13] data extracted from real-world testing of vehicles from a variety of OEMs, including BMW and VW. These papers demonstrate how DCA has come to be recognised as a source of

significant interest by major players in the automotive sector, and highlights the importance of achieving a better understanding of the factors influencing DCA performance.

Two papers, [7, 8] present the application of modelling and simulation techniques to describe the underlying electrochemical processes which are responsible for the charge acceptance behaviour seen. This work is, of course, useful in and of itself in furthering the understanding of DCA, but of particular interest to this project is the experimental validation of the results described by [7]. This presents one of the first descriptions in literature of a test procedure specifically designed to characterise DCA performance, taking account of the various factors previously identified, such as SoC and history. The procedure proposes the use of a series of repeated charge and discharge pulses of varying currents to test the charge acceptance performance of the battery. This represents the beginnings of the development of a standardised method for testing and characterising the DCA performance of batteries.

The remaining papers reviewed in this area expand on this. The work reported in [10] presents a detailed review of the previous literature and identifies all the key factors which have been shown to influence battery performance in micro-hybrid vehicles; these being SoC, rest time between charges, temperature and history. This is then built upon by [11], which proposes a detailed test procedure to fully analyse battery behaviour in such applications. This test procedure includes specific features to measure the DCA performance across a range of SoC and also considers the effects of history by measuring DCA performance at the same SoC with both charge and discharge history.

This is further extended by [12], which presents a comparison of several variants of a DCA test procedure. This paper attempts to identify the most appropriate method to achieve a consistent, realistic assessment of DCA performance in a sensible time-scale. This work concludes that the most important factor in achieving a consistent DCA result is that the battery be properly conditioned to a known SoC before the beginning of the DCA testing phase. The end result of the above literature is the adoption of a European Standard DCA test procedure, EN 50342-6, also known as the ‘A3’

test procedure, and described by [14]. This test, however, does have some shortcomings. It does not fully account for all the factors shown to influence DCA performance, particularly in respect to SoC; further, the currents specified in the test are far lower than those reported in practice.

2.2 High-Frequency Ripple Effects

A review of the current literature on this subject has been found somewhat lacking; there are relatively few papers discussing the topic, and of those several performed their analyses at frequencies only around twice that of the mains supply (100 – 120 Hz) [15–18]. Only three papers discuss battery behaviour at higher frequencies [19–21], but even these go no further than 4, 8 & 20 kHz respectively — far below that of current-generation converters. No mention at all has been found of any work dealing with the effects of ripple currents on DCA performance, although several recent studies have examined the effects of ripple currents on charging performance of cells [22–25], albeit these papers all concern themselves with lithium cells. Despite these shortcomings the literature does provide useful information regarding the current state of research and the potential failure modes of batteries when exposed to ripple currents.

2.2.1 Typical Converter Frequencies

The first stage of analysis was to determine the typical operating frequency of converters. This would be critical to informing the project as it determines the frequencies of most interest, both in terms of literature review and the investigation itself. Of most use in this area is a paper dealing with the reliability of power converters [26], as this provides much detailed information regarding the characteristics of contemporary power converters.

The paper is an exercise in establishing the limiting factors to converter reliability, however it is the approach taken — that of a survey of power converter manufacturers — which yields the most useful data. As part of the background analysis the industry respondents were asked about their

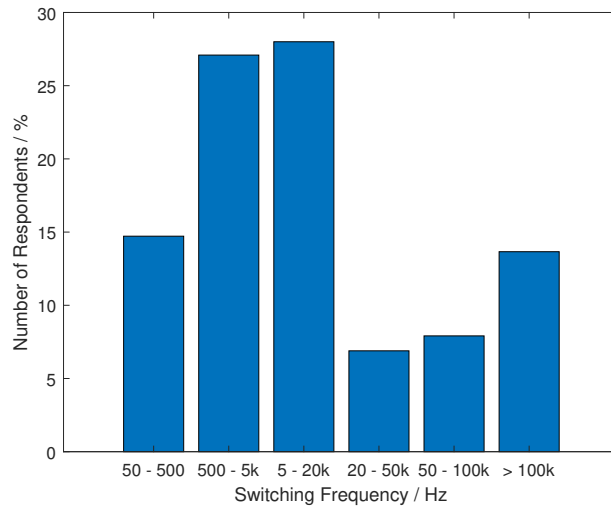


Figure 2.2: Converter Switching Frequencies Data [26]

current converter designs, such things as device types, power rating and, crucially, switching frequency. This broad, industry-based approach makes the results extremely useful as it not only aggregates the individual responses of many manufactures (56 in total), it also shows the specifications of current generation technology. These are exactly the kinds of converter designs that would be installed alongside modern battery systems.

The results of the survey itself are also highly informative. The most interesting results, in this case are those regarding converter switching frequency — these are reproduced here as figure 2.2. Of the respondents, the majority switching frequency (around 28 %) lay in the 5 kHz – 20 kHz bracket, although a very similar number were in the range of 500 Hz – 5 kHz. This suggests that the majority of current converters will be operating in the range of 500 Hz – 20 kHz. However the results also show a significant number of responses in the range of 20 kHz – >100 kHz, when taken as a whole, more than half the responses indicated a frequency of greater than 5 kHz. This clearly shows that high-frequency converters are already in common use today, and this is likely to increase further in coming years given the benefits they provide in terms of reduced size and weight over lower frequency designs.

It should be noted that switching frequency is, at least in part, a function of converter power and whilst the paper does group respondents into power

levels, it does not map typical frequency to power level in any way. That said, the results remain useful as an indication of the typical range of switching frequencies which may be encountered by batteries in modern systems.

2.2.2 Low-Frequency Ripple

The papers dealing with low-frequency effects concern themselves with the current ripple produced as a result of the second harmonic of the line frequency. Such a ripple is typically produced by the use of Flyback, Cuk [15] or H-bridge converters [17] to charge the battery. These papers deal with the effect this ripple has on the charging of the battery [15–17] and its long-term capacity [16].

In all cases no differences were observed between charges performed with or without a ripple current present. This is despite differences in the chemistry of the batteries used in the studies (lead-acid [15], lithium polymer [16] and lithium iron phosphate [17]). Furthermore, in comparative trials, ripple-charged batteries did not experience any additional loss of capacity over those charged with pure dc [16].

These findings suggest that low-frequency ripple charging does not affect either the battery’s ability to accept charge or its long-term capacity.

2.2.3 Heating Effect

A second factor considered by the majority of the ‘low-frequency’ papers is the effect of current ripple on the internal heating of the battery. Ripple currents will cause I^2R losses within the battery, leading to the generation of heat. The assumed risk here is that the battery will be subjected to ripple currents while ever the converter is connected to the battery, even when the dc load is very small. Whilst the magnitude of this heating will be no greater than the RMS dc equivalent, the long-term effects of this heating could be detrimental to the battery. As a battery is essentially an electrochemical system, the rate of internal reaction is strongly linked to temperature by the Arrhenius equation [18].

At higher temperatures internal reactions will proceed more quickly, with resultant advantages and disadvantages for battery performance. Higher temperatures will speed the rate of the reversible reactions allowing for faster charges, but will also increase the rate of non-reversible reactions such as plate corrosion and (in the case of lead-acid) sulphation. These non-reversible processes are the cause of battery degradation — clearly the hotter the battery the more quickly it will degrade. As the heat loss occurs within the structure of the battery itself, the effect is likely to be more pronounced than a similar degree of external heating which would have a lesser effect due to the thermally-insulating properties of the electrolyte material.

In practice, whilst the papers do report a mild heating of the battery in the presence of ripple currents [15, 17, 18], the magnitude of the increase is limited to a degree or so. This increase is insufficient to cause any appreciable additional degradation.

2.2.4 Ripple Charging

An area which has been the subject of some research in recent times is the use of ripple currents to reduce the charge time of batteries, whilst not directly applicable to DCA performance, this area does share some similarities. Reviewing the literature however, the results appear somewhat confused.

The work described in [22] investigates a method of charging lithium-ion cells using both sinusoidal and pulsed charge currents. By determining the frequency at which the cell exhibits the lowest impedance, around 1 kHz in this case, and charging using a pure sinusoidal ripple current at this frequency, with an amplitude of $3 A_{pk-pk}$ and an offset of 1.5 A, the charging time is seen to be improved by 17 % over those cells charged at 1.5 A dc. This paper also reported that the ripple-charged cells exhibited a 16 % improvement in lifetime over those charged with dc alone.

A similar approach is reported by [23], using a 14.6 V LiFeMgPO₄ battery. In this case the optimal frequency is determined to be 400 Hz, the charge profile used consists a 10 A dc component with a superimposed 7.5 A_{pk-pk} ac ripple. This results in an improvement to charge time and efficiency of

5.1 % and 5.6 % respectively over dc charging alone, due to the reduction in the effective impedance of the battery.

The same basic methodology is used by [24], with the addition of a phase-locked loop (PLL) to automatically determine the optimal ripple current frequency, which for the lithium-ion battery used in this study is determined to be around 800 Hz. Although this paper does not report the level of improvement seen when charging with this method, it does demonstrate once again the importance of determining the optimal frequency for the ripple current if its effect is to be maximised.

The three preceding papers show a consensus that charging with ripple currents in the range of 500 Hz – 1 kHz is beneficial in producing a faster charge, and [22] suggests that such frequencies may also help to extend lifetime in lithium cells.

These results are disputed by [25], which tested a range of charge current profiles (pulse, sinusoidal, and triangular) with a wide range of frequencies on lithium-ion cells, and found no benefit in any case over pure dc charging. Further, this paper presents a physics-based model which shows that no benefit should exist due to the ac ripple having no effect on the reactant concentrations within the cell.

Clearly these results are somewhat confusing and contradictory, and only examine lithium chemistries. Despite these limitations however, they all do demonstrate that at the frequencies examined, whilst ripple charging may not necessarily improve battery performance, it certainly does not cause it to worsen. This therefore further contributes to the findings of the papers dealing with low-frequency ripple which also suggest no detrimental effects from ripple currents at similar frequencies.

2.2.5 Mid-Frequency Ripple

Of the papers which discuss mid-frequency behaviour (4 kHz – 20 kHz), the one discussing the highest frequency — closest to that of a real-life application — unfortunately provides the least information [21]. This paper is primarily concerned with developing a battery model, therefore, whilst it discusses the

electrical properties of batteries at higher frequencies, it does not analyse the effects such frequencies will have on the long-term performance of the battery.

The remaining two papers reported a similar test procedure, whereby one set of batteries were exposed to ripple currents at up to 4 kHz and 8 kHz respectively [19, 20], whilst a second set were cycled with conventional dc. The methods by which the ripple was achieved however, varied between the papers. That described in [19] used a controlled, sinusoidal ripple to test over a range of frequencies (0.1 Hz – 4 kHz), whilst [20] applied a fixed frequency of 8 kHz to an inductor to generate the required ripple. Despite the differing methods, frequencies and battery chemistries (lead-acid [19] vs. lithium-ion [20]), neither paper reported any degradation of the batteries according to the metrics used.

The testing described in [19] measured the capacity change and predicted life cycle of the batteries exposed to ripple currents and found the ripple current to have no effect on the charge capacity, and only a negligible (1 %) increase in discharge capacity. In terms of life cycle, the inherent distribution of the battery life cycles was far greater than any change caused by the ripple currents.

Different metrics were used by [20], which measured both the discharge and regen resistance and the discharge and regen power for the batteries tested. The current ripple had no measurable effect on any of these metrics as compared to non-rippled batteries. Further it was found that temperature has a far more pronounced effect on resistance and peak power than any applied ripple. Which implies, although it is not explicitly stated by the paper, that the heating effects of the ripple losses are insufficient to affect the battery performance.

2.2.6 Microcycling

The final paper examined stands alone from the others in that it discusses the effects of microcycles on the battery [27]. Note that the term microcycle here is used to denote any general, short-duration, charge–discharge cycle;

when applied to the DCA test procedure, microcycle — as introduced in Chapter 3 — has a different, specific meaning; these should not be confused.

This is in contrast to the other papers which discuss only uni-directional current. The paper deals with the use of batteries in renewable systems where monitoring periods are long (≈ 1 hour). In such cases it is possible for microcycling to occur without being recorded by the monitoring equipment. The lack of monitoring causes predictions of energy throughput and SoC to be inaccurate for such systems. It is not clear from the paper however if the microcycles cause increased battery degradation, or how this is related to the microcycle frequency.

2.3 Conclusions

Dynamic Charge Acceptance is relatively new area of research, whose appearance coincides with the rise of practical hybrid electric vehicles in the last 10 years or so. Despite this, much research has been performed in this area and applications for DCA have been identified beyond the automotive sector. The factors which are important in influencing DCA performance have been identified and described, and numerous test procedures have been proposed to quantify charge acceptance, one of which has been adopted as a European Standard. This test, however, has its limitations, and does not fully account for all relevant factors, this leaves open the prospect of further investigation to improve the existing procedure to better represent real-world performance.

From the literature available it appears that the effects of ripple current on batteries has not been extensively covered, especially at high-frequencies. That said however, the papers above clearly indicate that such ripple has no adverse effect on battery life or performance — this appears to hold true for various battery chemistries and across a range of frequencies, although the supposed benefits of ripple-charging would seem to be open to questioning. Perhaps the lack of papers stems from the apparent absence of any interesting phenomena at the frequencies previously studied. It is also clear however that there is significant scope for investigation into the effects (if any) of higher

frequency ripple currents.

That there is no published literature relating ripple currents to DCA performance is perhaps not surprising, given the paucity of papers considering ripple at all, and the relatively recent rise of DCA as an important phenomenon. It does however demonstrate a clear gap in the current body of scientific knowledge, and therefore provides broad scope for research.

Chapter 3

Analysis of DCA Test Conditions for Lead-Acid Cells

3.1 Introduction

Battery technology and performance has become increasingly prominent over recent years, particularly in the automotive sector. Rising fuel costs and increasing concerns over emissions have driven a shift in the function of automotive batteries, from a purely auxiliary power source to providing a significant contribution to vehicle performance. This is particularly true for fully electric vehicles, where the battery is the only source of energy. When coupled with ever more complex and power-hungry on-board devices, such as driver-aids, HVAC and entertainment systems, this is making it particularly important that the behaviour of batteries in automotive applications is well understood.

3.1.1 Battery Use in Vehicles

Traditional IC engined vehicles carry a single lead-acid battery as a stand-by power source, used only when the IC engine is switched off. Once started the engine is used to provide all the vehicle's power, both electrical, via the alternator and mechanical via the gearbox and drive-train. In such a vehicle the battery is subjected to infrequent discharges for short periods when the

engine is started. Despite their limited duration, however, the discharge currents are significant; around 16 times the 1-hour rate, C_1 . Once running the engine is used, via the alternator to recharge the battery at a modest rate back to full SoC, typically this will be done with a current of no greater than $1 C_1$ [6]. Thus, in this method of working, the battery is only used infrequently, being subject to shallow discharges and is always immediately recharged and maintained at or near 100 % SoC. This is a duty which is well suited to the characteristics of lead-acid batteries, which when combined with their low cost, robustness and safety has made them the universal standard chemistry for automotive use for decades. The use of lead-acid batteries in this way, for SLI and their failure modes under these conditions is well understood.

An addition which is becoming increasingly common is the fitting of a stop-start system to an otherwise standard IC vehicle. Under such a system the IC engine is automatically stopped when the vehicle is stationary for a certain period of time, and restarted before moving off, without intervention from the driver. This type of system is intended to significantly reduce the amount of time the engine is running whilst the vehicle is stationary, thereby reducing emissions and fuel-usage. This method of working does result in a more demanding duty for the battery, as the number and frequency of starting events, and hence the number of discharge–charge cycles is increased over the more traditional method of operation, but the fundamental mode of operation and mechanism for recharging remains the same.

More recently, with advances in battery technology, together with increasing fuel costs and environmental concerns, vehicles are using batteries to augment the IC engine, or replace it entirely. The batteries in these vehicles are used in a very different way to those of a traditional IC vehicle, and can be divided into two main duties.

Where the battery has replaced the IC entirely, as in full EVs, the demands placed on the battery become very cyclic. Driving the vehicle uses energy from the battery, causing it to discharge. Energy may be recovered using regeneration during braking, but due to losses inherent in the electrical and mechanical systems of the vehicle, and the fact that the charge efficiency

of any battery is less than 100 %, not all of the energy available can be recovered and stored. Whilst such a system can therefore help to increase the range of the vehicle, it can never fully replace the energy lost in driving, eventually the vehicle must be plugged into an external power supply to recharge the batteries. This leads to the battery being subject to a repeating cycle of charges and discharges. Such a duty places a premium on cycle-life, charging time and battery capacity. Given such a duty, lithium-based batteries are the obvious choice, their long cycle-life, fast-charge ability, and high energy-density and specific power all work in their favour to offset the initial expense and the difficulty of their recycling [28]. Even with these properties, however, EV battery packs often have a lifetime significantly shorter than that of the vehicle in which they are installed. The aforementioned difficulty and expense of recycling lithium cells has led to growing interest in second-life applications, beyond their original automotive use [29].

Aside from completely replacing the engine, many hybrid vehicles are now using batteries alongside the existing IC engine to provide traction power. In this application the battery acts as a power buffer, being able to provide short, high-power bursts during rapid acceleration, such as starting or overtaking, more efficiently than the IC could. There are several possible configurations for the drive arrangement of such vehicles [30], depending on whether the power is delivered in series or parallel, but the principle of operation is similar. In most cases it is possible for the vehicle to be powered by either the engine or batteries alone, or by the two together. This allows such vehicles to drive quietly and with zero emissions at low speeds, such as within cities. It also allows for the fitting of a smaller, more efficient IC engine sufficient for most driving, but maintain performance when needed, such as accelerating to overtake by using their batteries to increase the available power.

The battery can be recharged regeneratively during braking to recover otherwise wasted energy, this is known as a brake energy recuperation (BER) system, which reduces brake wear. Unlike in an EV however, the battery can also be charged by the IC should the need arise. This eliminates the need to plug the vehicle in to recharge – although plug-in Hybrid Electric Vehicles

(PHEVs) retain the ability to do so – and means the user can operate it in the same way as they would a conventional IC-engined vehicle. As the electrical power requirements are much greater in a HEV, the installed batteries are by necessity much larger than in a conventional vehicle, but less than that of a full EV, and thus standard automotive alternator is not sufficient to recharge them. Therefore recharging is typically performed by using the electrical machine fitted within the drive-train as a generator [30].

The duty imposed on a HEV battery is much less predictable than either that of an EV or a traditional SLI application and dominated by short, high-power pulses of either discharge or charge. Aside from the large discharges associated with starting the IC engine, there are additional discharge spikes caused by acceleration, together with longer periods of lower discharge currents where the vehicle is running in purely electric mode. The charging profile is similarly modified, the batteries are no longer steadily charged back to full SoC, instead operation is often at partial SoC. Charging from the engine is controlled to a modest rate as before, but is now interspersed with large charge spikes due to the BER system; these spikes can reach up to $30 C_1$ under heavy braking [6]. The operation of batteries under these conditions of HRPSoC is becoming increasingly common as the number of HEVs increases and thus the ability to perform reliably under these conditions becomes a crucial factor for HEV batteries, other aspects such as capacity and cycle-life assume a lesser priority.

In such applications lead-acid batteries remain a viable proposition [31–33]. The physical size of HEV batteries is less than that of EV batteries as they must share space with the IC engine, and their capacity need not be as great, so the weight penalty associated with lead is reduced. This is combined with the low initial cost and ready availability of lead recycling infrastructure, which makes lead economically attractive in this application.

3.1.2 Charge Acceptance

The chief benefit of a HEV drive-train over a traditional IC vehicle, from the users' perspective, is its lower fuel consumption resulting from the lo-

wer demands placed on the installed IC engine. To obtain the maximum benefit from this system it is critical that as much energy as possible must be recaptured and stored during any and all regenerative braking periods; this is ‘free’ energy which would otherwise be wasted as heat in the braking system. The main factor limiting the ability to capture this energy is the charge acceptance of HEV batteries under HRPSoC. As the batteries used in such applications are now required to provide more of the electrical power to the vehicle it is crucial that they are able to be recharged sufficiently quickly and that the performance of batteries under these conditions is well understood. To this end numerous testing methodologies have been developed to characterise the performance of automotive batteries, from stand-alone tests such as DCA and Hybrid Pulse Power Characterisation (HPPC) tests to full simulated drive-cycle tests like New European Drive Cycle (NEDC) and Worldwide harmonized Light vehicles Test Procedure (WLTP).

Understanding the DCA performance of automotive batteries has been identified as a key requirement for the development of electric vehicles [3, 4, 12], and standard test procedures have been designed to characterise the DCA performance of batteries [14]. This chapter describes an investigation into how varying the conditions and parameters of the standard DCA test regime can provide a superior evaluation of DCA performance and lead to a better understanding of the behaviour of the cell under real-world conditions.

3.2 DCA Overview

DCA is a measure of the charge efficiency of a battery, the higher the DCA value the better the charge efficiency and the more energy may be stored. The standard test for determining DCA performance involves the application of a defined current waveform to the battery under test, the response of the battery to this waveform is used to calculate DCA performance. The test procedure is composed of two primary operations run sequentially, these being: conditioning and microcycling.

Conditioning

The nominal or rated capacity of the tested cell, C_{nom} , is insufficient to properly characterise its DCA performance, therefore the conditioning phase is provided to experimentally determine the capacity of the battery prior to performing the DCA analysis. This is achieved through a series of charge and discharge cycles applied as shown in table 3.1. All charges are performed with a constant-current, constant-voltage (CCCV) methodology, whilst the discharges use a CC-only approach; with the per-cell voltage and current limits and end conditions as shown in table 3.1. The capacity delivered during step 6 of this sequence is used as the experimentally determined capacity of the cell, C_{exp} . Step 7 recharges the battery to 80 % SoC using a coulomb-counting method; this is achieved by charging until 80 % of the capacity released in step 6 has been returned to the battery.

This closely matches the regime given by the European Standard DCA Test A3 specification (EN 50342-6) [14], with the exception of the final rest period, step 8; this has been reduced to 1 hour from the 20 hours given in the test. It has been shown that for batteries which have previously been charged, as is the case here, the rest period between the end of the charge and the commencement of the testing phase has little effect on the DCA result [12]. This has allowed the rest time to be reduced in order to speed up the testing process.

Figure 3.1 shows the SoC profile for the conditioning phase of the standard

Table 3.1: Conditioning Operation Sequence

Step	Mode	V_{limit}	I_{limit}	End
1	Discharge (CC)	–	$2.0 C_{nom} A$	$V = 1.75 V$
2	Charge (CCCV)	$2.47 V$	$0.5 C_{nom} A$	$I = 0.02 C_{nom} A$
3	Discharge (CC)	–	$2.0 C_{nom} A$	$V = 1.75 V$
4	Charge (CCCV)	$2.47 V$	$0.2 C_{nom} A$	$I = 0.02 C_{nom} A$
5	Rest	–	–	$t = 1 h$
6	Discharge (CC)	–	$0.2 C_{nom} A$	$V = 1.75 V$.
7	Charge (CCCV)	$2.47 V$	$0.2 C_{nom} A$	$C = 0.8 C_{exp}$
8	Rest	–	–	$t = 1 h$

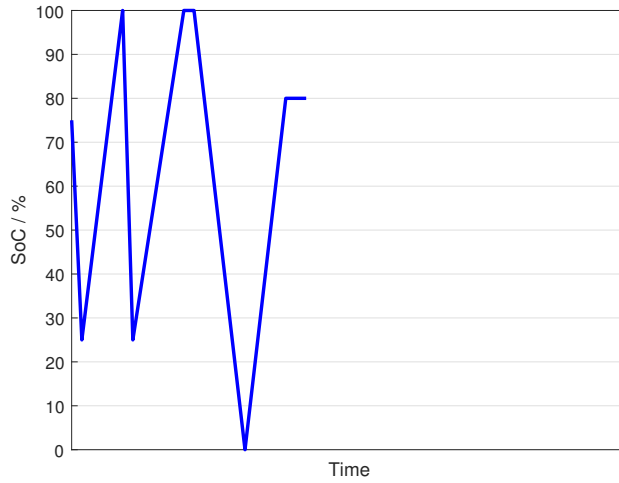


Figure 3.1: DCA Test A3 Conditioning Phase SoC Profile

A3 test procedure. It is not necessary for the initial SoC of the battery to be known, nor is the SoC at the end of the first two discharges defined, therefore this section of the profile is an approximation. This is implicit in the published test procedure and does not affect the ability of the test to determine C_{exp} as all SoCs after step 4 are well defined.

3.2.1 Microcycling

At the heart of the DCA test is the microcycle, it is this which defines the current applied to the battery, and from which the performance may be determined. The standard microcycle, as defined by the A3 DCA test specification is given in figure 3.2, this is summarised in tabular form in table 3.2.

DCA performance is calculated from the response of the battery to the

Table 3.2: Standard DCA Test A3 Microcycle Current Profile

Step	Mode	V_{limit}	I_{limit}	End
1, $(t_1 - t_2)$	Charge (CCCV)	2.47 V	$1.67 C_{exp}$ A	$t = 10$ s
2, $(t_2 - t_3)$	Rest	–	–	$t = 30$ s
3, $(t_3 - t_4)$	Discharge (CC)	–	$1.00 C_{nom}$ A	$C = C_{step\ 1}$
4, $(t_4 - t_5)$	Rest	–	–	$t = 30$ s

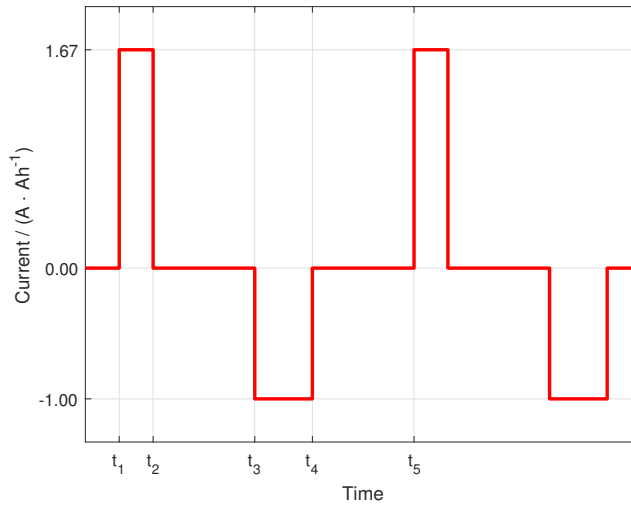


Figure 3.2: DCA Test A3 Microcycle Current Profile ($t_1 - t_5$)

charging phase of the microcycle (step 1). During this phase the test procedure replicates the high-rate charge pulses seen in HEV applications. This is achieved by attempting to charge the battery with a current of $1.67 C_{exp}$ A for 10 seconds. This charging will cause the terminal voltage of the battery to rise, if voltage reaches the set limit of 2.47 V per cell (equivalent to 14.8 V for a standard 6 cell battery) at any point during this step, the charge current is reduced to maintain the battery at the voltage limit; a reduction in charge current equates to a reduction in the charge accepted by the battery. DCA is thus determined by the difference in the amount of charge actually accepted by the battery compared to the total theoretically available from the charge pulse. All current limits used during the microcycle are normalised to the measured capacity of the battery (C_{exp}), which is obtained experimentally during the conditioning phase.

This behaviour may be seen from figure 3.3, which has been produced from the test data resulting from this study. Figure 3.3a shows the ‘ideal’ case, here the applied charge current causes the cell voltage to rise, but it does not reach the maximum allowable voltage. In this case all the charge available from the pulse is accepted. Figure 3.3b, on the other hand, shows the alternative. In this case the same charge current is applied, but now the voltage immediately rises to the limit, at which point the current must

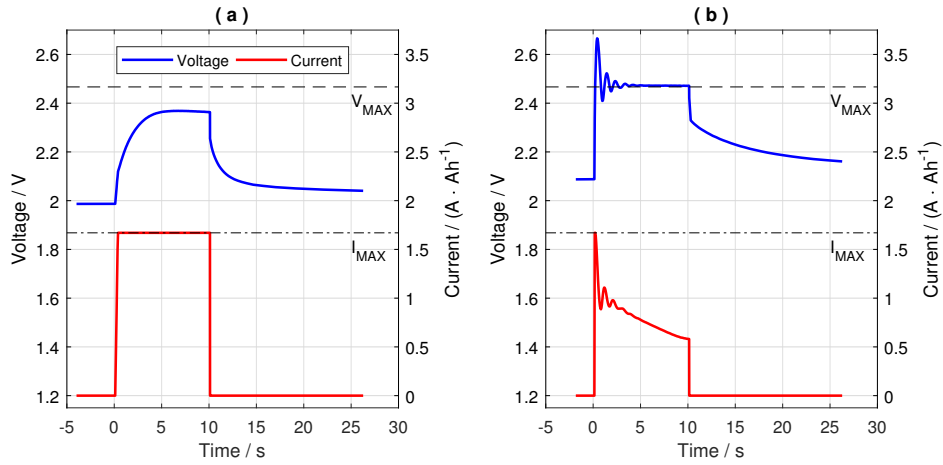


Figure 3.3: DCA Performance Examples. (a) All Charge Accepted, (b) Reduced Charge Acceptance

be reduced to avoid damage to the cell. Whilst the same amount of charge was available as in the first case, in this instance only a fraction of this was actually able to be accepted by the cell.

Microcycles are applied repeatedly to the battery in blocks of 20 to form a DCAPP. Each microcycle, and hence each DCAPP, is inherently energy-balanced. The amount of charge removed during the discharge in step 3 is equal to that accepted by the cell during the charge step, i.e:

$$\int_{t_1}^{t_2} I(t) dt = - \int_{t_3}^{t_4} I(t) dt \quad (3.1)$$

This is achieved by varying the length of the discharge cycle dynamically during the test procedure, which ensures that the SoC of the battery does not change between microcycles, and therefore does not drift over the course of the DCAPP. Note that this assumes equal efficiencies for both charge and discharge, in practice the difference between these efficiencies will have little effect due to the small energy throughput and the tests being conducted away from the extremes of SoC; this assumption is also implicit in the A3 test specification.

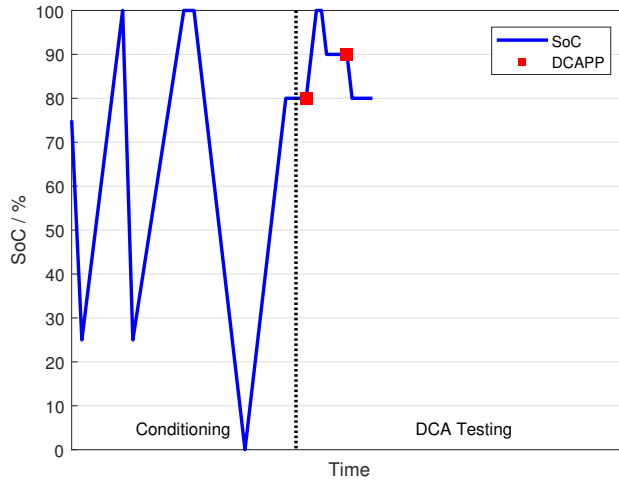


Figure 3.4: DCA Test A3 SoC Profile & DCAPP Locations

3.2.2 Standard DCA Test A3 Procedure

Figure 3.4 shows the SoC profile and DCAPP locations as specified by the standard DCA test procedure. The test begins with the conditioning phase, consisting of two heavy discharges to establish the reserve capacity performance of the battery, each followed immediately by a full recharge to 100 % SoC. The battery capacity, C_{exp} , is then determined by a standard-rate discharge to a minimum voltage of 1.75 V per cell. After this conditioning the battery is recharged to 80 % SoC where the first DCAPP is performed, this tests the DCA performance of the battery with charge history, i.e. after having been previously subjected to charging. The battery is then fully charged before being discharged to 90 % SoC for a second DCAPP, this time testing with discharge history. As with the conditioning phase, coulomb-counting is used to determine the SoC levels. The test then continues to perform various configurations of simulated drive-cycles, but these are beyond the scope of this investigation. Throughout the entirety of the test, the battery is maintained at an ambient temperature of 25 °C.

3.2.3 DCA Calculation

DCA is generally expressed as the average recuperation current, I_{recu} , in units of $A \cdot Ah^{-1}$ (often simplified to C [12]), for the time of the charge pulse. Thus, for a charge of arbitrary length, DCA is given by:

$$I_{recu} = \frac{Ah_{recu} \cdot 3600}{C_{exp} \cdot t} \quad (3.2)$$

where Ah_{recu} is the amount charge accepted during the pulse in ampere-hours, C_{exp} is the capacity of the battery in ampere-hours and t is the length of the pulse in seconds.

The DCA Test A3 calculates I_{recu} from the average current of all 20 charge pulses in the DCAPP. As both the number of pulses and their length and are specified (as 20 pulses and 10 seconds respectively), this allows for the simplification of equation 3.2 to

$$I_{recu} = \frac{\left(\sum_{n=1}^{20} Ah_{recu}(n) \right) \cdot 18}{C_{exp}} \quad (3.3)$$

3.3 Experimental Setup

The testing described below was performed using small form-factor 6 Ah carbon-enhanced valve-regulated lead-acid (VRLA) cells, of an experimental prismatic construction specifically designed for HEV applications [34] and manufactured by Banner GmbH (figure 3.5). This makes them ideal for testing of this nature as the cells have been designed specifically to be optimised for performance under HRPSoC conditions. Prior to this testing they were used to evaluate the performance of the design and were known to be in good condition. The nominal capacity of the cells, C_{nom} , is 6 Ah.

The testing described below was conducted using a Maccor Series 4000 automated test system (figure 3.6). This allows for the complete test procedure to be pre-programmed into the tester and run on demand. The system logs, in high-resolution, all important parameters (current, voltage, tempe-



Figure 3.5: 2 V, 6 Ah, VRLA Cell

perature, etc) during the running of the test, this data was then analysed using Matlab software to generate the results presented below.

Coupled to the testing equipment are environmental chambers, in which the tested cells are placed (figure 3.7). These chambers are capable of both heating and cooling and may be programmed to a specific temperature to ensure the tested cells are maintained in known and controlled environmental



Figure 3.6: Maccor S4000 Test System (l) & Environmental Chambers (r)



Figure 3.7: 8 Cells in Environmental Chamber

conditions for the duration of the procedure. Usually testing of this nature would be performed with the cells placed in a water bath, in this case however the form-factor of the cells — with terminals at opposite ends — prevents this. Instead the cells have been placed in free air within the temperature controlled chambers, this method has the advantage that it has been possible to perform tests at temperatures below 0 °C. Throughout the course of testing the Maccor has been used to record temperature data for the cell under test, this has been achieved by attaching a single type-T thermocouple, as required by the Maccor system, to the upper exterior surface of the cell, in the centre. Additionally a second type-T thermocouple placed inside the chamber is used to record the ambient temperature within. Testing has been conducted at -10, 0, 10, 25 & 40 °C, this range of temperatures covers the normal operational range which may be expected to occur in real-world service.

3.4 Test Procedure Modifications

The standard DCA A3 Test is somewhat limited in its ability to characterise the DCA performance of batteries. This is caused firstly by the fact that it only performs DCA analyses at two points, both with similar SoC levels. As DCA performance is critical to HEVs and the batteries in HEV applications are likely to be cycled across a wide range of SoC it is important that DCA performance be measured across a similarly wide range. A second concern is that it has been shown that history has a large influence on DCA performance. Whilst the standard test does assess performance with both charge and discharge history, it makes this assessment at different SoC levels, this makes any attempt to determine the influence of either SoC or history alone much more difficult.

3.4.1 Modified SoC Profile

The shortcomings discussed above are addressed by the modified SoC profile proposed by figure 3.8. The principal differences are the number and location of the DCAPPs and the SoC at which they are performed. In this profile DCA is measured in 10 places and five SoC across the SoC range, these being 90 %, 70 %, 50 %, 30 % and 10 % SoC, which is intended to assess DCA performance over a range similar to that which may be experienced by a HEV battery.

As the test procedure determines C_{exp} during the conditioning phase it is simple to achieve the desired SoC for each DCAPP using the same coulomb-counting method described above; starting from the fully charged state reached at the end of the conditioning process, the cell is discharged until $0.1 C_{exp}$ Ah have been removed and the cell is at 90 % SoC. $0.2 C_{exp}$ Ah is then removed following the next four DCAPP, thus reducing the SoC of the cell by 20 % each time. After the fifth DCAPP the cell is discharged until 1.75 V is reached and its SoC is 0 %, this process is then repeated, but with charges rather than discharges, for the next five DCAPPs as SoC increases. The effects of the immediate charge and discharge history, that is, the last operation performed on the battery, are also considered by measuring the

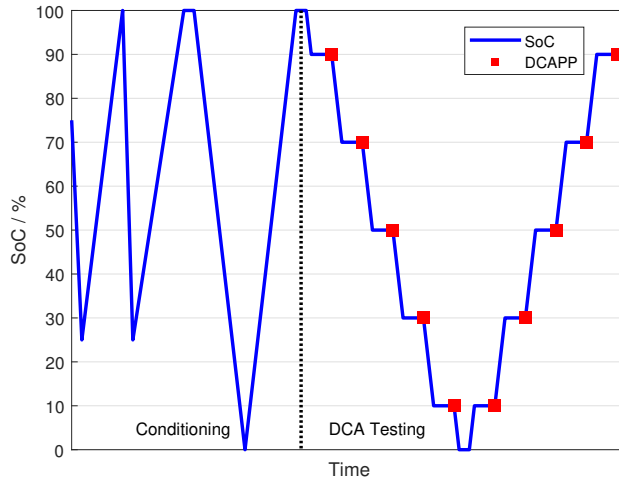


Figure 3.8: Modified DCA Test SoC Profile & DCAPP Locations

DCA at the same SoC with both charge and discharge history.

3.4.2 Modified DCA Calculation

To better assess the performance of the cells tested, the DCA has been calculated for each charge pulse within the DCAPP, rather than just as the average for the whole pulse profile as specified by the A3 test. This allows for any trends present during the DCAPP to be identified, the charge acceptance has therefore been calculated using a modified form of equation 3.2. Given that the length of the charge pulse is known to be 10 s, the calculation may be simplified to give

$$I_{recu} = \frac{Ah_{recu} \cdot 360}{C_{exp}} \quad (3.4)$$

Figure 3.9 shows the typical result of the DCA analysis obtained from the modified test procedure. The abscissa is divided into five discrete sections, one for each SoC of the test procedure. Within each of these sections are plotted the DCA results for each microcycle, arranged in chronological order from left to right; each section thus contains 20 individual data-points. Charge acceptance, in $A \cdot Ah^{-1}$ is shown on the ordinate axis. Two plots are provided, giving the results of the testing with both discharge and charge

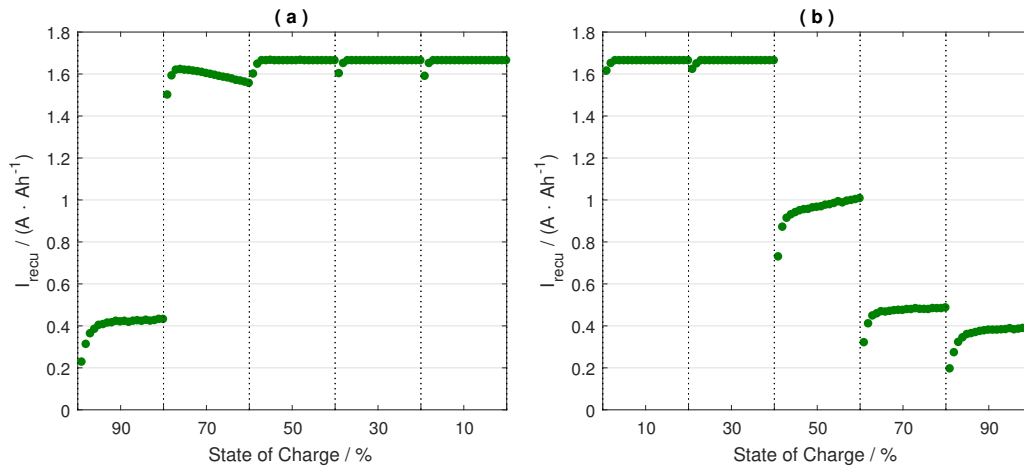


Figure 3.9: DCA Analysis Result at 25 °C, Modified SoC Profile. (a) with Discharge History, (b) with Charge History

history.

It may be seen from figure 3.9 that the modified test profile provides far more information regarding the DCA performance across a range of SoC. Despite this however there is a clear limitation imposed by charge current used, it may be seen that at many of the SoC examined the cell is capable of accepting all the charge available and thus the result is artificially limited to the maximum charge current of $1.67 \text{ A} \cdot \text{Ah}^{-1}$ specified by the test procedure. This result does however, begin to show the benefits of considering history, as there are clear differences in the charge acceptance performance at the same SoC levels, but with differing histories.

3.4.3 Increased Charge Current

To address the artificial limitation of charge acceptance discussed above, the microcycle profile has been modified to increase the current during the charge (step 1) to $4.00 \text{ A} \cdot \text{Ah}^{-1}$. This is a value which more closely equates to the charge currents likely to be experienced by HEV batteries, whilst avoiding the application of excessive stress to the cells. All other parameters of the microcycle profile remain as indicated in figure 3.2 and table 3.2. Figure 3.10 shows the results following these modifications.

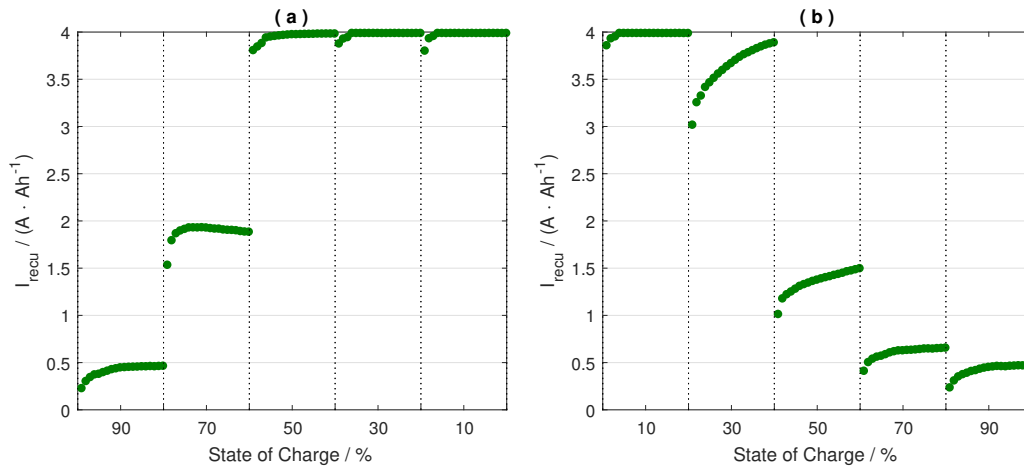


Figure 3.10: DCA Analysis Result at 25 °C, Modified Microcycle Profile and Increased Charge Current. (a) with Discharge History, (b) with Charge History

This result shows three main points of interest. Firstly it demonstrates the trend in DCA performance with varying history and SoC much more clearly than the previous method. This is most clearly demonstrated with the variation in charge acceptance with SoC, broadly DCA improves as SoC reduces. This is to be expected as the total capacity of a battery is finite, and as SoC may be considered analogous to the current battery capacity at any given point, the further below 100 % SoC the more readily the battery will accept charge at a given rate.

Secondly, by calculating and plotting the charge acceptance for each microcycle, performance trends within the DCAPP which would normally be overlooked become apparent. It may be seen that there is typically a large increase in performance between the first and second charge pulses, beyond this, although performance continues to generally improve as the DCAPP progresses, the rate of improvement slows with time. This effect is seen to be more pronounced at lower SoC levels.

Finally, it can be seen that history of the cell results in a large difference between charge acceptance at some SoC levels. Whilst the results at 90 % SoC correlate well, at all SoC below this, tests with discharge history show significantly improved DCA performance, reaching $4 \text{ A} \cdot \text{Ah}^{-1}$ at 50 % SoC;

with charge history this level of charge acceptance is not observed until SoC reduces to 10 %. This behaviour has previously been observed in lead-acid batteries when subjected to the standard DCA test and similar profiles [11, 12].

This result clearly indicates that DCA performance is not merely governed by the SoC of the cell at the time of testing, the electrochemical processes occurring within the cell also affect the results. All testing was prefaced by a 1-hour period where the cell was allowed to rest, open circuit, to allow for these processes to reach an equilibrium. Despite the rest however, the effect of operational history remains significant, thus it must also be considered as a fundamental factor when assessing DCA performance.

3.4.4 Rest Period Variation

Whilst the 30 s rest period between operations in the microcycle specified by the A3 test is perfectly reasonable for determining DCA performance and is, of course, necessary for defining a standard test procedure, in real-world applications the rest periods between charge pluses are likely to vary considerably. To assess the effect of this variation on the test cells the microcycle was further modified by altering the length of the rest periods used (steps 2 & 4). These were both increased and decreased by an order of magnitude to test cell performance with rest periods of 300 s and 3 s, as well as the standard 30 s; figures 3.11a & 3.11b show the results from this testing.

In this case, the most general observation is that charge acceptance is indeed affected by the rest period, with shorter rest periods being seen to improve DCA performance. It is also apparent that the rest period affects the way charge acceptance changes throughout the DCAPP. With the shorter, 3 s rest periods the charge acceptance increases more rapidly during the initial pulses before beginning to plateau. As the length of the rest period is increased, however, this process becomes less pronounced, with the 300 s rest tests showing little change in performance throughout the entire DCAPP. There is also one isolated case (at 70 % SoC with discharge history) where the 300 s rest period led to a pronounced decrease in charge acceptance over

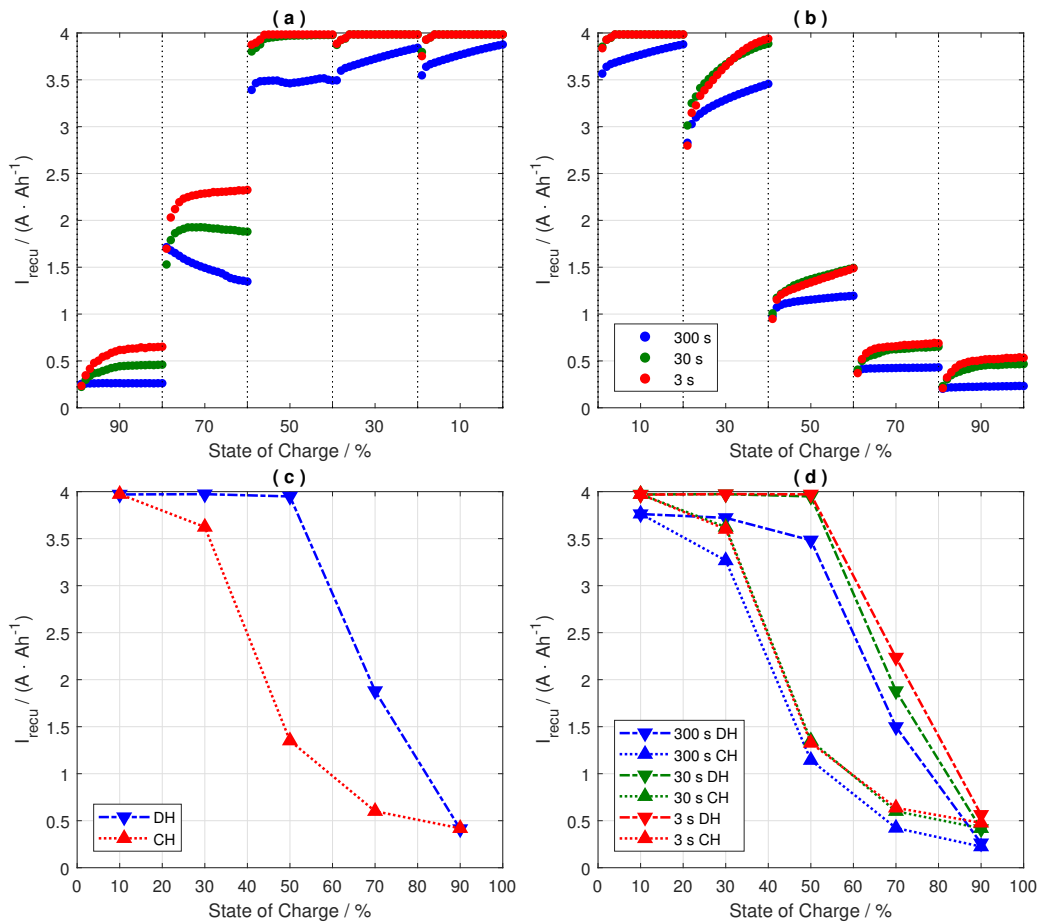


Figure 3.11: DCA Analysis Result, Variation with Rest Period at 25 °C. (a) with Discharge History, (b) with Charge History, (c) Average Charge Acceptance Variation with 30 s Rest Period, (d) Average Charge Acceptance Variation for all Rest Periods

the DCAPP. No satisfactory explanation has been found for this behaviour, however.

To better illustrate the variations caused by history, the results were recalculated using the DCA Test A3 method, as given by equation 3.3. This produces a single, average DCA value for each DCAPP allowing history to be more easily compared. Figure 3.11c shows the result of this recalculation for the 30 s rest period alone, clearly demonstrating the effects of history, and revealing the hysteresis-like behaviour resulting from this influence. The greatest variation in performance lies within the mid-SoC range, which is the

typical range of operation of a HEV battery. This clearly indicates the need to properly analyse the behaviour of such batteries under these conditions if their real-world performance is to be properly assessed.

Considering the average charge acceptance for the other rest periods, shown in figure 3.11d, again the effects of history are apparent, with the behaviour previously observed being exhibited regardless of rest period. It may also be seen that the effect of the rest period is broadly consistent across the SoC range. This is a very useful result, as in real-world applications the rest periods between charge pulses are likely to vary significantly, this shows that such variation does not have as great an impact on DCA performance as other factors, such as SoC.

Although history continues to have a large influence, there is much greater differentiation between rest periods for those results with discharge history. When the cell has charge history however, there is very little difference between the 30 s and 3 s rest periods in either the start and end points or shape of the result. This is interesting and suggests that whilst DCA performance is poorer when the cell has charge history, it is also more consistent with regards to rest period.

3.4.5 Temperature Variation

As with rest period, it is necessary in order to define a repeatable standard, for the A3 Test to fix the ambient temperature during testing to 25 °C. However, in practice this will not be the case, instead the batteries in HEVs will be subject to significant variations in ambient temperature during their operation. They are subject to the variation in climatic temperature conditions experienced by the vehicle, becoming very cold during winter nights or very hot during the height of summer. Similarly, the very act of using the battery, particularly at high rates, will cause heating due to internal losses. To examine performance across a range of temperatures, the test procedure was repeated with the cell at an ambient temperature of -10, 0, 10, 25, or 40 °C, which were chosen to best represent the likely real-world conditions HEV batteries may be exposed to.

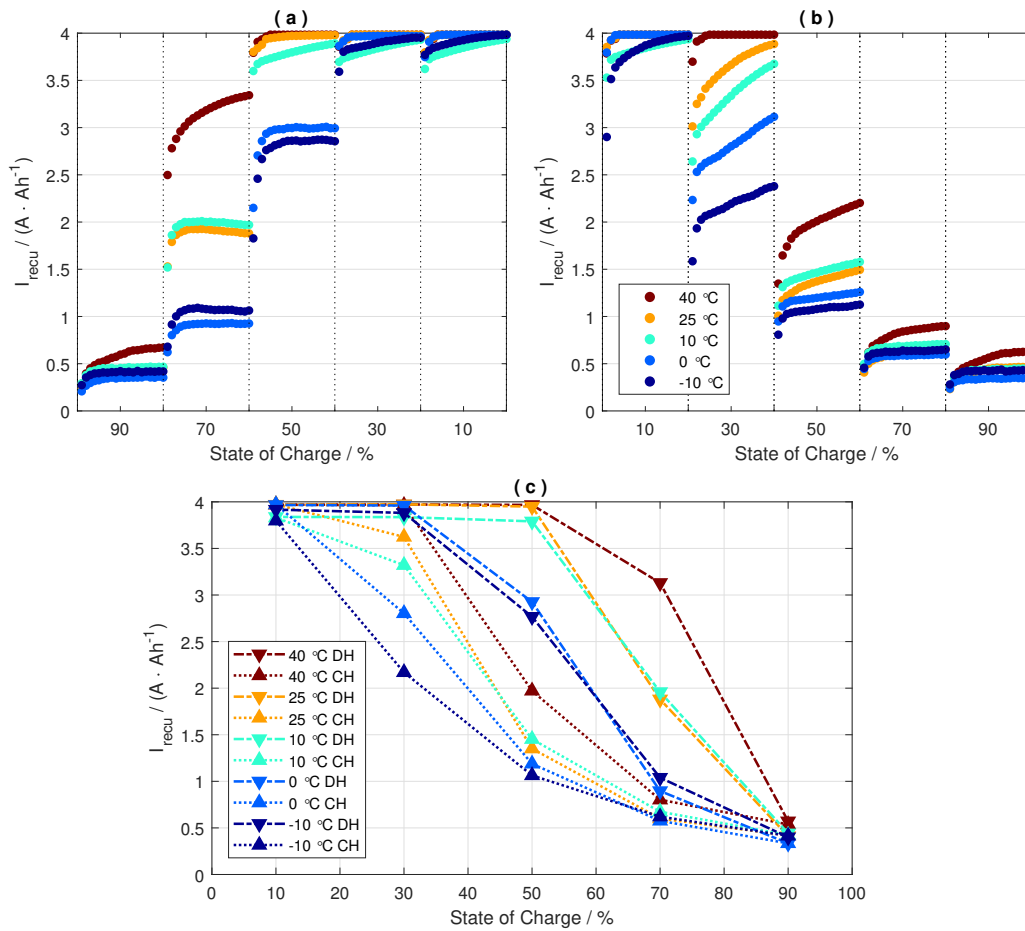


Figure 3.12: DCA Analysis Result, Variation with Temperature with 30 s Rest Period. (a) with Discharge History, (b) with Charge History, (c) Average Charge Acceptance

Prior to beginning the test procedure the cell was maintained at the desired temperature for a period of 24 hours to allow the ambient and internal temperatures to equalise. One complete test was then performed before the ambient temperature was adjusted and the cell was again allowed 24 hours to equalise. Figures 3.12a & 3.12b show the results of this testing, which, for brevity, was conducted using only the standard rest period of 30 s.

The general trends in the shape of the charge acceptance throughout the DCAPP and the effects of history are again present and much as previously identified; the major point of interest here is the significant worsening of DCA

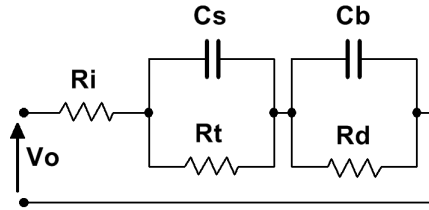


Figure 3.13: Randles' Cell Equivalent Circuit

performance as temperature decreases. It is well known that the effective capacity of a battery is reduced as temperature decreases, but the DCA test should account for this effect by measuring the capacity of the battery at the beginning of the procedure and scaling the charge pulses appropriately, so this alone cannot explain the results observed.

The standard electrical model of a lead-acid cell is the Randles model [35], as given in figure 3.13, which models the cell as a pair of series connected capacitors. From the Randles model, R_d represents the self discharge resistance of the cell and R_i the resistance of the cell's internal connections. The elements of most interest in this case are C_b , C_s and R_t . C_b is the main charge storage element of the cell, whilst C_s and R_t together model the transient effects of current densities and ion concentrations on the plates of the cell. C_b is typically several orders of magnitude larger than C_s [36].

The short-duration, high-current nature of the DCA charge pulse makes it primarily a test of the surface capacitance of the cell. The DCA profile shares many similarities with a Pseudo-random Binary Sequence (PRBS) profile, which has been shown to be a good indicator to the values of the discrete components comprising the Randles model [37]. This testing also showed a significant reduction in the value of C_s as temperature is decreased. Clearly a reduction in the surface capacitance will translate into a corresponding reduction in the ability of the cell to accept charge.

The reduction in temperature will also affect the value of C_b . This is to be expected as the electrochemical processes with the battery, modelled by C_b , are governed by the Arrhenius equation [18]. This relationship, first identified by Swedish chemist Svante Arrhenius in the late 19th century relates temperature to the rate of a chemical reaction, for example, those

occurring within a cell [38]. Nowadays, this is seen as a useful generalisation for many reactions occurring around room temperature, where it is usually given that the reaction rate will double for every 10 °C increase in temperature [39, 40]. At lower temperatures the rate of reaction will be slowed, meaning the amount of charge the cell will be capable of storing in C_b during the 10 second DCA charge pulse will also be reduced [41]. Together these phenomena have the effect of significantly reducing the ability of the cell to accept charge efficiently under HRPSoC conditions as temperature decreases.

Considering the average charge acceptance, figure 3.12c reveals that the hysteresis-like behaviour is again present, but the effect of temperature is far more pronounced than that of the rest period, and has the effect of shifting the entire curve downward as temperature decreases. The result of this downward-shift is that at lower temperatures, the results with discharge history begin to look very similar to those for charge history at higher temperatures. This suggests that the effects of charge history may be considered analogous to those of temperature, with the difference in performance between charge and discharge history being roughly equivalent to the difference in performance associated with a 50 °C change in temperature for these cells. This may be observed by comparing the results at 0 or -10 °C with discharge history to those at 40 °C with charge history.

3.5 Comparison with Standard Lead-Acid

The test methodology described above has been shown to yield informative results regarding the DCA performance of carbon-enhanced lead-acid cells across a range of conditions. The addition of carbon to the cell, specifically the negative plate, has the effect of producing a capacitor-like action, which has been shown to significantly improve charge acceptance under HRPSoC conditions [13]. To quantify this level of improvement and to confirm the validity of the test procedure described above, the methodology has been extended to investigate the performance of standard lead-acid cells under the same conditions. This testing phase used standard lead 2 V, 2.5 Ah, EnerSys ‘Cyclon’ VRLA cells (figure 3.14), which were brand new and unused at the



Figure 3.14: 2 V, 2.5 Ah, EnerSys ‘Cyclon’ VRLA Cell

time of testing.

The results of the analysis for standard lead-acid are shown in figure 3.15. As would be expected, they share many similarities with the carbon-enhanced cells given their similar chemical composition, some differences are nevertheless apparent. The most obvious of these is in the effect of history, this is much more equal for both discharge and charge history, also the trends within each DCAPP exhibit much the same shape (both 30 & 3 s rests being steeper than 300 s) regardless of charge history. It can also be seen that the variation in DCA performance with respect to SoC is more linear for the standard lead than that of the carbon-enhanced cells. As previously observed DCA is improved with reduced rest periods.

Whilst this more uniform behaviour would at first seem to be advantageous, as it makes the charge acceptance more predictable and reliable, it may be seen that this uniformity comes at the expense of DCA performance when the cell has discharge history. Figure 3.15d shows the average charge acceptance performance of the cells tested against that of the carbon-enhanced cells previously examined, with $\Delta I_{recu} > 0$ indicating a better performance for standard lead. From this it can be seen that for equivalent SoC, with discharge history the DCA performance of standard lead is much poorer than those cells with carbon enhancement, whilst for charge history the improvements are only negligible.

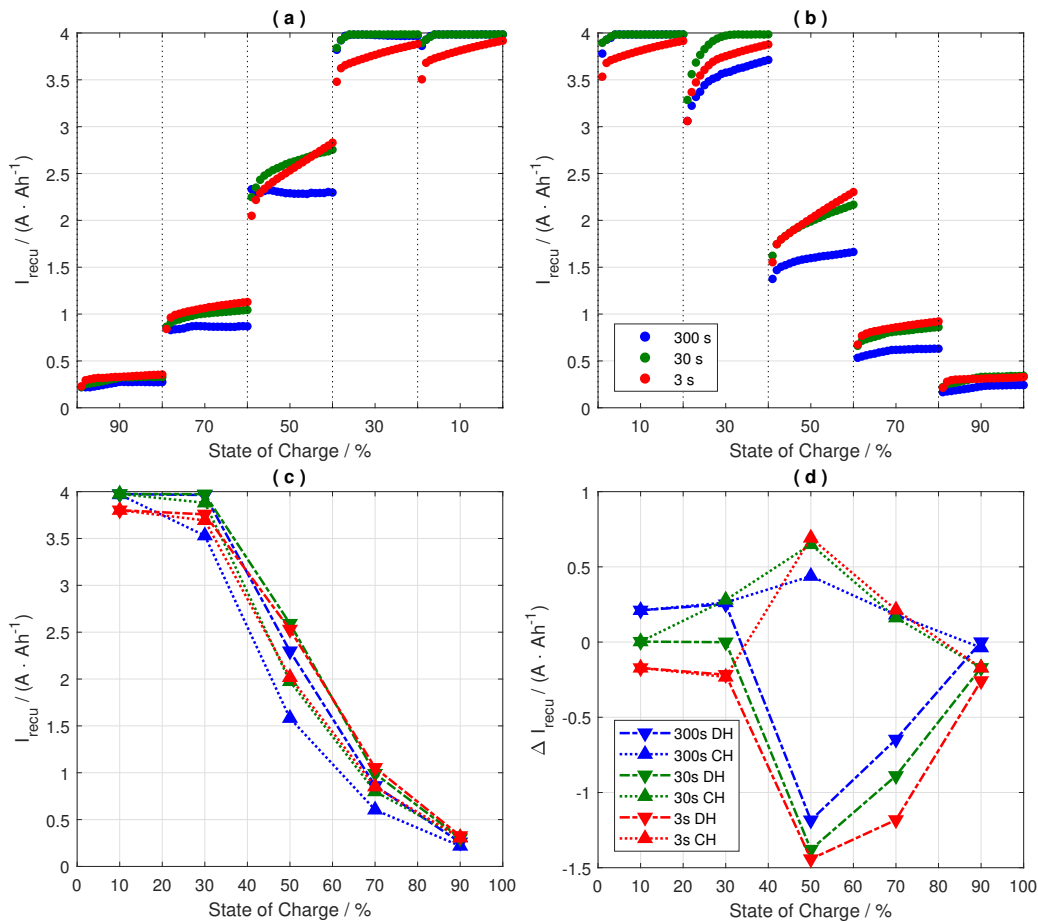


Figure 3.15: DCA Analysis Result for 2 V, 2.5 Ah Standard VRLA cell, 25 °C. (a) with Discharge History, (b) with Charge History, (c) Average Charge Acceptance, (d) Difference in Average Charge Acceptance between Carbon-Enhanced and Standard Lead

3.6 Extended Testing

After the completion of the initial testing with the carbon-enhanced lead-acid cells, and the validation of the results against standard lead-acid, an additional series of tests were performed to further analyse some interesting features noticed in the results. All these tests were performed using the carbon-enhanced Banner cells.

The first feature of interest is the DCA performance of the cells with higher recuperation currents. The testing thus far had been limited to

4.00 A·Ah⁻¹ to avoid excessive stress on the cells, however as with the standard A3 test, this places an artificial limit on the maximum charge acceptance and thus leaves uncertainty over the true capabilities of the cells. To definitively determine this, the tests were repeated with a much increased current limit.

The second area of interest was the effect of the rest period on the DCA performance within the DCAPP, this is most evident in figure 3.11a from the results at 70 % SoC. Here it can be seen that DCA performance increases slightly across the DCAPP in the case of the 3 s rest test, whilst it remains broadly flat for the test with 30 s rest, and decreases significantly with 300 s rest. This would seem to be a critical point in terms of SoC where the DCA performance is highly dependent on the rest period, however the 20 microcycles of the standard DCAPP are insufficient to draw any solid conclusions, therefore an additional test series was performed with a much increased DCAPP length.

3.6.1 High Current Testing

The initial testing was performed with a charge current limit of 4.00 A·Ah⁻¹, this had the effect of artificially limiting the maximum charge acceptance to this level. To fully understand the performance of the cells, the tests have been repeated with the maximum charge current increased to 12.00 A·Ah⁻¹, this limit has been chosen as it is the maximum capability of the test equipment. By increasing the limit it is possible to reveal the maximum charge the cells are capable of accepting across the whole range of test parameters. This gives a truer picture of the performance the cells under the typical HRPSoC conditions they are likely to experience in HEV applications.

In this case the testing has examined the effects of rest period and temperature. Whilst all three rest periods have been examined, for the sake of brevity, only three temperatures were assessed, these being 40, 25 & 0 °C, which cover both the A3 standard temperature, and two alternative extremes. The results of this testing are shown by figure 3.16.

These results show broadly similar trends to those previously observed,

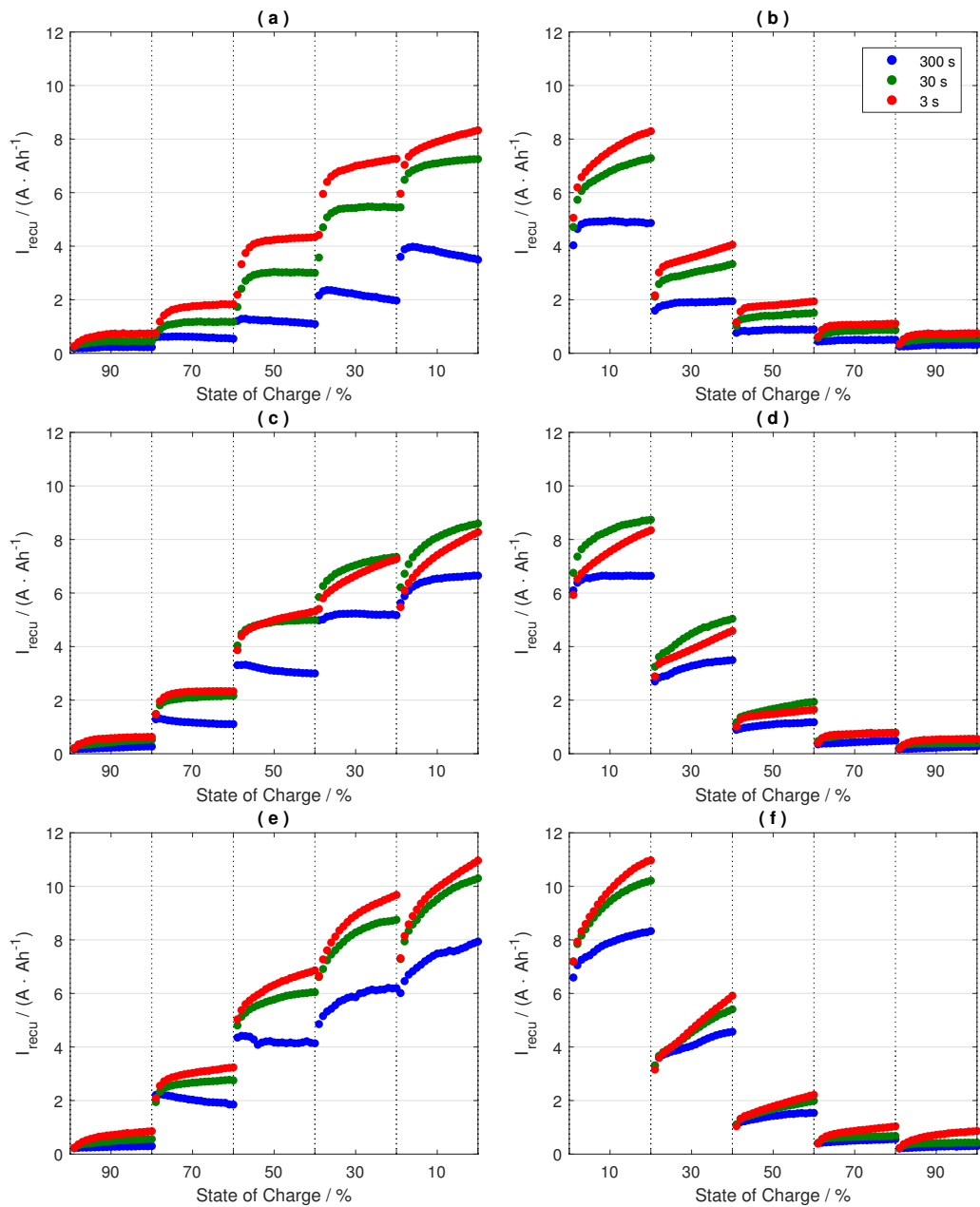


Figure 3.16: DCA Analysis Result, Increased Current Limit. (a) 0 °C with Discharge History, (b) 0 °C with Charge History, (c) 25 °C with Discharge History, (d) 25 °C with Charge History, (e) 40 °C with Discharge History, (f) 40 °C with Charge History

namely that increased temperature results in improved DCA performance. Also observed in this case is that the rate of increase in charge acceptance

during each DCAPP is greater at higher temperatures, this is most pronounced with long rest periods. It may be seen from figures 3.16a & 3.16b at 0 °C, for the tests with 300 s rests, the DCA performance generally falls during the DCAPP, this is in contrast to that of figures 3.16e & 3.16f at 40 °C where at 300 s rests the DCA is generally flat or rising.

These results finally show the true capability of these cells, with charge acceptance no longer being limited by the test procedure. From this it may be seen that at the standard temperature of 25 °C charge acceptance exceeds 4 A·Ah⁻¹ at 50 % and 30 % SoC with discharge and charge history respectively; and goes on to reach a maximum of around 7 – 8 A·Ah⁻¹ at very low SoC. At the higher temperature of 40 °C charge acceptance improves still further to a maximum around 10 A·Ah⁻¹.

An interesting observation is the effect of rest period at 25 °C. In this instance it would appear that there is little difference between 30 s and 3 s, and indeed at low SoC levels, a 30 s rest period results in the best charge acceptance. This result is in contrast to all previous testing which has shown consistently that a shorter rest period produces better charge acceptance in all cases. This is indeed true for the other temperatures examined in this testing phase.

To confirm the behaviour observed at 25 °C, the test was repeated on a second cell, the results of which agree with the original test at this temperature, indicating the results are valid, although the reasons for this anomaly remain unclear. What it does demonstrate, however, is the critical dependence of charge acceptance performance on environmental factors and test conditions.

3.6.2 Extended Microcycle Testing

A second area of interest is the DCA performance of the cells during the DCAPP period. Analysis of the tests already performed shows that this is not constant across the period, rather DCA is seen to either increase or decrease as the DCAPP proceeds, apparently dependent on the rest period within. This behaviour has only been noted due to the presentation of DCA

results on a per-microcycle basis, the standard A3 test only requires that they be reported as the average charge acceptance across the whole DCAPP period, thus obscuring any changes which may occur during that time.

To investigate this phenomenon, a new test procedure has been designed with the length of the DCAPP increased. A series of tests have been performed using this procedure, the results of which appear highly promising. It has been shown that even with the longer period, DCA performance shows significant variation, also the way the results are presented is key to revealing the underlying performance. Initially testing took place using a modified DCAPP consisting of 100 microcycles. This was performed with the cell at 70% SoC and with both discharge and charge history.

Figure 3.17a shows the analysis result when plotted against microcycle number. From this it appears as if the DCA for all rest periods has essentially stabilised by the end of the 100 pulses, this seems to be true for both charge and discharge history. However it is clear to see from Figure 3.17b, which shows the same data, but plotted against time, that this is far from true. In fact only the result at 300 s has stabilised, the others continue to show change. Of particular interest are the results with discharge history, here the trend seems to show that the DCA follows a similar profile for all rest periods, but is shifted up with reduced rest time. For cells with charge history it is obvious that those with 3 s and 30 s rest periods have not stabilised, also they do not appear to be following a common trend; certainly, at least, not in the way those with discharge history do.

In light of these results the test was modified such that the DCAPP was applied for a specified period of time, regardless of rest period. In this case the test was run for 60,000 seconds (16.67 hours), which gives around 100 cycles with 300 s rest period, thus allowing for a comparison with the previous test results. The result of this test is given in Figure 3.17c.

Considering first the results when the cell has charge history, this agrees with that previously observed, in that the responses diverge quite significantly with the two shortest rest periods increasing rapidly. It can also be seen that the increase leads to a convergence between the charge and discharge histories, although even after a significant period of cycling, the two

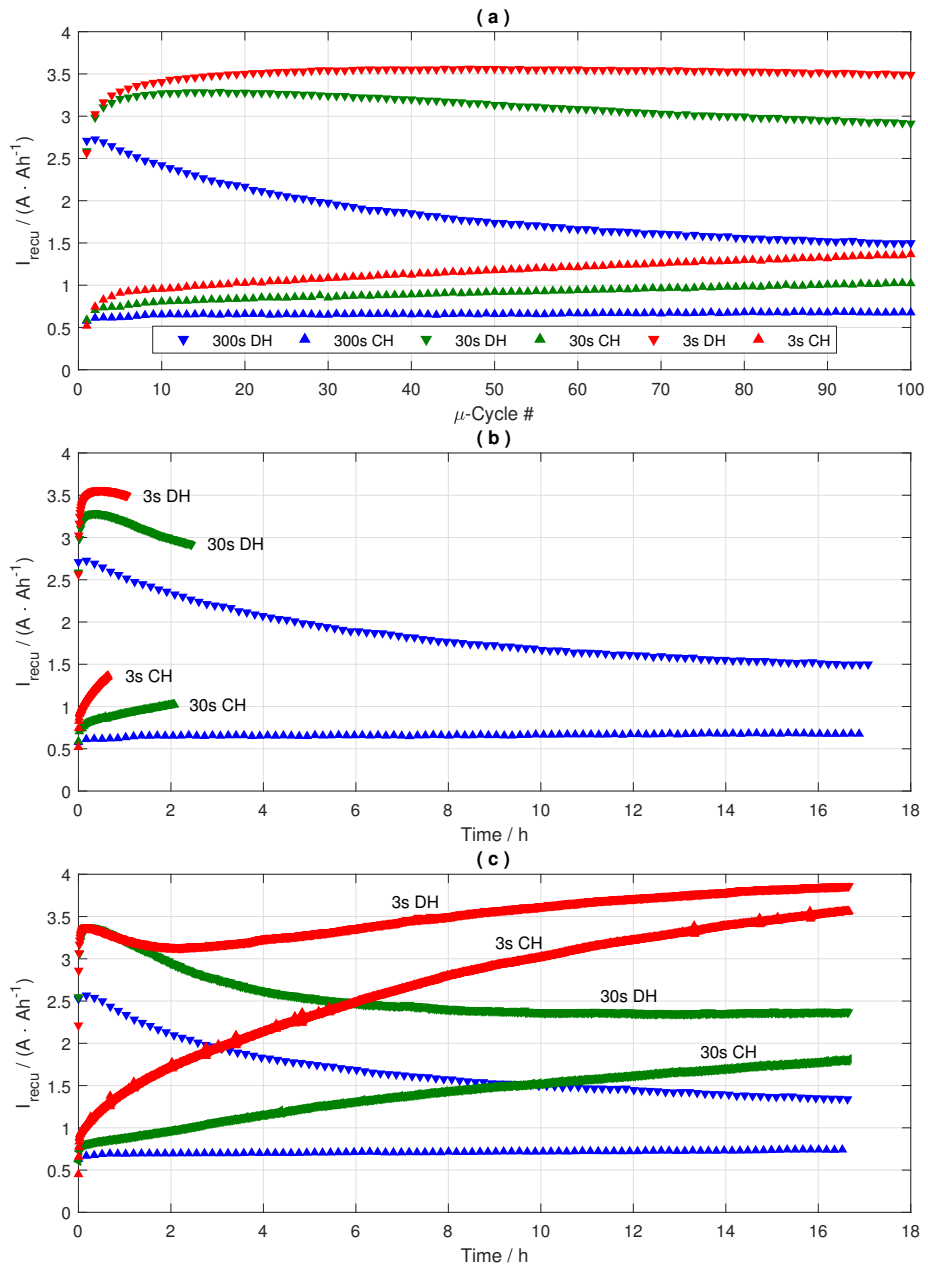


Figure 3.17: DCA Analysis Result, Extended DCAPP at 70 % SoC and 25 °C. (a) against Microcycle #, (b) against Test Time, (c) Test with Constant Time

never actually meet. This convergence is also observed with the 300 s rest period, although in this case the result with discharge history reduces to meet

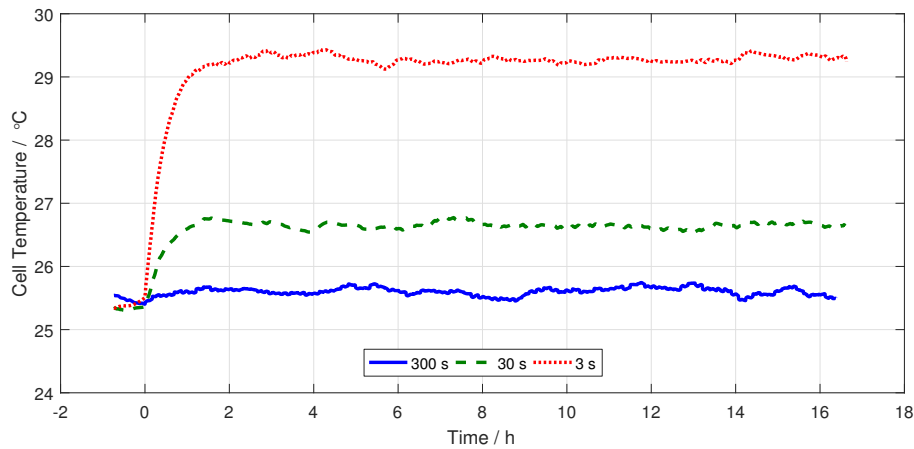


Figure 3.18: Cell Surface Temperature for Extended DCAPP test, with Discharge History

that with charge history. Again, the two never meet.

The picture for discharge history is slightly more complex. Initially the results appear to follow those previously observed, with all three rest periods displaying a similar shape, shifted along the y-axis. This remains true for the 300 & 30 s rest periods, which correlate well across the test period. For 3 s rest however, the trend diverges quite significantly from around the 2-hour mark onwards. This divergence is possibly attributable to the increase in cell temperature due to the much higher energy throughput associated with the shortest rest period. As has been previously shown, DCA is partially dependent on temperature, so the effect of this increase must be considered when analysing these results.

Figure 3.18 shows the temperature measured on the surface of the cell for the duration of the tests conducted with discharge history. It may be seen that during 3 s rest section of the test procedure, the cell temperature rose by around 4 °C. The maxima of this rise occurs around 2 hours after the start of the test, at a similar time to when the divergence in DCA performance becomes significant. This may be compared to the temperature increase of around 1 °C seen for the equivalent test with 30 s and the negligible increase with 300 s rest periods.

3.7 Conclusions

Following the testing of carbon-enhanced lead-acid cells carried out over a range of SoC, rest periods and temperatures there is clear correlation between DCA and both SoC and temperature. DCA is improved at higher temperatures and at lower SoC, furthermore there is some evidence to suggest the cells may exhibit a ‘memory effect’ leading to improved DCA following a period of discharging. It has also been shown that the rest period used within the test regime affects the DCA response of the cells, in all cases reducing the rest period improves charge acceptance. These trends have also been shown to be present in standard lead-acid cells without carbon additives, whilst carbon-enhancement is seen to improve DCA performance when the cell has discharge history.

Secondly the work shows that to select a battery based on DCA performance it is important to consider the range of SoC over which the battery will be operated — picking a narrow SoC window to base results on risks missing important changes in performance as SoC varies, which could lead to sub-optimal performance in certain conditions. A second issue to consider is the magnitude of the recuperation current, especially at low SoC. Even increasing the current to $4 \text{ A}\cdot\text{Ah}^{-1}$, far in excess of the A3 standard of $1.67 \text{ A}\cdot\text{Ah}^{-1}$ does not reveal the full capabilities of carbon-enhanced lead cells, which reach $4 \text{ A}\cdot\text{Ah}^{-1}$ at around 50% SoC and will accept recuperation currents of $6 - 8 \text{ A}\cdot\text{Ah}^{-1}$ at lower SoC.

These tests also show that DCA is not a static parameter, fundamental to the cell. Rather it is critically dependent on environmental conditions, the history of operations performed on the cell and the electrochemical balance within the cell at any given time. In order to properly understand DCA performance a more thorough test procedure is required than that provided by the A3 Test, one that examines the charge acceptance at various SoC and accounts for the effects of history.

Chapter 4

Analysis of the Effects of Cell Degradation on DCA in Lead-Acid Cells

4.1 Introduction

A major problem often cited with the use of lead-acid batteries in HEV applications is their apparently poor DCA performance. The previous chapter has demonstrated that the standard test for determining DCA performance has several shortcomings, and does not fully represent the conditions found in real-world situations. This indicates that the performance of lead-acid batteries in HEV applications is likely to be better than predicted by the standard testing methodology.

4.1.1 Lead-acid Cycle Life

A second criticism frequently made regarding the use of lead-acid cells in automotive applications is their poor cycle life when compared with lithium-based chemistries. Whilst this initially seems to be a reasonable argument, and it is certainly true that a lithium cell will exhibit longer cycle life than lead under the same conditions, there are other factors to be considered in the HEV scenario which make such an argument less sound. Firstly, the

batteries in a HEV are subjected to relatively few cycles, certainly fewer than those in a full EV. Secondly the ability of the HEV to charge its battery from the IC engine means that operation at very low SoC, which is known to cause high levels of degradation, particularly in lead-acid cells, can be avoided. Furthermore, as illustrated by the previous chapter, cycle life is not the primary consideration for HEV batteries, rather it is their performance under HRPSoC conditions and DCA which are the key features.

These factors combine to suggest that the shorter cycle life of lead-acid cells may not be as much of a drawback as might first be expected; particularly when the relative costs, both of initial purchase and end of life recycling, of the use of lead vs lithium are considered. That said, however, there has been little work published on the effects of cell degradation on DCA performance, and thus an investigation has been performed to determine how DCA is affected by cell degradation.

This is important not only for the automotive sector, but beyond that there are numerous applications where batteries are used as buffers to absorb short high-power transients similar to those seen in HEV applications. Typically these are large grid-connected storage systems, however some applications such as wind or solar PV energy storage are candidates for smaller domestic applications, and many may be able to take advantage of second-life EV and HEV batteries [29, 42].

4.1.2 DCA and Battery Degradation

Battery degradation is inevitable. Degradation occurs even if the battery is simply stored, unused; this is known as calendar ageing, and in lead-acid batteries is primarily due to corrosion of the positive plate [43]. This process is slow however, and does not usually contribute significantly to overall degradation, far higher levels of degradation are unavoidably caused by using a battery. This results from several factors, in lead-acid batteries it is primarily due to sulphation and corrosion of the plates [43]; lithium-based batteries also suffer with lithium plating of the negative electrode and oxidation within the cell [44].

Regardless of the cell chemistry or source, degradation manifests itself in three main ways: reduction in capacity, increase in internal resistance and increase in self-discharge. Of these effects, capacity loss is the simplest to diagnose, this being possible on-line using coulomb-counting [45]. Capacity loss is also the most obvious symptom of degradation to the user, where it is seen as a reduction in run-time and the resultant need for more frequent recharging, therefore capacity loss alone is commonly used as a measure of battery degradation, where it is referred to as the State of Health (SoH) of the cell, which is generally defined as [44, 46, 47]:

$$\text{SoH} (t) = \frac{C_t}{C_{nom}} (\%) \quad (4.1)$$

where C_t is the measured capacity at time t and C_{nom} is the nominal capacity of the cell. This change in capacity with degradation presents a problem when considering DCA performance of a cell, as there are now two variables at work. Firstly there is the actual loss in performance due to degradation, but there is also the influence of the test procedure itself.

The DCA test in its standard form, as described in Chapter 3, normalises all currents to the measured capacity of the battery, C_{exp} , thus giving I_{recu} units of $\text{A}\cdot\text{Ah}^{-1}$. This is desirable and necessary when comparing the relative performance of different batteries as it compensates for the effect of differing battery capacities, but has the potential to present a problem when assessing the change in DCA performance over time of batteries which have degraded. As a degraded battery will have a lower capacity, the standard DCA test will apply a lower current during the testing phase. This effectively makes the test easier which may mask the true effects of the degradation. In reality, of course, the demands placed on the battery will not be reduced simply because it has degraded, therefore this should be accounted for when assessing a battery's DCA performance.

4.2 Test Procedure

To determine the effects of degradation on DCA performance, and to assess the effect the DCA test itself has on the results, a test procedure has been developed. This procedure consists of two main components, the DCA testing phase, to assess charge acceptance performance and the cycling phase to stimulate controlled degradation of the cells.

Within a battery there will be differences in the individual cell performance and rates of degradation. These differences, and their effect on overall battery performance, are often hard to determine due to the impossibility of accessing the individual cells to perform measurements. To overcome this, single cells have been used for this study; these were of the standard lead-acid EnerSys Cyclon 2 V, VRLA type, with a nominal capacity, C_{nom} , of 2.5 Ah as used in the previous investigation, and were all new and unused.

4.2.1 DCA Testing

The previous work, described in Chapter 3 has shown that the standard A3 DCA test as outlined in [14] has some shortcomings when measuring performance under HRPSoC conditions. The chief concerns are that it only measures DCA performance in a narrow SoC window and makes the assessment of the influence of history difficult to assess.

SoC has been shown to have a large impact on DCA performance so this must be accounted for during the test procedure, particularly where cells will be operated across a wide SoC range, such as those in HEVs. The history of a cell, that is, whether it has previously been charged or discharged, also significantly affects DCA performance. The standard DCA test attempts to account for this, but measures charge and discharge history at different SoC levels, which complicates any attempt to analyse the effects of charge history in isolation. Both of these shortcomings have been addressed by the test procedure adopted for this study; the DCA test has been performed using the SoC profile shown in figure 4.1. This is modified slightly from the method proposed in Chapter 3, the heavy discharges in the conditioning phase have been dispensed with as there is no need to assess reserve capacity

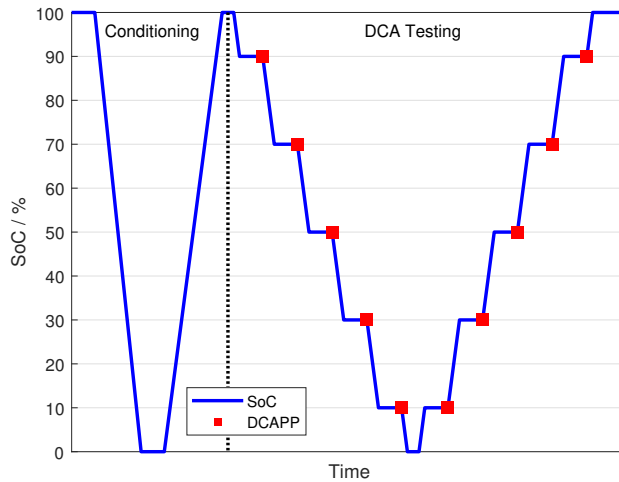


Figure 4.1: DCA Test SoC Profile & DCAPP Locations

in this test, and omitting them allows the testing to proceed more quickly and avoids additional unnecessary degradation of the cells.

Starting from 100 % SoC the cell is initially discharged to 0 % SoC, from this C_{exp} is calculated. The cell is then recharged for the beginning of the DCA testing phase. This consists of 10 distinct DCAPPs applied across the SoC range from 90 % – 10 % SoC, the first five of these assess performance when the cell has discharge history, whilst the second five consider the effect of charge history. The SoC levels are the same for both histories, allowing the effect of this to be easily compared, and cover a wide SoC range, which is typical of what may be expected in HEV applications. Upon completion of the DCA test procedure the cell is recharged to 100 % SoC in preparation for the continuation of testing. All charges and discharges (except those within the DCAPP) are performed at 0.5 A ($0.2 C_{nom}$ A) and all rest periods are of 1 hour in length.

The charge current applied by the standard A3 test within the DCAPP is only $1.67 C_{exp}$ A, this is far less than the actual currents seen in many HRPSoC applications, particularly in HEVs [6]. It has been shown in Chapter 3 that increasing this current to $4 C_{exp}$ A yields results which better represent the real-world performance of cells. This change is reflected in the microcycle current profile given in figure 4.2, and is the profile used for this

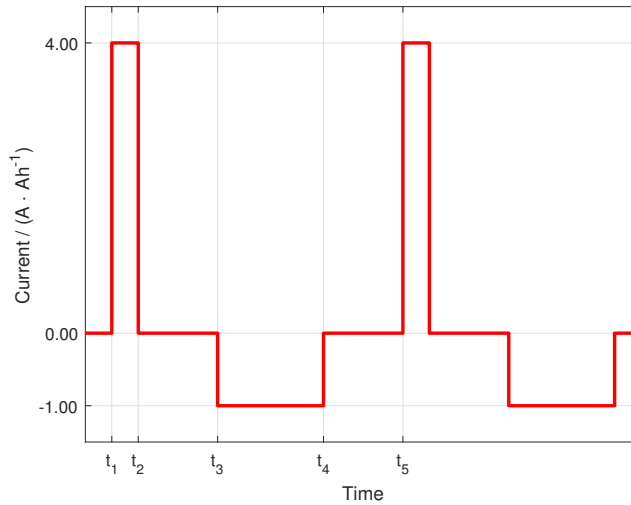


Figure 4.2: DCA Test Microcycle Current Profile ($t_1 - t_5$)

investigation.

The other concern here is the normalisation itself; as discussed above the choice of normalising value may have a significant influence on the apparent DCA performance of the cell. To assess this, two variants of the test procedure were performed, the first with currents normalised to $4 C_{exp}$, resulting in a charge current which varies with capacity throughout the testing period. For the second, normalisation was to $4 C_{nom}$, in this case there was no change in applied DCAPP current as the cell degraded.

4.2.2 Cycling

The second phase of the test procedure was that of cycling to degrade the cells. The objective was to cause an accelerated ageing process to occur, thereby degrading the cell more quickly than would be the case in reality, whilst at the same time maintaining the relevance to real-world scenarios by ensuring that the method of degradation was the same. To this end a procedure was developed to subject the cell under test to 24 cycles at a rate of $1 C_{nom}$ A, with a SoC range from 100 % – 20 %, and a 1-hour rest period between discharging and charging.

This cycle profile is not intended to represent the duty a cell would be

subjected to in real-world HRPSoC conditions, rather it is designed to cause the cell to degrade in a timely manner whilst avoiding the very low SoC regions where a real-world system would not be operated. Operation at very low SoC causes additional stresses on the cell and is likely to lead to forms of degradation which would not be seen in real-world applications.

Defining an end of discharge SoC of 20 % is simple, achieving this in practice is rather more involved, however. Clearly it would not be possible to use the method described in Chapter 3, as determining C_{exp} requires discharging the cell to 0 % SoC, thus defeating the whole purpose of the exercise. Nor would it be possible to determine C_{exp} periodically, as the capacity of the cell will change with each passing cycle as its SoH degrades. What is required is a limit which can be determined in advance, and which remains constant regardless of cell degradation; fortunately, such a metric exists: the cell voltage.

It is possible to determine the relationship between SoC and voltage simply by performing a single discharge test, although in practice the average of several tests is used to compensate for minor variations in performance between cycles. The process is simple, during the discharge both the cell voltage and capacity are measured, capacity is converted to SoC by linearly scaling between 0 Ah being 100 % SoC and the capacity at the end of the test being 0 % SoC; SoC is plotted on the abscissa, whilst the corresponding voltage is plotted on the ordinate. From this it is simple to determine the voltage required to achieve any given SoC. The relationship between voltage and SoC for the Cyclon cells, as determined experimentally, is shown in figure 4.3.

Whilst simple and effective, to use this method properly requires understanding of its limitations. Firstly the result is only valid for the operation from which it was measured, thus the curves derived from a discharge are only valid for discharges, a second curve must be calculated for charging. Secondly, the voltage given is not the open-circuit voltage (OCV), rather it is the voltage reached at a given point in the discharge cycle, and thus it has an associated current. This results in different currents resulting in different voltages at the same SoC, this may also be seen from figure 4.3 which shows the curves for two discharge currents.

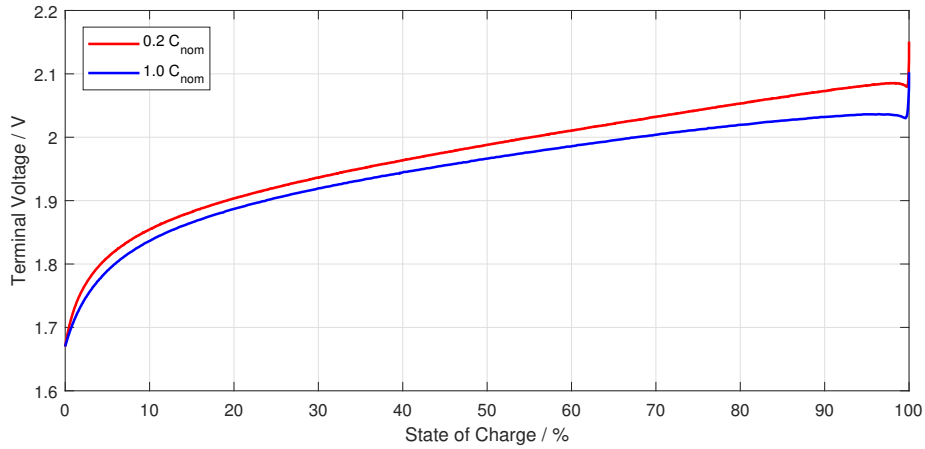


Figure 4.3: Discharge Curve for Cyclon Cells at Various Currents

This effect has two primary causes, one physical and one chemical. Firstly, the fundamental construction of any cell results in the internal connections having a non-zero impedance, thus at higher currents there will be a greater voltage-drop across these connections and therefore the voltage measured at the cell terminals will be further from that across the plates of the cell. This has the effect of shifting the curve in the y-direction, for discharge this shift will be downwards, whilst for charge it will be upward. It is this process which accounts for the initial, rapid drop in terminal voltage, and is a result of the battery reacting to the transition from open circuit conditions before the test, to the applied discharge current. Secondly, the chemistry of the cell has an effect; in this case lead-acid cells obey Peukert's Law [48], which states that at higher discharge rates the total capacity delivered will be less [49]. This has the effect of compressing the curve in x-axis at higher rates. For this test procedure, the discharge current was chosen to be $1 C_{nom}$ A, therefore 20 % SoC will be reached when the voltage falls to 1.89 V and discharging should be terminated at this point.

The complete test procedure began with an initial DCA test to establish baseline values for charge acceptance and C_{exp} , this was then followed by repeated applications of the Cycling and DCA testing phases. The initial discharge within the DCA test making for an effective 25 cycles between each analysis of DCA performance. The testing was continued until 200 cy-

cles had been completed in total, and was conducted using a Maccor Series 4000 test unit. As was the case for previous testing, the cells were tested in an environmentally-controlled chamber with the ambient temperature maintained at $25\text{ }^{\circ}\text{C} \pm 2\text{ }^{\circ}\text{C}$ throughout.

4.3 Results & Discussion

Four cells were subjected to the test procedure described above: A, B, C & D, all of which were new and unused. Cells A & B were tested using the modified DCA test method, proposed above, with normalisation to their nominal capacity of 2.5 Ah throughout, whilst cells C & D were tested using the standard C_{exp} normalisation.

4.3.1 Degradation

Figure 4.4 shows the reduction in cell capacity throughout the test, as measured from the $0.2 C_{nom}$ A discharge prior to the DCA testing phase. All the tested cells are seen to have similar baseline capacities, which indicates they are well matched. All four are also seen to follow a similar trend of capacity loss as they age. This further suggests that they have performed equally and shows that the differing currents used during the DCA testing phase do not have any significant effect on the rate at which the cells degrade.

The results show the typical cycle life performance trend expected for lead-acid cells: initial capacity loss within the first 25 cycles was minimal, this soon increased however as the cells settled in to a trend of roughly linear degradation between cycles 25 and 150. During this period a typical loss of 0.4 % per cycle, or around 10 % between every 25-cycle capacity measurement, was observed. As the deterioration reached more severe levels, however, the rate again reduced toward the end of testing. This shows that whilst the test procedure has caused the cells to degrade more quickly than would be seen in service, it has not changed the way in which this has occurred, and therefore the results can be considered representative of real-world conditions.

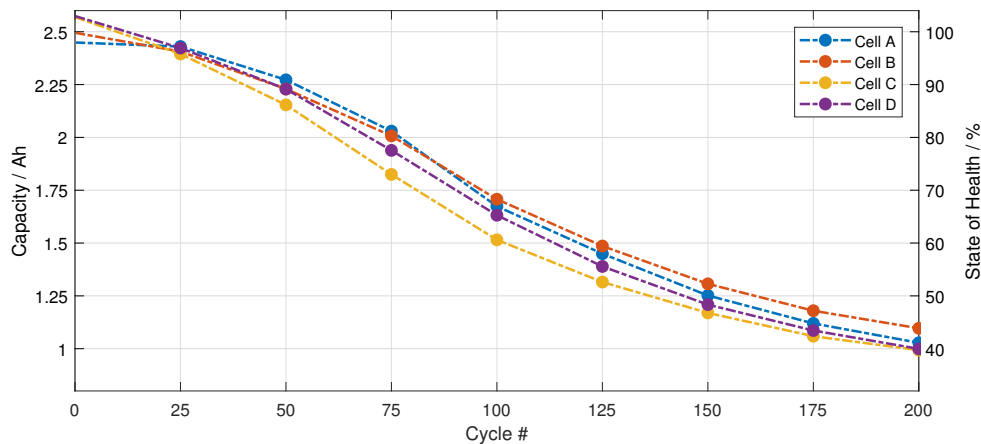


Figure 4.4: Capacity Loss with Degradation

Three of the cells took 75 cycles to degrade to around 80 % of their initial capacity, this is the point at which they would usually be considered to have reached their end-of-life condition in a HEV application, and hence can be considered as the starting condition of cells for second-life applications. The final cell (cell C) had degraded slightly quicker but still remained above 70 % capacity at this point. By the end of the test, after 200 cycles, all four cells had degraded to around 40 % of their initial capacity. This is a very severe level of degradation and it is unlikely that they would ever reach this condition without replacement in any real-world application.

4.3.2 DCA Performance

Figure 4.5 shows the DCA performance for cells C and D. Note that in order to aid comparison, all results are given in terms of absolute current, rather than being normalised to either C_{nom} or C_{exp} .

It is apparent that the results for the two cells are well correlated and the results clearly show the importance of considering multiple SoC levels and operational history when assessing DCA performance; in general terms, DCA is improved at lower SoC and when the cell has discharge history.

Considering the effects of degradation, it is clear that the results may be divided into two broad regions, depending on the performance of the cell in the baseline test (cycle 0). For SoC above 70 % and 50 % for discharge and

charge history respectively, the performance is determined by charge acceptance alone; it can be seen that under these conditions DCA performance is always below the maximum current provided by the test, therefore the charge acceptance capability of the cell is the only limiting factor. As degradation occurs, the effects of history become important, the results with discharge history (figures 4.5a & 4.5c) show performance gradually improving to reach a maxima around 75 cycles, before falling back gradually to end with no significant loss of performance after the entire 200 cycles; this despite the significant loss in capacity suffered by the cell during the same

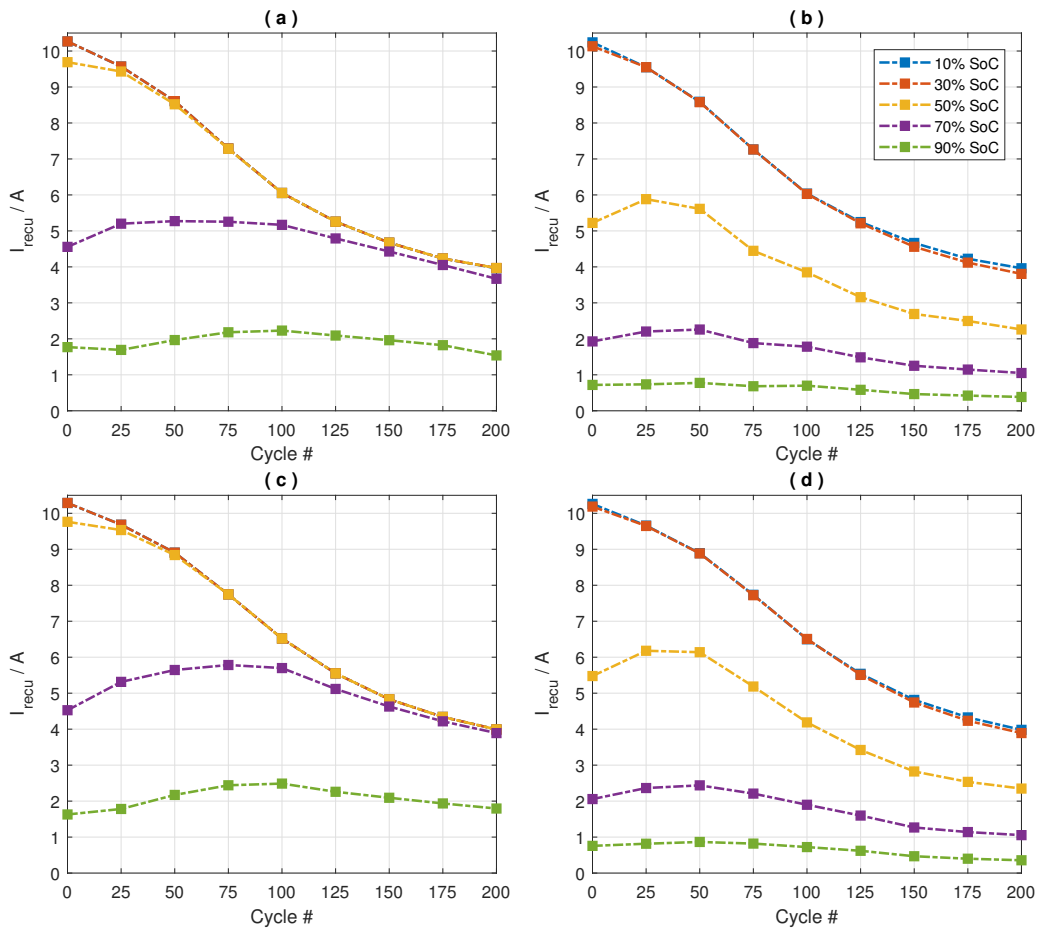


Figure 4.5: DCA Performance at Various SoC Levels with C_{exp} Normalisation. (a) Cell C with Discharge History, (b) Cell C with Charge History, (c) Cell D with Discharge History, (d) Cell D with Charge History

period. With charge history (figures 4.5b & 4.5d) the rise is again present, but is less pronounced with the maximum being reached after 50 cycles; following this however, the loss of performance is much more pronounced, with charge acceptance falling to around 50 % of the baseline performance after 200 cycles.

For the remaining SoC levels, regardless of history, DCA performance follows a consistent downward trend for the entirety of the test, this trend closely corresponds to the loss in capacity seen in figure 4.4. In this case performance is limited by the maximum current provided by the test procedure, which reduces in line with C_{exp} . From these results it is impossible to determine the actual performance of the cell at lower SoC, as it is being masked by the effects of the DCA test procedure. This clearly demonstrates the shortcomings of using the standard DCA testing methodology to characterise cells as they degrade.

Figure 4.6 shows the DCA performance for cells A and B, again there is a good correlation between the results for the two cells. It can be seen that there is a demarcation depending on SoC as before, and the DCA performance at high SoC levels is very similar to that previously observed for cells C & D. This further confirms that the results seen in these cases is due to the effects of cell degradation alone and is not being influenced by the DCA testing methodology.

At lower SoC, however, the true picture now becomes more apparent. In this case performance remains broadly constant up to the 75-cycle mark, regardless of history, this must be due to charge acceptance being limited by the DCA test itself. In this region greater charge acceptance would be possible if the charge current within the DCA test were increased. Beyond 75 cycles the performance begins to decrease across the board, this can only be as a result of the degradation of the cell as the maximum available current remained at 10 A, the same as for the baseline case.

It may be seen that history again has a significant effect on performance. As seen at higher SoC, charge acceptance reduces much more quickly when the cell has charge history. Taking 30 % SoC as an example, performance drops from 10 A at 75 cycles to around 4.5 A at 200 cycles, with charge

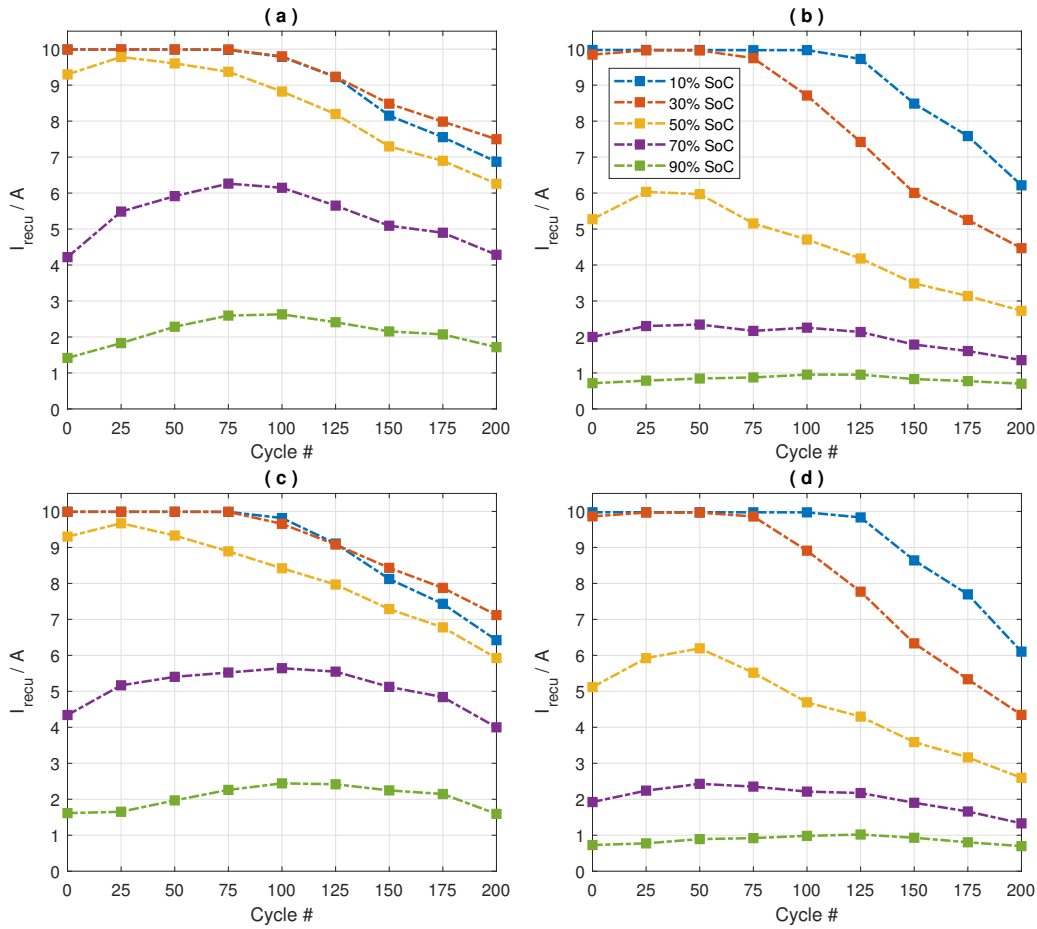


Figure 4.6: DCA Performance at Various SoC Levels with C_{nom} Normalisation. (a) Cell A with Discharge History, (b) Cell A with Charge History, (c) Cell B with Discharge History, (d) Cell B with Charge History

history; a loss of around 0.45 % per cycle. Over the same period with discharge history, performance had only fallen to around 7.5 A; a loss of 0.20 % per cycle. Again, this illustrates the importance of ensuring that the test procedure fully reflects the operating conditions of the cell if the results are to be accurate and informative.

It is also interesting to consider the results after 75 cycles. At this point the cells had degraded to 80 % of their baseline capacity, the point at which they would usually be considered too degraded to continue in HEV use. At this point however, charge acceptance performance in all cases was at least

as good as the baseline case, better, in some cases. This suggests that in situations where DCA performance is more important than absolute capacity, such as HEV applications or energy storage buffers, effective cell lifetime could be greater than would be predicted from capacity loss measurements. It also suggests that the DCA performance on-delivery of second-life batteries is likely to be little changed from the performance when they were new; although, of course, they will begin to show signs of degradation more rapidly.

4.4 Conclusions

It is apparent from this investigation that the effects of cell degradation on DCA performance are complex, and not well correlated to capacity loss alone. It is also clear that the DCA test procedure itself has a significant influence on the observed performance. Together these factors highlight the importance of ensuring that the DCA test procedure accounts for the actual operating SoC window, and maintains a constant charge current as the cell degrades if an accurate assessment of the true DCA performance is to be achieved.

In this investigation the results were achieved with the current normalised to the nominal cell capacity, but there is nothing inherently special about this value. What these results show is that to obtain a true picture of DCA performance as a cell degrades, it is crucial to use a consistent, fixed normalisation point, specific to that cell. In this case, the nominal capacity was chosen, but similarly valid results could be achieved by normalising to an experimentally determined baseline capacity, or indeed any other fixed value, if this were more convenient.

The results further suggest that reduction in capacity may not be the best indication of the end-of-life point for cells. In applications where DCA performance is more important than capacity, it is possible that the useful life of the cell may be much longer than would be suggested by capacity loss alone. This also has implications for second-life applications; in these situations, although the cell has degraded and lost capacity, its DCA performance may be very similar to that of a new cell.

Chapter 5

Analysis of the Influence of High-Frequency Ripple Currents on DCA in Lead-Acid Batteries

5.1 Introduction

Previous chapters have shown that lead-acid batteries are a viable proposition for HEVs. It has been shown that real-world DCA performance can be expected to be better than that predicted by the current standard test procedure and that degradation of the battery will not significantly lessen DCA capability across the normal SoH window for such batteries. Up until this point, however, the work has been concentrated on determining the factors which influence DCA performance and how it changes with time. This work is now extended to examine the possibility of applying an external stimulus to batteries to improve their DCA performance. The previous chapters have demonstrated that reducing the rest period within the DCAPP results in better charge acceptance; it is therefore considered if the application of a sinusoidal ac ripple current will have a similar effect, as these ripple currents will be present as a matter-of-course in any system fitted with modern swit-

ched mode converters. Continuing from the previous work, this exercise has also used lead-acid batteries as the basis for its investigation.

Whilst most efforts have focussed on DCA for automotive applications, the underlying principle has much wider applications and is important in any system where it is desirable for a battery to accept charge in a time-limited fashion. Such applications include grid-connected storage systems, particularly when operating in Enhanced Frequency Response (EFR) mode [50], and smaller scale renewable energy systems. Clearly then, a greater understanding of the factors influencing DCA performance, and methods for improving it could have broad applications across the whole energy storage sector.

Previous work by the author, and others, has identified four main factors which influence the DCA performance of batteries, and which therefore may provide scope for improving it. These factors: SoC, temperature, history and microcycling are now considered in turn.

The SoC of the battery has a very significant effect on DCA performance, with much greater levels of charge acceptance being possible at low SoC. Intuitively this makes sense as the main physical limitation on charge acceptance is the terminal voltage of the battery, a battery at a lower SoC will have a lower terminal voltage, and therefore have a greater ability to accept charge than one at a higher SoC. In practice, however, it is rarely practical to take advantage of this. Whilst it is possible to arbitrarily limit the maximum SoC of the battery to achieve better DCA performance, this results in the battery storing less energy than it is capable of. To achieve the same energy storage ability, would thus require the use of a larger battery. Clearly, in automotive applications where the size and weight of the battery pack is fundamentally limited, this approach is not desirable.

Battery temperature is also important in DCA performance, with higher temperatures promoting improved charge acceptance as seen in Chapter 3. Again this is to be expected as the underlying electrochemical reactions governing battery performance obey the Arrhenius equation [18], and thus proceed more easily at higher temperatures. Again, though, it is difficult to take advantage of this effect as the high currents to which automotive batteries are subjected cause internal heating due to losses within the battery. To

avoid excessive temperatures being reached the batteries are cooled to around $40\text{ }^{\circ}\text{C} - 50\text{ }^{\circ}\text{C}$, allowing the temperature to rise above this level would improve DCA performance, but would also risk long-term damage or sudden, catastrophic failure being caused in the process. It is also the case that this natural heating of the battery takes some time to occur. The precise time taken for this process will obviously vary depending on the ambient temperature of the battery and the level of current applied, but the fact remains that during the early part of the drive the batteries will be cold and thus unable to accept charge as well as when they have had chance to heat up.

The history of the battery, whether it has been recently charged or discharged, also has a large influence on DCA performance, Chapter 3 shows that higher charge acceptance is possible when the battery has discharge history. This effect is due to the differing electrochemical environment within the battery between charge and discharge. Clearly, there is no way to reliably take advantage of this effect, as it is impossible to predict in advance the operations which will be performed on the battery.

The final method for influencing DCA performance is microcycling, which involves repeatedly applying short charges and discharges to the battery. This has been shown experimentally in Chapter 3 to improve charge acceptance in lead-acid cells, and simulations have shown that this effect is due to the microcycling improving the homogeneity of the current distribution within the cell [8]. This allows for charge to be accepted as efficiently as possible. It has previously been identified by the above work that with microcycles consisting of square-wave like pulses, increasing the frequency of the pulse results in increased charge acceptance. This chapter presents the results of an investigation to determine if a similar result could be achieved by injecting a sinusoidal ripple current at a higher frequency, but of a lesser magnitude than that used in the previously reported testing.

This approach represents the most practical method of improving charge acceptance in real-world applications. The main benefit of microcycling is that it is essentially independent of the battery's current state, and thus can be applied at any point as required. With a balanced microcycle the amount of energy added during charge is equal to that removed during discharge,

therefore the overall SoC of the battery remains unchanged. This allows the microcycling to be applied at any SoC, without risking over-charging or -discharging the battery. Microcycling using sinusoidal currents also has the potential to be highly efficient, by using a resonant circuit to produce the ripple current, the energy used is simply cycled between the battery and the reactive components in the resonator; in this approach the total efficiency of the system is primarily governed by the charge efficiency of the battery and the efficiency of the resonator, typically both of these would be better than 95 %. Alternatively, the natural tendency of switched mode converters to produce ripple currents as a fundamental part of their operation could potentially be harnessed, thereby avoiding the need for any additional hardware.

5.2 Battery Analysis

The batteries used in this study were RS Pro 698-8091 VRLA type (figure 5.1), consisting of six cells in series, with a nominal voltage of 12 V and a rated capacity (C_{nom}) of 4 Ah. To maximise the effectiveness of the applied ripple current and to minimise losses within the battery, it is important that the frequency-dependent behaviour of the battery is understood [22–24]. Thus, before proceeding to the main testing phase, the batteries were analysed to determine their impedance response across a range of frequencies.

5.2.1 Spectroscopy

This analysis was performed using a Solartron Analytical 1260 and 1287 Electrochemical Impedance Spectroscopy (EIS) instrument, in conjunction with an environmentally controlled chamber to maintain the ambient temperature of the battery at $25\text{ }^{\circ}\text{C} \pm 2\text{ }^{\circ}\text{C}$ throughout the analysis period. This is crucial, as the impedance response is highly dependent on the temperature of the battery.

Prior to performing the analysis on each battery, it was discharged to



Figure 5.1: 12 V, 4 Ah, RS Pro VRLA Battery

70 % SoC, this is the same as that at which the DCA testing was performed (see below for details) and the battery rested. This ensures that the results of the spectroscopy are representative of the performance of the battery during the DCA test, as the frequency response will change with SoC [51]. The analysis was performed with the EIS instrument in potentiostatic mode, after discharging to 70 % SoC the cell was rested for 10 hours to determine the OCV, the test instrument then maintains this OCV potential throughout the test period. Superimposed on the OCV potential is a sinusoidal ac voltage; this causes a current to flow in the battery which is measured by the test instrument. From the applied voltage and measured current the impedance of the battery is determined by the Solartron software. This process is performed repeatedly with the frequency of the applied voltage varying, in this way a spectrum is produced giving the impedance of the battery across a range of frequencies.

For this analysis the frequency range selected was 10 mHz – 1 MHz, using a logarithmic sweep with 20 points per decade and a ripple voltage of 30 mV_{pk-pk}. This range was selected to be representative of both the low frequency components typical of the DCA test procedure as well as higher

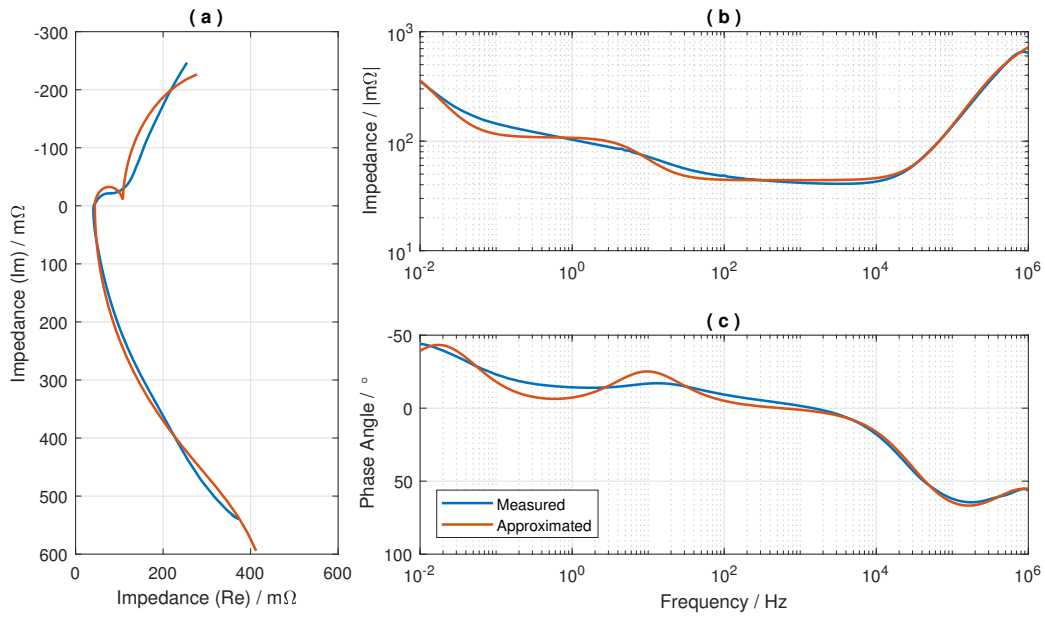


Figure 5.2: EIS Spectra. (a) Nyquist Plot, (b) Bode Plot - Magnitude Response, (c) Bode Plot - Phase Response

frequencies commonly produced by power-electronic switching devices. The range chosen also gives a wide spectrum which allows for a better understanding of the underlying performance of the battery. Figure 5.2 shows the results of the analysis, with the measured response shown in blue.

From the spectroscopy result it is clear that the behaviour of the battery can be separated into two broad regions. At low frequencies the response is capacitive, as indicated by the imaginary component of the impedance, $Im(Z)$, and the phase angle being negative. Conversely, as frequency increases $Im(Z)$ and the phase angle become positive, indicating an inductive response. The crossover frequency between these two regions occurs at around 1.5 kHz. To better understand the performance of the battery, each region was considered individually for modelling before the two models were combined to produce a full representation of the battery behaviour.

5.2.2 Modelling

A commonly used electrical model for the low-frequency behaviour of a battery is the Randles model [35], this models the battery as a pair of series connected, parallel RC circuits, as shown in figure 5.3a. Whilst improvements have been proposed to this model [36], the basic Randles circuit is well regarded and provides a simplified second-order model, suitable for this application.

The software provided with the EIS instrument (*ZPlot & ZView 2*) allows for the fitting of models to measured data. When provided with an equivalent circuit and some initial parameter estimates, the software performs an iterative fitting process to determine the component values which best approximate the measured data; i.e. the smallest weighted error between the measured and approximated frequency spectra. The results of this process for the Randles model applied to the measured frequency spectrum from 10 mHz – 1.5 kHz are given in table 5.1–A.

A high-frequency battery model is proposed by [21]. This replaces the capacitive elements of the Randles model with inductors and simplifies the

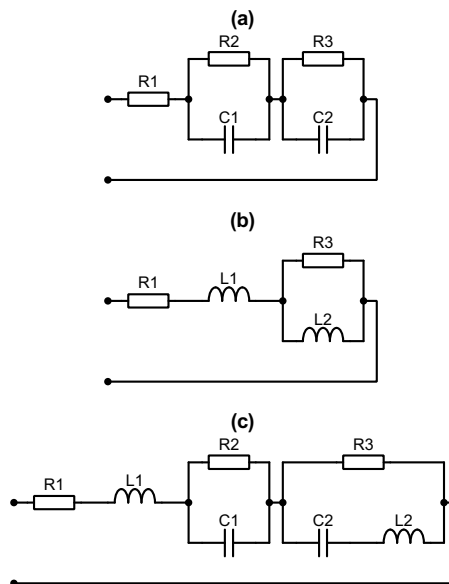


Figure 5.3: Battery Equivalent Circuit Models. (a) Randles, (b) High frequency from [21], (c) Hybrid

Table 5.1: Model Component Parameters

Component	Model		
	A	B	C
R_1	46.1 m Ω	41.1 m Ω	44.0 m Ω
R_2	63.7 m Ω	–	64.1 m Ω
R_3	530.0 m Ω	412.6 m Ω	472.0 m Ω
C_1	397.8 mF	–	398.2 mF
C_2	45.0 F	–	45.0 F
L_1	–	66.1 nH	63.5 nH
L_2	–	140.4 nH	141.8 nH

parallel branches, to better represent the electrical behaviour of the battery at higher frequencies. This model is shown in figure 5.3b, note that the components have been numbered such that those representing the same elements as in the Randles model share their numbers with those from the Randles circuit. The results of the fitting process using this high-frequency model applied to the measured frequency spectrum from 1.5 kHz – 1 MHz are given in table 5.1–B.

It may be seen that the components common to both the models described above, R_1 & R_3 , have similar values. This is a good indication that the models are describing the same system but at different frequencies, as the resistive elements should be independent of frequency. Combining both models to produce a hybrid model results in the equivalent circuit given in figure 5.3c. This is similar to previously described models [51–53], but with the reactive components replacing constant-phase elements.

Using the component values previously determined as a starting point and the whole measured frequency spectrum, the results of the fitting process for the hybrid model are given in table 5.1–C. The performance of this hybrid model to the same stimulus as the actual battery is shown in figure 5.2, in red. The similarities between the measured and approximated responses are clear and suggest that the model is a reasonable and accurate description of the behaviour of the battery. It should be noted, however, that these parameters are only valid for the conditions at which they were determined, in this case, 70 % SoC and 25 °C.

5.2.3 Ripple Frequency Selection

Aside from providing a model describing the behaviour of the battery, the spectroscopy results also allow for the selection of likely frequencies for affecting the performance of the battery. As the hybrid model includes both inductive and capacitive elements, this indicates that the battery will behave in a similar way to a resonant circuit.

As $f \rightarrow \infty$ the impedance of the inductors becomes significant and the battery impedance will be dominated by that of L_1 , this being in series with all other elements. As $f \rightarrow 0$, conversely, the capacitive elements dominate; as these are in parallel branches, the battery impedance will tend toward the sum of R_1 , R_2 and R_3 . This behaviour can clearly be seen from the measured impedance spectrum in figure 5.2b, the impedance is relatively high at low frequency; as frequency increases, the impedance falls to a minimum at around 50 Hz. It then remains broadly flat until around 10 kHz, at which point the inductance becomes significant and the impedance rises rapidly.

The main charge storage elements of the battery are modelled by the capacitors, C_2 in particular, therefore in order to affect the performance of the battery as a whole it is important that the ripple current affects these elements. At low frequencies the bulk of the current will flow in the resistances, whilst at high frequencies although C_1 will be the favoured current path through the network of C_1 & R_2 , L_2 will restrict current flow through C_2 . Therefore, to maximise the current flow through the capacitive elements, the frequency should be selected to lie in the range at which the total impedance of the battery is at a minimum.

The spectroscopy result given in figure 5.2b shows the battery impedance to be at a minimum in the range of circa 50 Hz – 10 kHz. From this broad range it is unclear which frequency would be best for influencing the battery. Simple ac circuit analysis techniques can be used to determine the current flow through any given component at a given frequency, this can then be compared to the total input current to give the proportion of any applied current which will be present in a component of interest at a specific frequency. This analysis has been performed for the circuit given by the hybrid

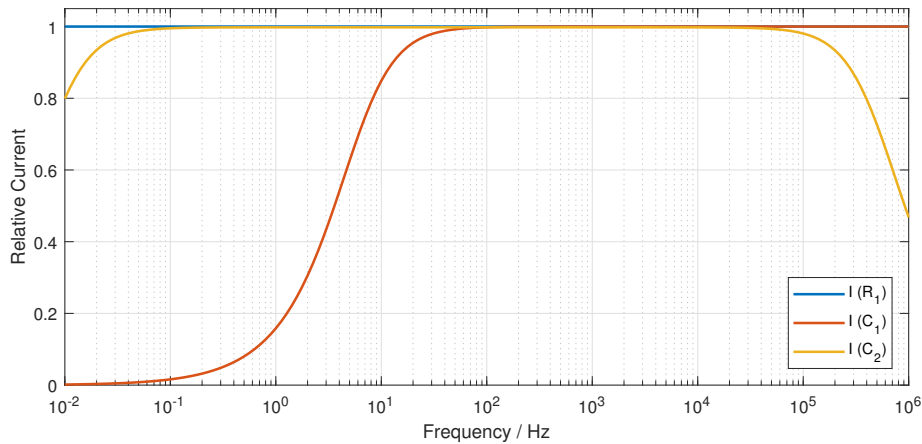


Figure 5.4: Relative Current Flow in Hybrid Model R_1 , C_1 & C_2

model from table 5.3–C, with the components of interest being R_1 , which should see all applied current across all frequencies, and C_1 & C_2 , the charge storing elements of the battery. The results of this analysis, with a frequency range of 10 mHz – 1 MHz, are given in figure 5.4.

As expected, this shows that all applied current flows through R_1 for all frequencies. For C_1 it can be seen that very little current flows in this element at low frequency, as frequency increases, however, the proportion rises until all the applied current flows through this element for frequencies greater than around 100 Hz. C_2 starts with a much greater proportion of the applied current, which soon reaches a maximum with all current flowing through it by around 100 mHz. At very high frequencies however, the effect of L_2 being in series begins to limit the current flow, with the proportion reducing as frequency increases above around 100 kHz. This analysis shows that to maximise the effectiveness of any applied ripple current, by directing as much current as possible through the charge storing elements of the battery, the ripple frequency should lie in the range of 100 Hz – 100 kHz, where both currents are at a maximum.

As with the EIS spectra, this is a broad frequency range, an alternative approach, to narrow this somewhat, is to note that R_1 & L_1 together model the impedance of the internal connections between the terminals and cells within the battery, as such they do not represent the performance of

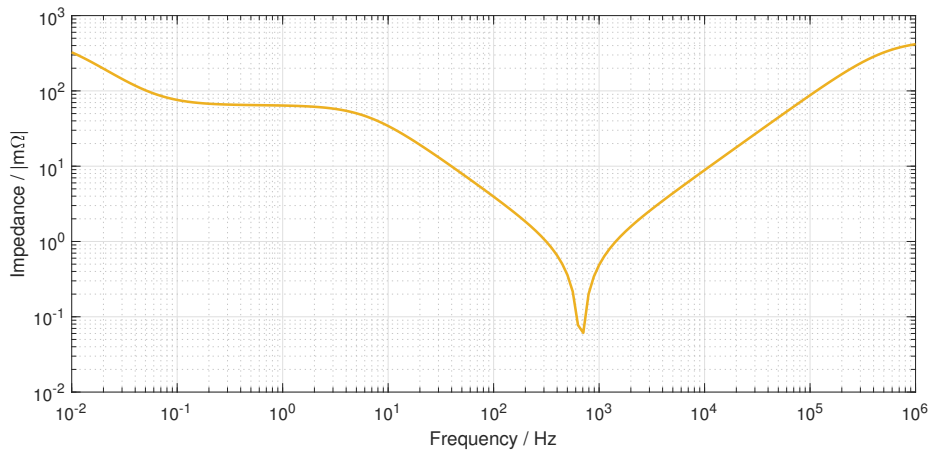


Figure 5.5: Impedance Spectrum for Hybrid Model, Neglecting R_1 & L_1

the charge storing structures. By neglecting these components a frequency spectrum for the charge storage elements alone may be produced, as shown in figure 5.5.

As can be seen, this much more closely resembles the classical resonant circuit impedance spectrum, with a clearly defined resonant frequency of around 700 Hz. This corresponds to the point of minimum impedance, and lies comfortably within the range of maximum effectiveness suggested by both the current analysis and EIS spectrum. This also represents the point of minimum battery impedance and thus the point of maximum efficiency for any applied ripple current, which has been shown to be important in maximising the benefits from the ripple current [22–24]; 700 Hz is therefore selected as the baseline frequency of the ripple current used for the testing described below.

5.3 Test Procedure

The test procedure is based on the previous work described in Chapter 3 to determine how DCA performance is influenced by the test parameters.

5.3.1 Effect of History on DCA Performance

A critical factor influencing DCA performance, as identified above, is the operational history of the battery. This refers to the operations which have been performed on the battery prior to the DCA test and may be divided into discharge history, where the battery has previously been discharged, and charge history where it was charged.

The effects of this history have been shown by Chapters 3 and 4 to be very significant, with large differences in DCA performance at the same SoC, dependent on the battery's history. It is crucial therefore that this influence be accounted for in the test procedure.

5.3.2 Test Rig

To perform the necessary testing, a custom test rig was constructed, which is shown, in overview, in figure 5.6; the full circuit schematics for this rig are given in the Appendix of this document. The rig consists of two current sources connected to the battery under test. This approach allowed for the ac ripple current to be applied independently of the dc currents used during the DCA test and to charge and discharge the battery.

The dc current source is provided by a Maccor Series 4000 battery test system, this is a commercial unit which is designed for the reliable and efficient testing of batteries. In this case the unit was configured to provide a maximum, bi-directional dc current of 20 A at up to 20 V. The system has the ability to log data during the testing process, in this case the tester was

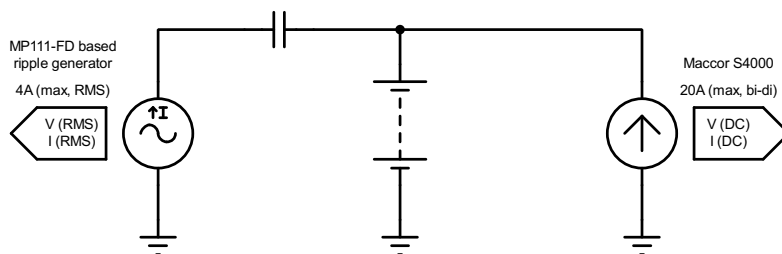


Figure 5.6: Test Rig Schematic



Figure 5.7: Ripple Generator

configured to log the dc battery current and voltage. The analogue signals were pre-filtered to remove the effects of the ac ripple before being passed to the Maccor system for logging.

To produce the necessary ac ripple current, a bespoke ripple generator was constructed (figure 5.7). This is based around the Apex Microtechnology MP111-FD Power Operational Amplifier, which was chosen for its wide power bandwidth and high current output. As constructed the generator is capable of producing ripple currents up to $4 A_{\text{rms}}$ across a frequency range from 100 Hz – 180 kHz, and contains the required circuitry to produce analogue outputs scaled to the rms values of the generated current and voltage. These signals were fed into auxiliary inputs on the Maccor system, so all logging and data storage was centralised.

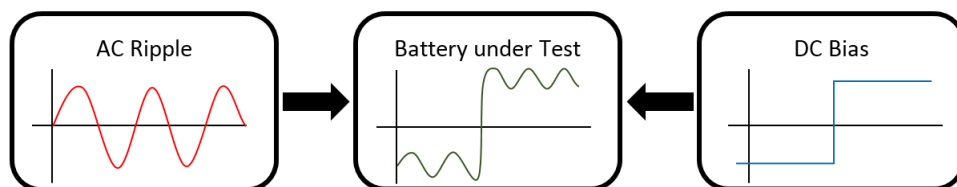


Figure 5.8: Superposition of ac and dc Components

The ac ripple current is capacitively-coupled onto the dc bias current, this eliminates the need for voltage matching between the generators and ensures the ripple current present on the battery is always superimposed on top of the existing dc voltage. This process is illustrated schematically by figure 5.8.

5.3.3 Test Description

Figure 5.9 shows the SoC profile for the test procedure. This begins with a high-rate discharge to test the reserve capacity of the battery, followed by a 1-hour rest and recharge to 100 % SoC. The battery is then discharged to 0 % SoC at the 5-hour rate, from this C_{exp} is determined. From this point the battery is then fully recharged, rested and discharged to 70 % SoC. Following another 1-hour rest the first DCAPP is performed, this testing the DCA performance when the battery has discharge history. For the duration of the DCAPP and the rest period leading up to it ($t_A - t_B$), a sinusoidal ripple current of $1.6 A_{rms}$, equivalent to $0.4 C_{nom} A_{rms}$, at 700 Hz is applied to the battery. This current level was chosen as it is high enough to influence the performance of the battery, without being unrealistically large.

The battery is then fully discharged, rested and recharged to 70 % SoC.

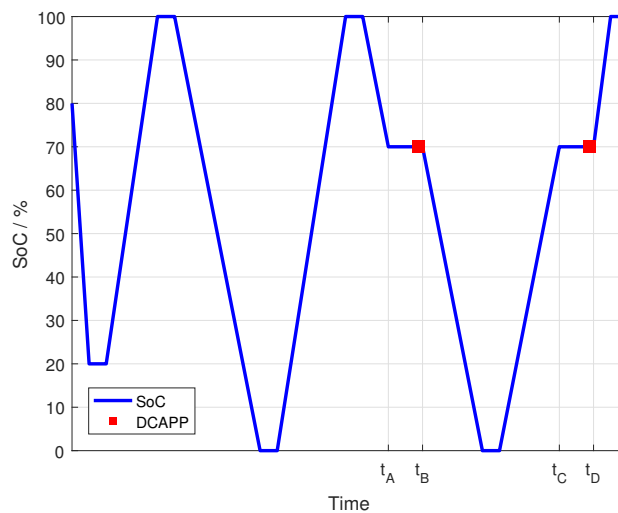


Figure 5.9: Test Procedure SoC Profile & DCAPP Locations

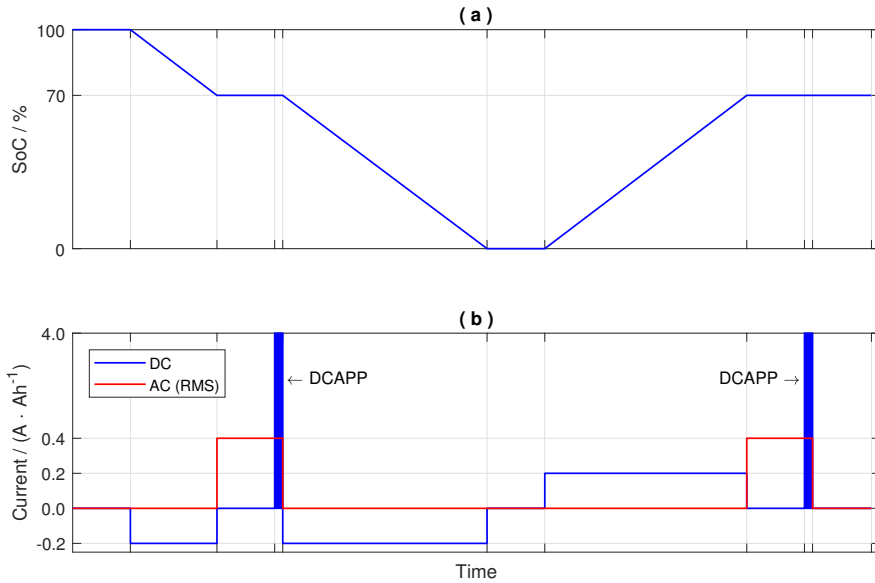


Figure 5.10: Test Procedure Details. (a) SoC Profile, (b) Applied Current Profile

Again, after resting for 1 hour a second DCAPP is performed, testing the DCA performance with charge history. As before the ripple current is applied for the duration of the DCAPP procedure and the rest preceding it, $t_C - t_D$. Figure 5.10 shows an enlargement of the time around the DCAPPs, allowing the SoC and ac and dc currents to be seen in more detail.

5.4 Results & Discussion

The initial testing focussed on the effect of ac ripple current at a frequency of 700 Hz, as identified by the battery characterisation above, later in this investigation this will be extended to include the effect of varying ripple frequencies. To establish a baseline performance, the test procedure described above was applied to the battery under test, but without any injected ripple current. The battery performance under these conditions is shown in figure 5.11, in blue. This figure shows the average charge acceptance for each of the 20 microcycles of the DCAPP, with charge and discharge history, this shows the typical DCA performance traits as previously identified.

The first and most obvious of these is the large difference in performance dependent on the operational history of the battery; with discharge history the performance is significantly better than when the battery has charge history. Secondly, the history influences the performance as the DCAPP progresses in different ways; with discharge history there is a general decrease in charge acceptance as the number of microcycles increases, whilst with charge history the performance is broadly consistent across the whole DCAPP.

5.4.1 Effects of 700 Hz Ripple

Figure 5.11 also shows the DCA performance of the battery when subjected to the full test procedure with the 1.6 A_{rms}, 700 Hz ripple current applied. It may be clearly seen from this figure that the injection of a ripple current improves the charge acceptance performance of the battery. The result shows the same traits as identified for the baseline are present, but in all cases the amount of charge accepted is greater.

This differs from the effect previously observed in Chapter 3 when the rest period within the DCAPP was reduced. In those cases whilst DCA performance was improved, the trend of charge acceptance within the DCAPP

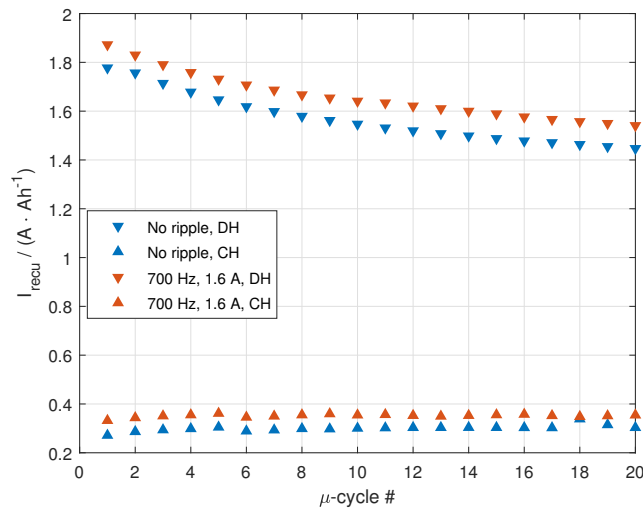


Figure 5.11: DCA Analysis Result - Effect of Injected Ripple Current

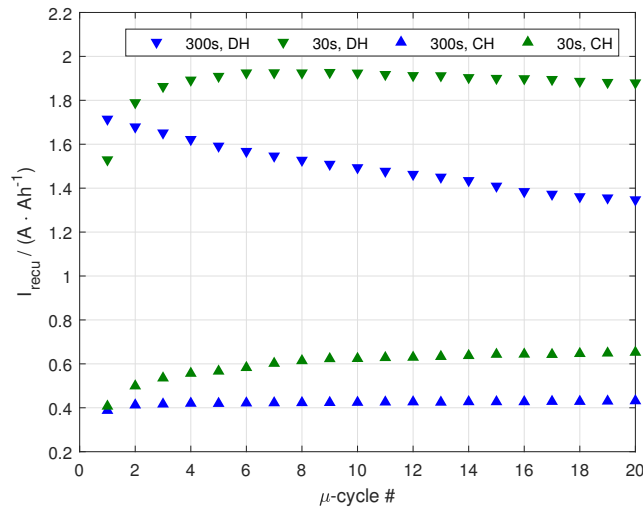


Figure 5.12: DCA Analysis Result - Effect of Reduced Rest Period

was also altered; tending to increase as the number of microcycles increased. This is illustrated by figure 5.12, which shows the effect on the DCA performance of a VRLA cell when the rest period is reduced from 300 s as used in this test, to 30 s; the data being taken from Chapter 3.

Comparing the results given in figure 5.12 with those observed from this study (figure 5.11), it may be seen that the effect produced by the injected ripple current is very different to that caused by reducing the rest period. Whilst both methods improve DCA performance, the injected ripple current does not alter the trend of charge acceptance within the DCAPP as reducing the rest period does.

The magnitude of the improvement seen is illustrated by figure 5.13, which shows the percentage increase in charge acceptance over the baseline for each microcycle. This result is of particular interest as it shows a significantly larger improvement in performance when the battery has charge history, this is important as the absolute charge acceptance is much poorer in this case, so this larger improvement will be more beneficial to the performance of the battery. For completeness, table 5.2 gives the average performance improvement for the complete DCAPP observed in this study.

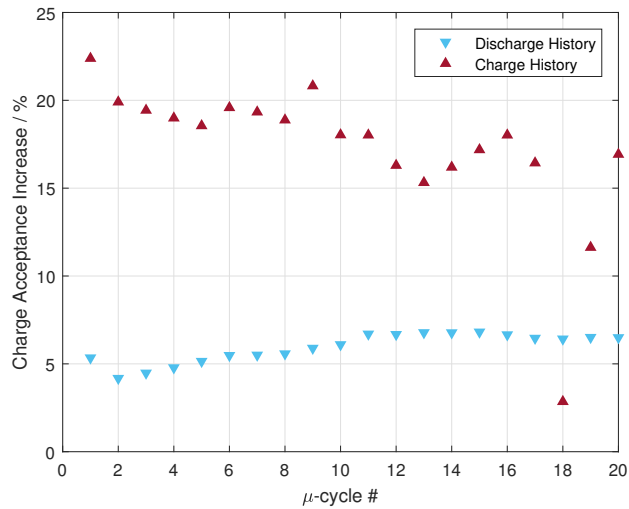


Figure 5.13: Charge Acceptance Improvement with 700 Hz Applied Ripple Current

Table 5.2: Average Charge Acceptance Improvement with 700 Hz Applied Ripple Current

History	Increase
Discharge	5.9 %
Charge	17.2 %

5.4.2 Effect of Varying Frequency

The above result shows that an injected ac ripple current can increase charge acceptance. From the previous work it was observed that increasing the frequency of the microcycles used within the DCA test also increased charge acceptance. To examine whether this trend continued with ac ripple currents, the investigation was extended to consider frequencies higher than 700 Hz. Three additional frequencies were selected, for further investigation: 4.5 kHz, 30.0 kHz and 180.0 kHz. These were selected as being evenly spaced, on a logarithmic scale, between 700 Hz and the maximum capability of the test rig; additionally they usefully bracket the most common converter frequencies as identified by [26]. It was decided not to investigate frequencies lower than 700 Hz as there would be little scope for a reduction in frequency before the limit of the test equipment was reached. Further it was determined

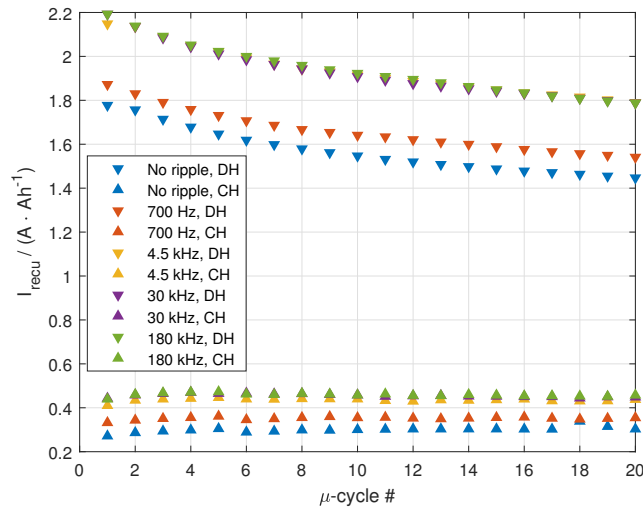


Figure 5.14: DCA Analysis Result - Effect of Injected Ripple Currents of Various Frequencies

from figures 5.4 and 5.5 that there was likely to be only minor performance differences across the available frequency range.

The test procedure described above was repeated at each of the frequencies of interest, the result of this testing is shown in figure 5.14, with the baseline result and that at 700 Hz included for completeness. From these results it is clear that moving to higher frequencies does improve charge acceptance, furthermore it can be seen that, as at 700 Hz, the trend in DCA performance throughout the DCAPP follows that of the baseline. This is important as it suggests that whilst the injected ripple current improves the battery's charge acceptance it does not significantly alter its other behaviour.

Figure 5.15 shows the average increase in charge acceptance for the whole DCAPP over the baseline, for each frequency of interest. This clearly demonstrates the benefits of increasing ripple frequency as charge acceptance improvement increases from around 6 % and 17 % with discharge and charge history respectively at 700 Hz to 24 % and 53 % at 180 kHz. It is also interesting to note that the increase is not linear, rather most gains are achieved with the initial increase from 700 Hz to 4.5 kHz. This is particularly true for discharge history, which showed virtually no additional improvement beyond this point. In the case of charge history, further improvement was observed

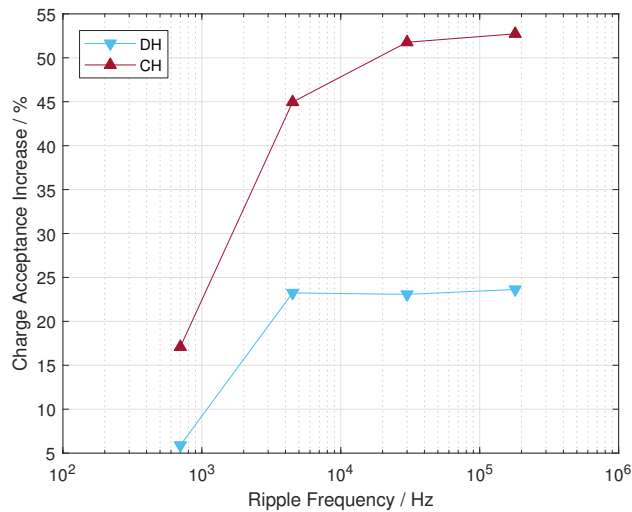


Figure 5.15: Average Charge Acceptance Improvement with Applied Ripple Currents

but at a far lesser degree than previously, and by 180 kHz this too shows virtually no increase in performance with increased ripple frequency.

Aside from the obvious charge acceptance increases, moving to higher ripple frequencies brings other benefits. Firstly, for a given power-rating the size of the reactive components required in generating the ripple current is reduced as frequency increases. This provides benefits in terms of material cost and size constraints. A secondary advantage of moving to higher frequencies is that the ripple frequency can be above 20 kHz, which is the upper limit of human hearing, by going above this frequency the ripple generator will produce no audible emissions.

Another important feature of this result is that charge acceptance is seen to improve significantly when subjected to ripple currents at frequencies typical of those generated by modern converter designs. Were it possible to harness these naturally-occurring ripple currents, it would seem possible that the DCA performance of the battery could be increased without the need for any additional ripple-generating hardware.

There are however disadvantages to higher frequency operation. As the impedance of the battery increases with frequency, generating ripple currents at higher frequencies requires more power and will increase the losses

Table 5.3: Battery Impedance and Power Requirements for Various Frequencies of Ripple Current

Frequency	Impedance	Power
700 Hz	42.25 m Ω	—
4.5 kHz	40.87 m Ω	0.97
30 kHz	60.72 m Ω	1.44
180 kHz	222.20 m Ω	5.26

within the system. This is illustrated by table 5.3 which shows the battery impedance for each frequency of interest and the relative power required to generate a ripple of a given current over that at 700 Hz.

Clearly, there is a trade-off to be made between the benefits of higher frequency ripple current in terms of charge acceptance and the disadvantages of much increased power requirements. In this case it would appear that operation around 30 kHz would provide an acceptable solution.

5.4.3 Effect of Ripple Current on SoC

A major potential drawback of the use of ripple currents of any frequency is the effect on the SoC of the battery. As the round-trip efficiency of the battery is less than 100 %, not all of the energy removed during the negative half-cycle will be returned during the positive half, even if the currents in both are equal. Whilst the net loss of charge per cycle will be negligible, over time the cumulative effect could produce a significant reduction of SoC.

Were this to be the case, it would add significant complexity to the system. Either the Battery Management System (BMS) would need to measure and account for the loss, which would require the use of high-frequency measuring equipment, adding to the cost of the BMS, or the ripple generator would need to produce a ripple current with a dc offset to compensate for the loss of SoC, again adding significant complexity and cost.

To assess the effect of injected ripple currents on SoC a second test procedure was devised. In this, a fully charged, well-rested battery was discharged to 70 % SoC. It was then allowed to rest, open-circuit, for five days whilst its OCV was logged every 10 seconds. This measured voltage profile was

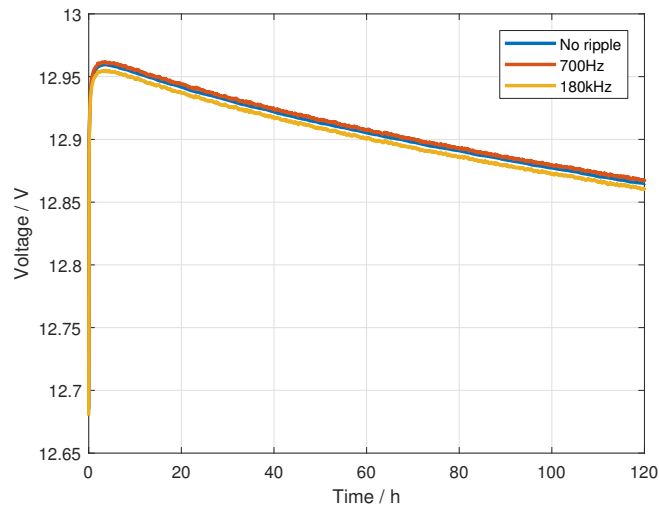


Figure 5.16: Voltage Profiles from 5-day SoC Test

used as a baseline, against which the effect of the ripple current could be assessed. The test was then repeated, but in this case as soon as 70 % SoC was reached and the dc bias current was removed, an ac ripple current was applied for five days. During this period the terminal voltage of the battery was again measured every 10 seconds. In this way, were the ripple current to have an effect on the SoC of the battery it would be shown by a deviation in the voltage profile from that of the baseline. The two extremities of the previously explored ripple frequencies were tested, 700 Hz and 180 kHz.

Figure 5.16 shows the results of this testing. From this it is clear that the presence of the ripple currents has no appreciable effect on the SoC of the battery, all three curves follow identical patterns, the only differences being due to a slight variation in the initial voltage. Table 5.4 summarises the starting and ending voltages for the test, it may be seen that there was a difference of only 1 mV between the tests with ripple current present and

Table 5.4: Battery Start, End and ΔV Voltages from 5-day SoC Test

Frequency	Start (V)	End (V)	ΔV (V)
No ripple	12.685	12.865	0.180
700 Hz	12.687	12.868	0.181
180 kHz	12.680	12.861	0.181

the baseline. This is well within the noise of the data and clearly shows that even after five days the presence of the ripple currents has not appreciably discharged, or indeed charged, the battery, and has thus not altered its OCV curve. It may therefore be inferred that the SoC has also not been changed by the presence of the ripple current.

5.4.4 Effect of Ripple Current on SoH

With the previous investigation showing the presence of ripple currents has no measurable effect on the short-term SoC of the battery, the work was extended to determine if the ripple current would cause any change in the long-term SoH of the battery. To establish a baseline result a new battery, of the same type used in the above study was subjected to a long-term cycle life test. This consisted of applying repeated charges and discharges at a current of $1 C_{nom}$ A to the battery, separated by rest periods of 2 hours. As with the degradation test described in Chapter 4, this cycling was performed between 100 % SoC and 20 % SoC. In this case the termination voltage was determined to be 11.625 V, as shown by figure 5.17. To eliminate the effects of varying temperature, this testing was again performed with the battery in a environmental chamber, maintained at an ambient temperature of $25\text{ }^{\circ}\text{C} \pm 2\text{ }^{\circ}\text{C}$ throughout.

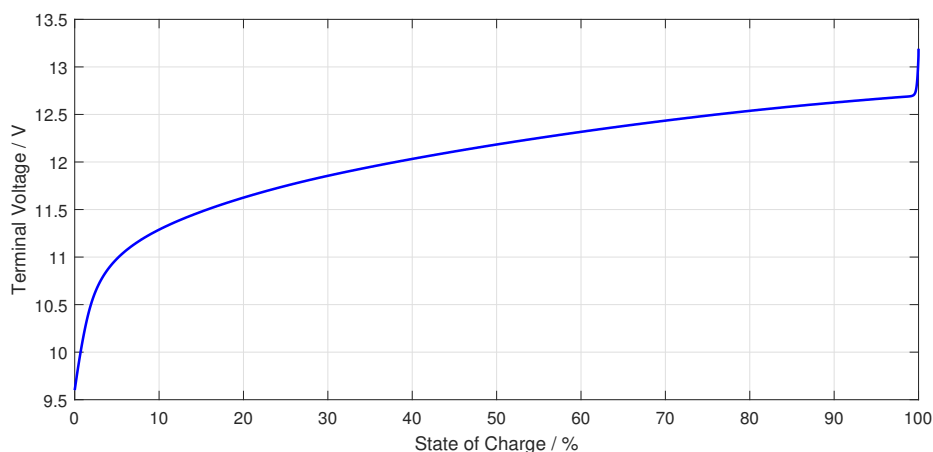


Figure 5.17: Discharge Curve for RS Pro Battery with $1 C_{nom}$ A Discharge

For each charge–discharge cycle the discharge and charge capacities were measured, from this the charge efficiency of the battery, that is, the proportion of the energy used to charge the battery which can be recovered during discharge, may be calculated. Additionally, before beginning the test, and after every 50 cycles, the battery was weighed and had its impedance measured using a Hioki BT3554 Battery Tester. This operates on the same principle as the EIS system, but applies a fixed ac current of 16 mA at 1 kHz to the battery whilst measuring the resultant voltage response, from which the impedance of the battery can be calculated.

The primary method used to determine degradation was again the SoH of the battery, determined by comparing the battery’s discharge capacity at cycle n against that of cycle $n = 0$, the first discharge. However the additional data gathered has also be used to assess the performance of the battery. As described in the previous chapter, as the battery degrades, its impedance will increase; any additional degradation caused by the ripple currents would therefore manifest itself as a greater increase in impedance over the same number of cycles than observed for the baseline. The mass of the battery is also important, mass loss in lead-acid batteries is a sign of the battery being overcharged, and losing electrolyte through gassing. By measuring the mass of the battery, any mass loss compared to the baseline will be indicative of the ripple currents causing overcharging of the battery.

Figure 5.18 shows the results of the baseline test, which ran for 500 cycles. Throughout the course of this test, the battery SoH fell to 50 %, giving an average rate of degradation of 0.1 % per cycle. The charge efficiency rapidly increased to around 97 % during the first 20 cycles and thereafter steadily increased before stabilising at around 99.5 % after 300 cycles. In the same period there was a linear loss of mass of 4 g, from 1.554 kg to 1.550 kg and a roughly linear increase in impedance of around 4 m Ω , from 29 m Ω to 33 m Ω .

To determine the effects of injected ripple currents, the test procedure described above was repeated with two additional batteries. All cycling and measurement parameters were as described above, in this case, however, a ripple current of 1.6 A_{rms} was injected during the 2 hour rest periods between charges and discharges. For one battery this current had a frequency of

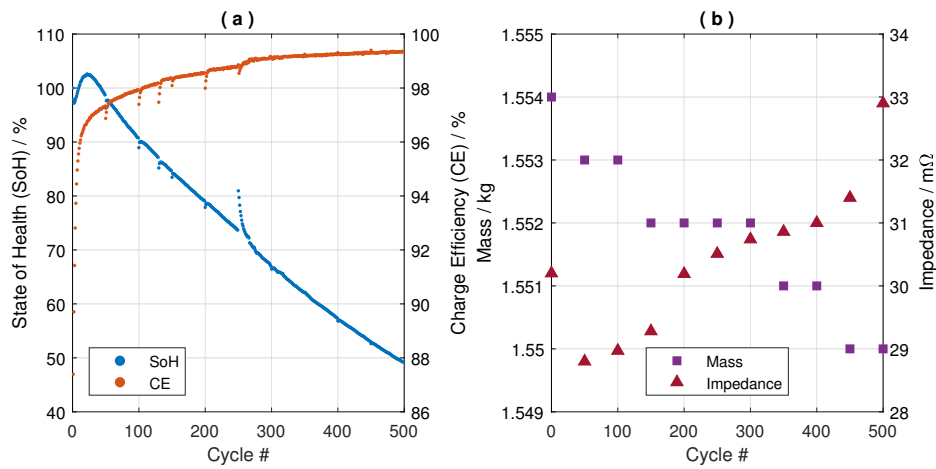


Figure 5.18: Long-term Cycle Performance for Baseline Test. (a) SoH & Charge Efficiency, (b) Mass & Impedance

700 Hz, and for the other it was 30 kHz.

Figure 5.19 shows the results of the test with 700 Hz ripple current, whilst figure 5.20 shows that for 30 kHz. In both cases the long term effects of the ripple current are negligible, the differences in SoH and charge efficiency between all three tests are virtually indistinguishable. Whilst figure 5.19 shows slightly lower, and figure 5.20 slightly higher degradation than the baseline test, the difference is so small as to be impossible to distinguish

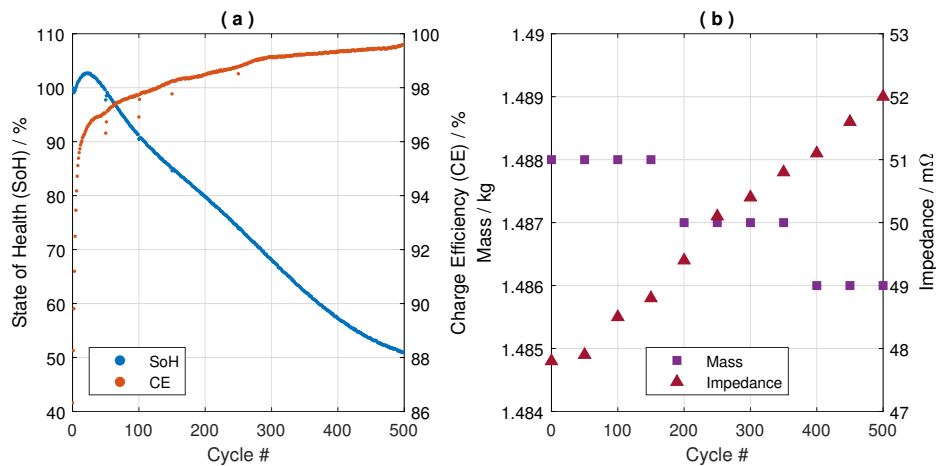


Figure 5.19: Long-term Cycle Performance with 700 Hz Ripple. (a) SoH & Charge Efficiency, (b) Mass & Impedance

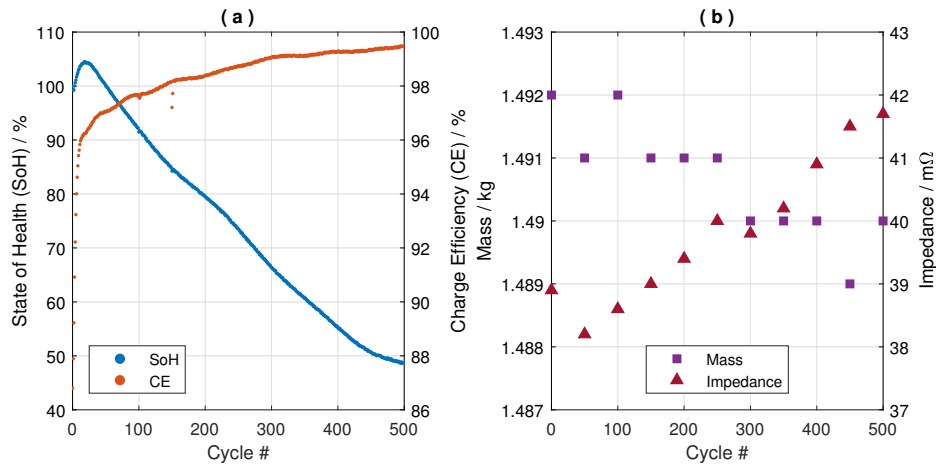


Figure 5.20: Long-term Cycle Performance with 30 kHz Ripple. (a) SoH & Charge Efficiency, (b) Mass & Impedance

between the effect of the ripple current or the natural variation in battery performance due to manufacturing tolerances.

A similar phenomena is observed for the other measurements. Whilst there are differences in the absolute values of mass and impedance for the batteries with applied ripple current, these are again within the tolerance one would reasonably expect to see between batteries of the same type. Any effect caused by the ripple current would be shown by the magnitude of change in mass or impedance throughout the tests, here, however the results are virtually identical to that of the baseline case.

In terms of mass, the loss was 2 g in both cases, compared to 4 g for the baseline case; in all cases the loss was around 0.25 % of the battery's total weight, which is so small as to be effectively zero. The impedance increase was also the same for both tests, at 4 mΩ, this also being the same as the baseline test. All in all, this suggests that, as in the case of short-term SoC, the injection of ripple currents has no measurable effect on the long-term SoH of lead-acid batteries.

5.5 Effect of Ripple Currents on Cell Balancing

Many battery systems, including those used in HEV applications, suffer from issues with cell balancing. If the injection of ripple currents is to be practical in real-world systems, it is important that they do not exacerbate these problems; ideally, of course, the ripple current would help to improve the situation. A further series of tests were therefore performed to assess the effect of ripple currents on cell balance.

5.5.1 Cell Balancing

Nearly all practical battery systems require a terminal voltage greater than that which can be provided by a single cell, this is achieved by stacking several cells in series to form a string with the desired voltage. If greater capacity is required, multiple strings can be connected in parallel until the required performance is achieved. This configuration, of several parallel strings is the basis of very many battery systems, in a wide variety of uses, from automotive HEV and EV to large grid-scale storage systems, and may consist of many thousands of individual cells. Cell balance issues affect any battery containing cells in series, and therefore are applicable to a vast array of battery applications.

The issues with cell balancing arise due to manufacturing differences leading to apparently identical cells, even those produced in the same batch at the same time, exhibiting slightly different performance characteristics, which then cause problems when such cells are operated in series. The performance differences can be considered as though the cells will charge at different rates; in practice, of course, the reasons are considerably more complex but essentially result in the cells having either differing capacities, impedances, or most commonly, both [54]. External factors, such as uneven temperature distribution within the battery pack, may also lead to imbalances [55].

Consider a battery comprised of two such cells C_0 & C_1 , where C_0 charges more quickly than C_1 . When charged, C_0 will reach full charge before C_1 ,

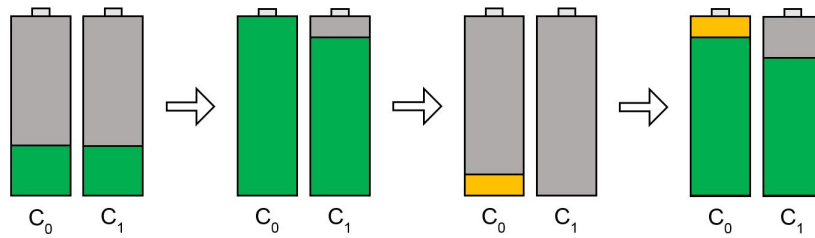


Figure 5.21: Cell Imbalance Example

and as the charging must be terminated at this point to avoid overcharging, the two cells will contain different amounts of energy, C_0 holding more than C_1 . When discharged the cell with the least stored energy, C_1 , will become depleted first, whilst energy is still stored in C_0 , again as the discharge must be terminated when any cell reaches its minimum voltage to avoid damage, the energy remaining in C_0 is stranded in the system and cannot be recovered.

The problem is then exacerbated when the battery is recharged as, not only will the performance imbalance again cause C_0 to charge faster than C_1 , but C_0 already contains some energy stranded from the previous discharge. Combined, this causes C_0 to reach full charge even quicker, and C_1 to store even less energy than before. If steps are not taken to correct this imbalance, the battery eventually becomes unusable as C_0 will tend to become fully-charged whilst C_1 tends toward fully-discharged, thus no operations can be performed on the battery and all energy stored in C_0 is rendered useless. This process is illustrated by figure 5.21.

There are three main methods to correct cell imbalance [56]. The simplest is to perform an equalising charge on the battery, this involves applying a higher charging voltage to the battery and allowing individual cells to become overcharged until all cells are fully charged. This method is only possible in batteries whose chemistries can tolerate being overcharged, such as lead-acid and nickel metal hydride. Other drawbacks of this method are that the cells which are overcharged are subject to higher degradation, and due to the charge current falling rapidly when the equalising voltage is reached, it can take a long time for all the cells to fully charge. For cells which cannot tolerate overcharging, such as those which are lithium-based, or where it is

desirable to avoid the degrading effects of overcharging, passive or active cell balancing may be employed instead.

Passive balancing is achieved by connecting a resistor and switch in parallel with each cell. The cells may then be balanced by discharging all but the least-charged cell through the resistors until the battery is balanced, at which point it is usual to apply a ‘topping-off’ charge to fully recharge the battery [57]. Although simple and requiring few components, passive balancing does have some disadvantages. Firstly, the energy removed from the cells during balancing is lost as heat in the resistors. This requires that the balancing current be relatively modest, lest the resistors become too hot or require heatsink mounting, thus increasing component count and cost. Limiting the balance current in this way also makes the process of cell balancing quite slow.

The concept behind active balancing is very simple: take the energy from cells which have an excess and transfer it to those with a deficit, until all cells are at the same level; implementing this concept, however, is rather more complex [56–58]. A typical system uses a dc-dc converter and a switch matrix to allow energy to be moved between a group of cells, as the number of cells in the battery increases so does the required number of converters and switch matrices. This makes an active balancing system far more complex and expensive than the other options, the benefits, however, are that very little of the stored energy is wasted and that balancing can be achieved in a timely manner.

5.5.2 Test Procedure

Whilst there are many possible causes for cell imbalance, they all manifest themselves as a difference in voltage between cells in the string. To determine the level of imbalance, therefore, it is necessary to measure the individual cell voltages within the battery, with the imbalance being given by the absolute difference between the lowest and highest cell in the battery. The batteries used previously in this investigation are constructed as a single sealed unit, making such a measurement impossible. To assess the effect of ripple current



Figure 5.22: 8 V, 4-cell Test Battery with Cell 0 Leftmost

on cell balance a bespoke battery was produced consisting of four EnerSys Cyclon cells in series (figure 5.22), giving a nominal voltage of 8 V and a capacity of 2.5 Ah. These cells were mounted to a PCB and provided with connections to allow for measurements to be taken of the cell voltages during testing. The test battery was also equipped to allow individual cells to be charged or discharged independently so manual balancing or imbalancing could be performed. Each cell was given an ID number, beginning with cell 0 at the negative end of the battery to cell 3 at the positive end.

Testing proceeded in two ways, firstly to determine the level of imbalance which would be typical when the battery was cycled, and an assessment of whether ripple current would affect this; and secondly, if the application of a ripple current in isolation would alter the level of imbalance within the string.

5.5.3 Cycle Imbalance

To obtain a baseline level of imbalance, the battery was subject to an equalising charge to minimise the differences between the cells. It was then subjected to five charge–discharge cycles at a rate of 1.25 A, equivalent to $0.5 C_{nom}$ A. To avoid causing excess degradation of the cells, the discharge was terminated when the battery reached 20 % SoC, recharging was to 100 %

SoC, however.

The results of this testing are shown in figure 5.23. It can be seen that for the majority of the time imbalance is very low, with a typical value of around 10 mV. There are short spikes where the imbalance briefly rises when there is a sudden, rapid change in battery voltage, such as at the start of a discharge, but these are corrected quickly and the imbalance returns to its initial value; nearing the end of charging, however, imbalance climbs rapidly.

Charging was performed with the standard CCCV approach as seen from figure 5.23a, as can be seen from this data the battery voltage is held constant once CV-mode is reached. Figure 5.23b, however, shows that the picture for

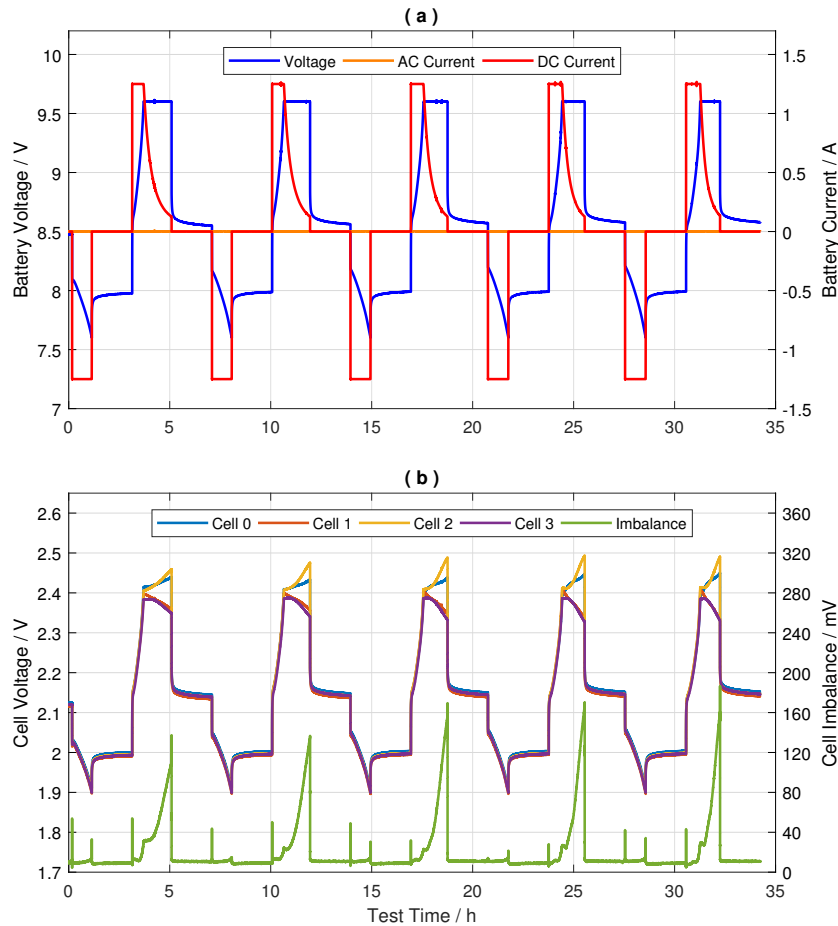


Figure 5.23: Cycle Imbalance Profiles for Baseline Test. (a) Battery Voltage & Current Profile, (b) Cell Voltage & Imbalance

the individual cells is very different. Despite the overall battery voltage being held constant at 9.6 V, there is an increasing spread of cell voltages as time passes, with two cells seeing a continued increase in voltage whilst the other two see a corresponding decrease. This may also be observed from the imbalance data, which shows a steadily rising imbalance until charging is terminated. As the number of cycles increases, it may be seen that the magnitude of the imbalance also increases, rising from around 130 mV for the first cycle to around 190 mV by the fifth; this illustrates, in practice, the cumulative nature of cell imbalance.

A second series of cycle tests was then performed, in the presence of an

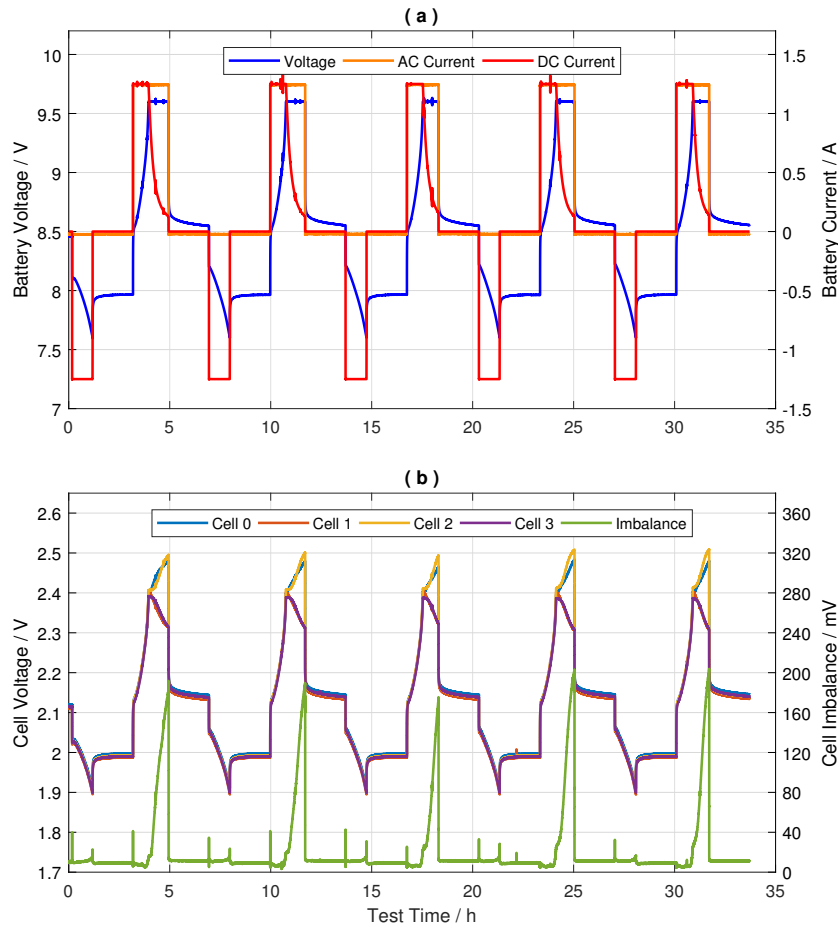


Figure 5.24: Cycle Imbalance Profiles with 30 kHz Ripple Current. (a) Battery Voltage & Current Profile, (b) Cell Voltage & Imbalance

applied ripple current. In this case, during the charge phase, when imbalance is seen to be at its worst, the battery was subjected to a 30 kHz ripple current of $1.25 A_{\text{rms}}$. The results from this test procedure are shown in figure 5.24.

Considering first the overall result for the battery, the presence of the ripple current appears to have had no effect, the CCCV charging profile has proceeded as before and the battery has not charged appreciably quicker, or slower than before. The same is true from the cell perspective, cell imbalance is still very low for much of the time, with the only real exceptions being during CV-charging of the battery. It is also apparent that the ripple current has not caused any great change in the level of imbalance either. The cells were not equalised between the preceding baseline test and this investigation, thus the imbalance continues from before, with a maximum of around 180 mV for the first cycle.

Interestingly, however, the rate of increase appears to be less than that observed in the baseline case, with the fifth cycle seeing a maximum imbalance of only 200 mV, and cycle three even saw a decrease. How much of this is due to the influence of the ripple current, and how much is simply the cells settling after equalisation is difficult to determine; what is clear, however, is that the presence of the ripple current has not caused the imbalance to become any worse than the baseline case.

5.5.4 Static Imbalance

The result of the above testing appears to indicate that ripple currents do not increase imbalance, and may possibly improve matters, however the full picture is somewhat difficult to determine due to the influence of additional factors. To eliminate these, a second test procedure was performed, with ripple current alone.

In this case individual cells of the battery were independently discharged to produce a deliberate imbalance, the battery was then allowed to rest for several hours for the cell voltages to stabilise, at which point a 30 kHz, $1.25 A_{\text{rms}}$ ripple current was applied to the battery for a period of 2 hours.

The results of this testing are shown in figure 5.25, from which it is very

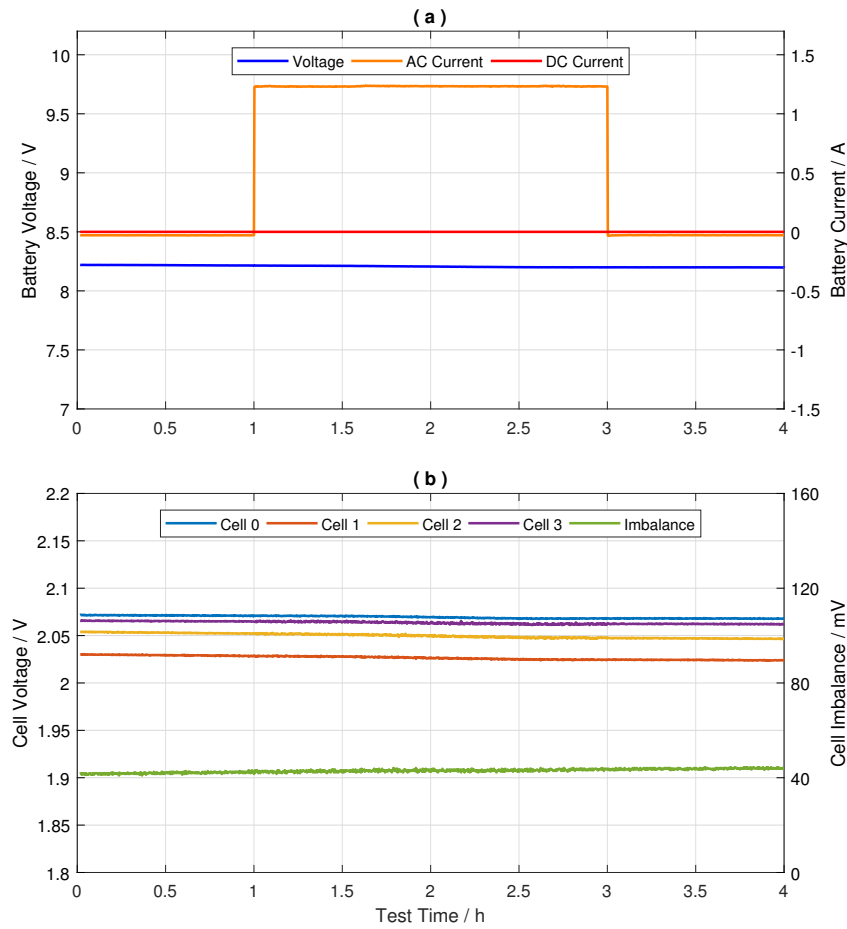


Figure 5.25: Static Imbalance Profiles with 30 kHz Ripple Current. (a) Battery Voltage & Current Profile, (b) Cell Voltage & Imbalance

clear that the ripple current has had no effect on the cell imbalance seen. It may therefore be further concluded that the slowing of the rate of imbalance increase seen in the cycle testing was caused by a stabilisation in battery performance following the equalising charge, rather than as a consequence of the ripple current.

5.6 Conclusions

The work has shown that the application of ac ripple currents to lead-acid batteries can significantly improve their charge acceptance. Improvements

in charge acceptance of over 50 % have been seen, with the use of ripple currents of $0.4 C_{nom}$ A. The improvements have been observed across a wide range of frequencies, and are seen to become greater as the frequency of the ripple is increased. The increase is not linear, however, and moving to frequencies greater than 30 kHz provides little practical benefit; especially when the increasing power requirements due to increased battery impedance are considered.

The application of sinusoidal ripple currents does not appear to have any detrimental effect on many crucial aspects of battery performance including SoC, where even after a period of five days no effect was measured; SoH, which showed no difference in performance across 500 cycles; and cell imbalance where neither cycling nor static imbalance were affected by the presence of a ripple current.

Chapter 6

Considering Lithium Chemistries

6.1 Introduction

Up until this point the work performed has focused solely on lead-acid cells, whilst these remain common and are appropriate in many applications, it cannot be denied that in many areas lithium-based cells are superior. As technology has progressed and systems have become more complex, portable, and power-hungry, the lithium cell has become fundamental to the operation of many everyday devices such as mobile phones and tablets. Lithium cells are also the basis for many large-scale battery systems, like those installed in electric vehicles or used for grid-scale storage.

As many of these areas also have requirements for the batteries to charge in a limited time or from charges which are infrequent but at a high rate, the work has been extended to consider the operation of lithium cells in such environments. Firstly by examining the DCA performance of lithium cells, and then to consider the most appropriate charging methodology to minimise degradation whilst maintaining cell performance. As this chapter examines two separate issues, which, although related, do not have quite as much coherence as other chapters, the conclusions are given within each section, rather than being combined at the end.

6.2 DCA Performance of Lithium-ion

The testing of both standard and carbon-enhanced lead-acid cells described in Chapter 3 yielded useful results regarding their performance. This investigation was extended to determine if the test methodology used in that work could also be applied to lithium cells. For this testing new Mottcell IFR26650 3.2 V, 3.3 Ah, 26650-type lithium iron phosphate (LFP) cells were used (figure 6.1). The only changes made to the test procedure described in Section 3.4.3 were to vary the voltage limits used, this being necessary to compensate for the differing voltages between lead-acid and LFP cells. As before, all testing was performed under environmentally controlled conditions at $25\text{ }^{\circ}\text{C} \pm 2\text{ }^{\circ}\text{C}$. Figure 6.2 shows the results of these tests.

The LFP results show some differences from those observed with the lead-based chemistries, although to some extent, all the trends previously identified are present. Firstly, in a trend reminiscent of standard lead-acid, variation with operational history is virtually eliminated, with lithium showing only a very slight reduction in DCA performance when the cell has charge history. Similarly, the effects of the rest period are clearly evident, across all SoC a reduced rest period improves DCA performance. As with the history behaviour, however, this effect is much more consistent and the shapes of the DCAPP remain broadly similar despite the changing rest periods.

The most dramatic change however is that the influence of SoC is much reduced compared to all previous results. This has the benefit of making



Figure 6.1: 3.2 V, 3.3 Ah, Mottcell IFR26650 LFP 26650 Cell

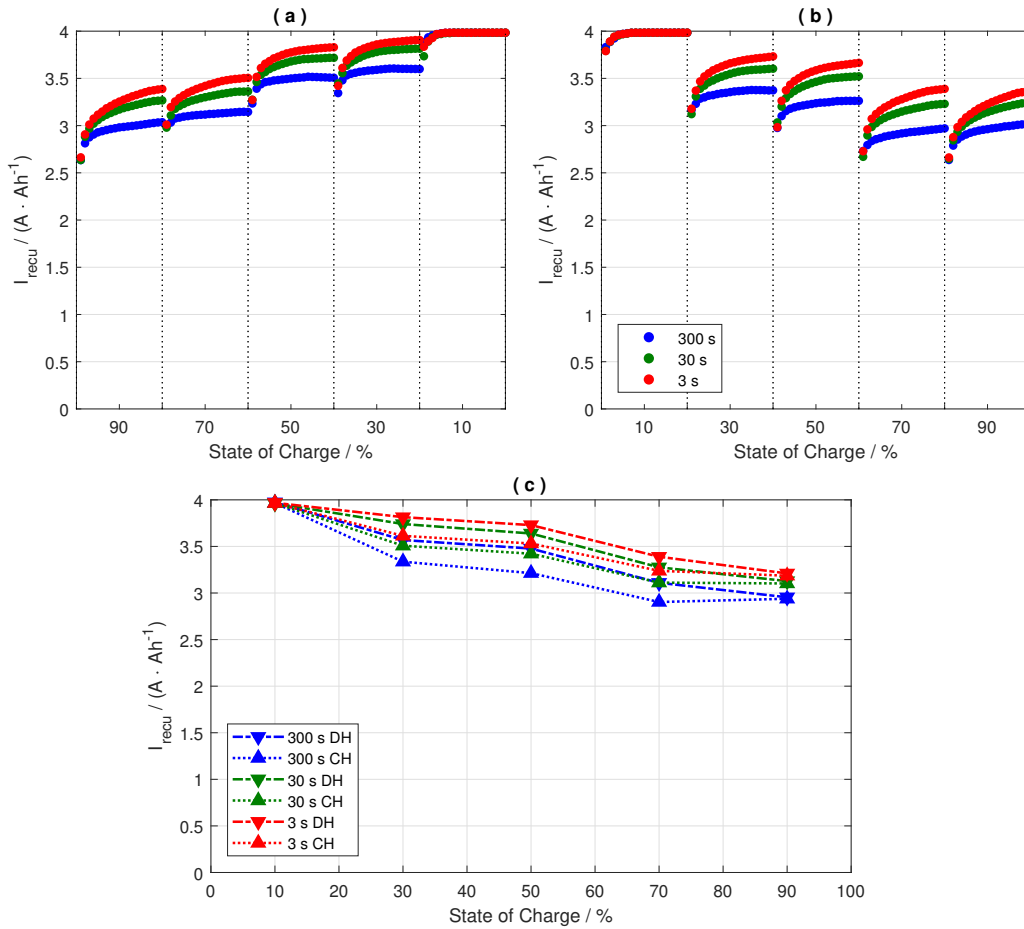


Figure 6.2: DCA Analysis Result for 3.2 V, 3.3 Ah, LiFePO_4 cell, 25 °C. (a) with Discharge History, (b) with Charge History, (c) Average Charge Acceptance

the DCA performance much more consistent across a wide SoC range, but does have some downsides. Whilst performance over carbon-enhanced lead is much improved at high SoC, as this reduces the lead-acid cells begin to show better performance, especially below around 30 % SoC. It has been shown that if the charge current is allowed to increase beyond $4 \text{ A}\cdot\text{Ah}^{-1}$ carbon-enhanced lead will accept up to around $8 \text{ A}\cdot\text{Ah}^{-1}$ (see Section 3.6). This compares favourably with the lithium cells which would seem unlikely to be capable of accepting more than around $4.5 \text{ A}\cdot\text{Ah}^{-1}$ under similar conditions.

These results also indicate that the test methodology described by Chap-

ter 3 is a useful device for determining the DCA performance of cells with a range of chemistries. It also reinforces the validity of the test and of the trends identified, as these too appear largely independent of the chemistry of the cell investigated.

6.3 Lithium-ion Charging Strategies

Lithium-ion (Li-ion) batteries have become very popular in recent years for the improved performance they offer over earlier chemistries, especially their increased energy density and cycle life. When first introduced, these benefits were used to increase the performance of the devices in which they were installed, by increasing run-time between recharges and reducing the need to replace degraded batteries. Over time, however, designers and engineers have come to recognise that, with a little circuitry to avoid overcharging or excessive temperatures, Li-ion batteries can also be charged more rapidly than previous chemistries.

Whilst rapid charging has allowed for devices to become more complex and powerful without needing to extend the time taken to charge, it does have its downsides. Charging at a higher rate causes greater cell degradation, and the increased power usage means the frequency of charging is also increased, further adding to the rate of degradation. In many cases, this is not major problem; laptop and smart-phone batteries may have an expected lifetime of 2 – 3 years of heavy use, by which point the user is likely to want to upgrade to better hardware anyway, regardless of remaining battery life. In such situations, the increased degradation is commercially viable, as the benefit of increased performance to the user outweighs the cost of reduced life.

Away from high-end consumer electronics, however, battery systems are being developed using Li-ion cells where the cost of degradation is far more significant and damaging to the operational and commercial viability of the system. One such area which is now seeing the increasing use of Li-ion batteries, and which also presents a particularly challenging environment for them to operate in, is the provision of portable power banks to extend electrification in developing countries.

6.3.1 Renewable Energy in the Developing World

Throughout the developing world, over a billion people have no access to mains power [59]; in the absence of this, many rely on diesel generators for electricity and oil lamps for lighting, neither of which are environmentally sound and pose significant health risks due to their emission of toxic fumes. Efforts are being made to combat this, with projects to expand the provision of renewable energy supplies to developing countries [60], but in many cases such systems remain economically unviable or are frustrated by regulatory or political factors [61].

An alternative approach is to use rechargeable Li-ion battery packs to provide power; an example of such a pack produced by Mobile Power Ltd of Sheffield, is shown in figure 6.3. In this model a central base-station is provided in which the packs are stored and charged by whatever means is most appropriate, typically solar PV. Users then rent the packs on a pay-per-charge model and are free to take the pack to where it is needed. Depending on the design, the packs can provide power to charge a mobile phone or laptop, run a television and may also include LEDs for lighting purposes. When the pack has been discharged, it is returned to the base-station where it is recharged ready for the next use.

This model provides the benefits of renewable energy, without the high costs associated with installing a micro-grid system, thus making it attractive



Figure 6.3: Portable Li-ion Battery Pack – Courtesy of Mobile Power Ltd

to low-income users. It also has the advantage that it requires no infrastructure aside from the base-station, thus reducing ongoing maintenance costs and making provision viable even in sparsely populated areas. Clearly, however, this is a challenging environment in which to operate batteries; the usage profile is very cyclic, with the battery pack typically being used until it is fully discharged before being returned to the base-station for a full recharge also, the largest market for these systems is sub-Saharan Africa, thus ambient temperatures are high. Both of these factors are known to contribute to degradation in Li-ion cells.

As the cells form the most expensive part of such a system as well as its main consumable, it is important that they be used in such a way to maximise their value. Typically this will be achieved by optimising for cell lifetime, energy stored, charging speed or some combination thereof.

6.3.2 Test Procedures

To determine the best optimisation strategy, three test procedures have been developed; each procedure has been designed to maximise either energy stored, cycle life or charge speed. The effects of each of these procedures on cell performance may then be compared to identify the most appropriate charging methodology to extract the maximum value from the cell. The test procedures described below were performed with a Maccor Series 4000 automated battery test system. The cells used in this investigation were Samsung ICR18650-26J, Li-ion 18650-type (figure 6.4) with a nominal capa-



Figure 6.4: 3.6 V, 2.6 Ah, Samsung ICR18650-26J Li-ion 18650 Cell

city of 2.6 Ah, and all testing was performed with the cells in free-air within temperature-controlled chambers maintained at an ambient temperature of $35\text{ }^{\circ}\text{C} \pm 2\text{ }^{\circ}\text{C}$:

Method 1

This method attempts to extract the maximum possible energy from the cell. The cell is to be charged and discharged at a rate of $1\ C_{nom}$ A, separated by 1-hour rest periods. The discharge cut-off voltage is 2.8 V and charging is to be performed using a CCCV profile with a charge voltage of 4.2 V and a cut-off current of $0.05\ C_{nom}$ A. This is similar to the method used by many cell manufacturers to determine cycle life, and thus will provide baseline performance data on the effects of cycling at increased temperature, but in an otherwise standard manner. The charging profile for this method is shown in figure 6.6a.

Method 2

This method attempts to maximise cycle life by reducing stress on the cell; this is achieved by limiting voltage excursions at the end of charging and discharging. As with method 1, the cell is to be cycled at a rate of $1\ C_{nom}$ A with 1-hour rest periods. The discharge cut-off voltage is increased to 3.25 V, charging is again CCCV with a cut-off current of $0.05\ C_{nom}$ A, but the cell is to be charged such that 1 hour after charge termination its OCV relaxes to 4.1 V; this specification was a requirement of the application for which these tests were undertaken. This means that the maximum voltage applied to the cell will be reduced from 4.2 V, to some lesser amount. By operating the cell within a narrower voltage window, this method attempts to maximise cycle life, at the expense of energy delivered. The charging profile for this method is shown in figure 6.6b.

Method 3

This test is similar to method 2 in that it attempts to reduce stress on the cell, but in this case the objective is to minimise charging time. All parameters are as in method 2 apart from charging. Here the cell is

once again to be charged to 4.2 V, but the current cut-off is increased to $0.2 C_{nom}$ A. This will result in the cell spending less time at the peak voltage and produce a faster overall charge. The charging profile for this method is shown in figure 6.6c.

All parameters required for testing are well defined, apart from the charge voltage limit for method 2, which has been determined experimentally. One cell was subjected to five cycles of method 2, for each cycle the charge voltage was increased from 4.115 V to 4.135 V in 5 mV increments. The results of this test are given in figure 6.5, which clearly demonstrates that to achieve an OCV of 4.1 V, 1 hour after charge termination, the cell should be charged to 4.12 V.

With the charge voltage limit for method 2 determined, all three test procedures can be fully specified; table 6.1 details the full parameters for each test and figure 6.6 shows the charging current and voltage profiles for each of the three methods as measured from the first test cycle. Two cells were subjected to each test, giving six tested cells in total, identified as cells A – F. Cells A and D were tested with method 1, cells B and E with method 2, and cells C and F with method 3.

The test procedure described above represents one discharge–charge cycle,

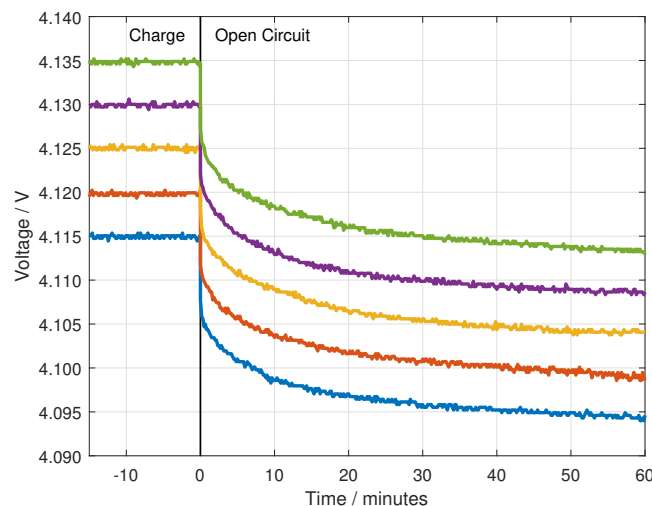


Figure 6.5: OCV Determination Test for Method 2 Charging

Table 6.1: Full Test Parameters for all Methods

Step	Operation	End condition		
		Method 1	Method 2	Method 3
1	1 C Discharge	2.80 V	3.25 V	3.25 V
2	1-hour rest			
3	1 C Charge	4.20 V, 0.05 C	4.12 V, 0.05 C	4.20 V, 0.20 C
4	1-hour rest			

in all cases after 100 such cycles the cell was subjected to a full capacity assessment, by performing a single cycle of method 1, and an impedance test. The results of these tests then can be compared to a baseline result taken

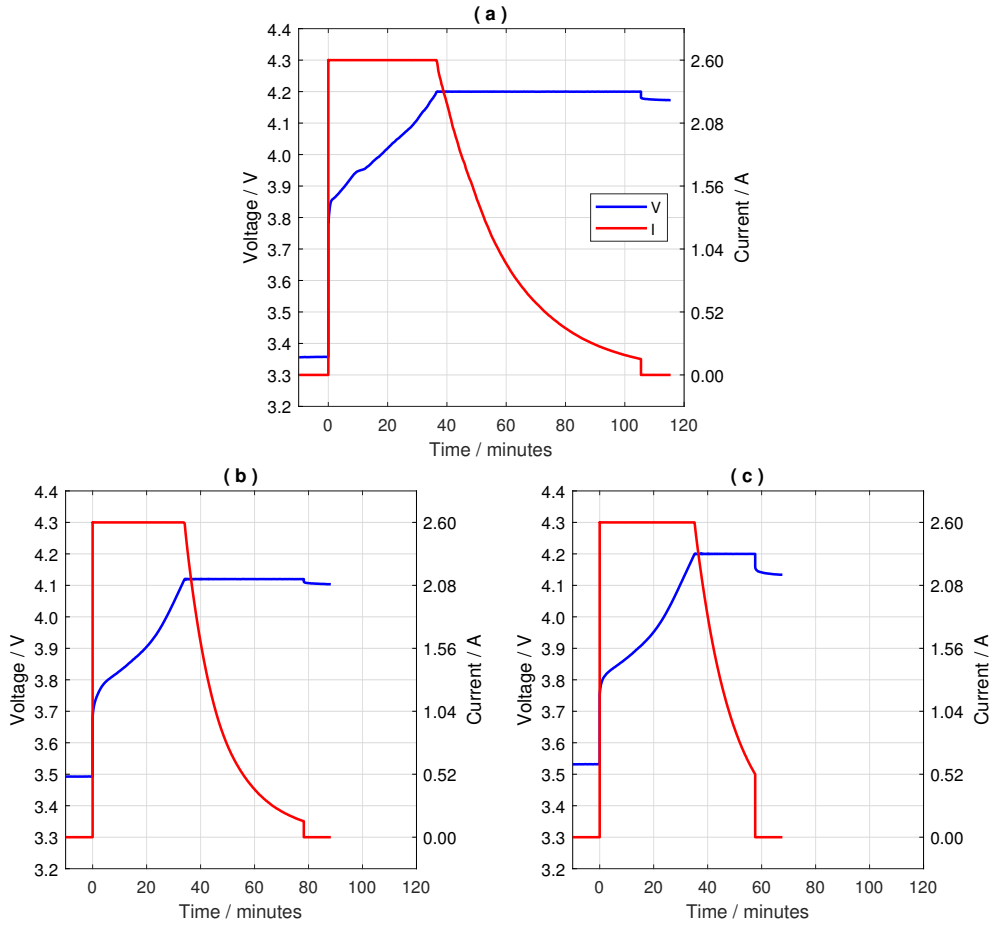


Figure 6.6: Charge Current & Voltage Profiles. (a) Cell A (Method 1), (b) Cell B (Method 2), (c) Cell C (Method 3)

before the commencement of the test procedure to determine the effects of the testing on the health of the cell. Following each 100-cycle profile, the condition of the cell was assessed, and if suitable, it was subjected to a further 100 cycles of testing.

6.3.3 Impedance Testing

Before beginning the test procedure, a single cell was subject to an EIS test to determine its frequency-dependant impedance. The effect of the various test procedures on the impedance of the cells would form an important part of the test process, therefore it was necessary to establish a baseline result and determine the most appropriate method to measure impedance. In this case the frequency range chosen was 5 mHz – 5 kHz, the results of this test are given in figure 6.7.

This shows two important features, firstly the difference in impedance caused by differing SoC is minimal. This indicates that power loss within

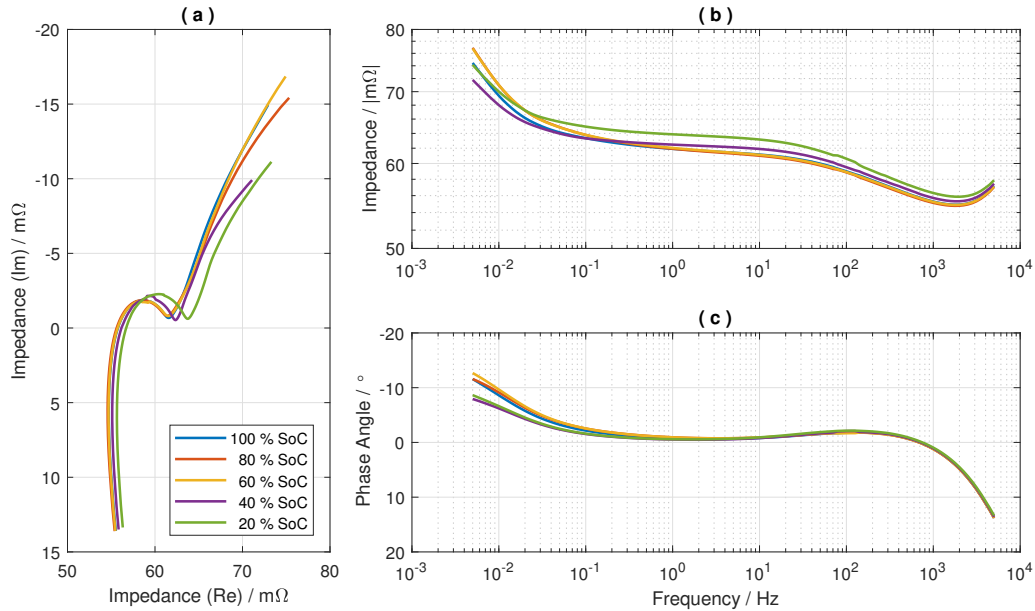


Figure 6.7: EIS Spectra for Samsung 18650 Cell at Various SoC Levels. (a) Nyquist Plot, (b) Bode Plot - Magnitude Response, (c) Bode Plot - Phase Response

the cell during charge or discharge is essentially constant regardless of the SoC and therefore there is no power-loss benefits to be gained by early termination of either charge or discharge, and such operation is not likely to lead to significant increase in cell temperature due to increased losses.

Secondly, it may be seen from figure 6.7b that the absolute impedance varies little across the whole range of frequencies investigated. This indicates that the complexity incurred by assessing impedance across a range of frequencies is unnecessary, a representative result may be obtained from a single-frequency assessment.

6.3.4 Results & Discussion

The results of this study can be divided into two broad areas, firstly the direct impact of the differing methods, such as the effect on the cell's energy storage ability or charge time. These effects are produced immediately as a direct result of the method chosen. The second area is that of the long-term impact of the various methods, such as the effect on cell lifetime. In these cases the influence of the various methods takes many cycles to become apparent.

Initial Capacity

All cells were tested for capacity prior to the start of cycle testing, the results of this are shown in table 6.2.

These show the cells were all very close to their nominal capacity and that there was very little variation between them; this is further reinforced by the mean capacity being 2.598 Ah with a standard deviation of only 0.004 Ah. This result confirms that prior to starting the testing process all the cells were well matched and in good condition, thus it is reasonable to conclude that performance variations observed during the testing process are as a result of the tests applied to the cells rather than some underlying condition present at the start of the test.

Table 6.2: Starting Capacity for all Cells

Cell	Capacity
A	2.604 Ah
B	2.600 Ah
C	2.597 Ah
D	2.598 Ah
E	2.597 Ah
F	2.591 Ah

Capacity Reduction

Due to the altered charge and discharge cut-off points used in methods 2 and 3, these cells will no longer deliver their rated capacity, instead it will be somewhat lower. Table 6.3 shows the magnitude of this loss as given by the average capacity delivered from the first test cycle for both cells of the given test procedure. The table gives the values in terms of both absolute capacity, and as a percentage of the cell's rated value of 2.6 Ah.

From this it may be seen that despite the differing charging profiles, the difference in available capacity between methods 2 and 3 is minimal. It is also apparent that the reduced voltage window of methods 2 and 3 only reduces the available energy stored in the cells by around 15 % compared to that of method 1.

Charge Speed

By limiting the charge termination point, either by reducing the peak voltage as in method 2 or by increasing the termination current as in method 3, the time taken to charge the cell will be less than that required for method 1. Allowing the cells to charge faster is an important benefit and may allow for improvements in cell utilisation as less time needs to be 'wasted' recharging

Table 6.3: Available Capacity from all Tests

Method 1		Method 2		Method 3	
Ah	%	Ah	%	Ah	%
2.601	100.0	2.174	83.6	2.249	86.5

Table 6.4: Charge Speed Improvement

Method	Charge Time	%
1	105.5 minutes	—
2	78.3 minutes	74.2
3	57.6 minutes	54.6

depleted cells.

Many factors influence the time taken to charge a cell, such as starting condition, temperature, and cell health, however an assessment of the potential benefits has been made by comparing the average times taken for the six cells to recharge after their first discharge cycle. At this point the cells are new and have been shown to be well matched, the only significant variable being the test procedure applied.

Table 6.4 summarises the result of this test, which may also be seen from figure 6.6. From these results it is clear that both methods 2 and 3 result in appreciably lower charging times, method 3 in particular nearly halves the time taken for the cell to charge. Some reduction in speed is to be expected, as less energy is being stored in the cells; however it may be seen in this case that whilst the stored energy is reduced by 15 %, the charge time is reduced considerably more. Whilst this is only a snapshot, it does give a useful indication of the likely benefits to charging speed of the modified charge profiles under investigation.

State of Health

As cells are cycled, they are subject to degradation. In Li-ion cells the main sources of this degradation are lithium plating of the negative electrode and cell oxidation [44]. This physical degradation leads to performance degradation which is exhibited as a reduction in the SoH of the cell. Figure 6.8 shows the capacity loss profile for all cells, as measured from the full capacity test taken every 100 cycles. This test yields C_t , and as C_{nom} is known to be 2.6 Ah for these cells, their SoH may also be calculated.

The first observation is that there is a significant difference in performance between the various methods, with some cells displaying very rapid

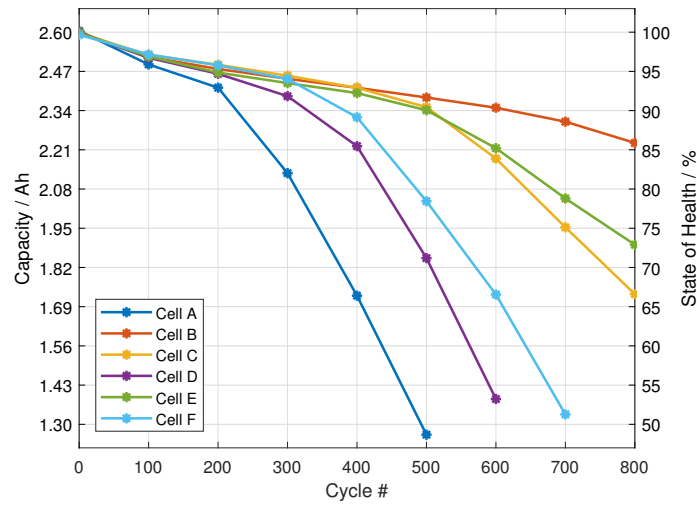


Figure 6.8: State of Health Profile for all Cells

degradation, whilst others show very little. Considering first the cells subjected to method 1 (cells A & D), it is clear that this is the most aggressive of the methods and results in the highest levels of degradation. For the first 200 cycles there is little difference with the other tests, however after this point the level of degradation increases rapidly. For this investigation it was determined that a cell had reached the end of its useful life when its SoH fell to around 50 %, for cell A this was reached after 500 cycles, at which point it was withdrawn from testing. Cell D fared somewhat better, reaching 600 cycles with a SoH above 50 %, however clearly this cell too is at the end of its useful life. The two cells in this test show quite significant variations in performance between them, however, this test is also the most strenuous and as such is likely to exacerbate any small variations which may exist between cells.

The cells subjected to method 2 (cells B & E), on the other hand, performed far better. These cells show very little degradation, both comfortably reaching 800 cycles with a SoH of 86 % for cell B and 73 % for cell E. They also exhibit much better consistency of performance, with the only appreciable difference in their SoH profiles becoming apparent after 500 cycles. Clearly method 2 is more suited to providing long cell lifetimes than either of the alternatives examined.

Table 6.5: SoH Cost by Cell & Method

Method	Cell	End Condition		SoH Loss (per Cycle)	
		Cycle	SoH	Cell	Method Average
1	A	500	48.69 %	0.103 %	0.091 %
	D	600	53.23 %	0.078 %	
2	B	800	85.88 %	0.018 %	0.026 %
	E	800	72.88 %	0.034 %	
3	C	800	66.61 %	0.042 %	0.056 %
	F	700	51.27 %	0.070 %	

The results for method 3 (cells C & F) show that it is an improvement over method 1, but not as good as method 2. Again there is a large variation in performance after around 300 cycles, where cell C performs almost as well as those from method 2 reaching 800 cycles with a SoH of around 67 %, cell F shows more rapid degradation, reaching end of life after 700 cycles with a SoH of 51 %.

To quantify these results a simple linearisation has been applied to determine the typical degradation per cycle for each cell, the results for the two cells subjected to the same test procedure have then been averaged to produce an indication of the typical degradation per cycle for each method, this is given in table 6.5.

Cell Impedance

A secondary measure of degradation is the impedance of the cell. This is a much more difficult metric to measure, requiring specialised equipment such as the EIS tester [62], thus it is not practical to perform in most real-life systems. Cell impedance is however an important factor governing performance, as increasing impedance causes increased losses within the cell. This results in lower charge efficiency, and greater heating of the cell. This is a significant concern when ambient temperatures are already high and the energy available for recharging the cells is limited. The Maccor test system used in this investigation has the ability to perform impedance measurements at a single frequency of 1 kHz. As the results of the EIS testing above in figure 6.7b sho-

wed that the impedance of the cells at 1 kHz is a representative figure, this has therefore been utilised to show the effects of the various test procedures on the impedance of the cells. Figure 6.9 shows the impedance measured for all cells across a range of SoC from 100 % to 0 %, in 20 % intervals.

The first observation is that in all cases there is very little change in impedance with SoC, as seen in the baseline case, and the initial impedance of all six cells was closely grouped in the 55 – 65 m Ω range, beyond that, however there is a clear difference in the impedance trend depending on the test procedure applied. Those cells subjected to method 1 (figure 6.9a & 6.9d) show a general trend of rapidly increasing impedance as the cycles progress. This is particularly true in the case of cell A, whose increase in impedance is well correlated with the decrease in SoH. Cell D exhibits somewhat different behaviour, with a large increase in impedance in the first 100 cycles, after which impedance stabilises before increasing again after 400 cycles. This trend is not matched by its SoH, however it is clear that both cells subjected to method 1 saw a large increase in impedance as the testing progressed.

For those cells tested with method 2 (figure 6.9b & 6.9e) the results show very consistent performance, with both cells exhibiting a gentle, linear increase in impedance as the testing progressed. Interestingly, cell B, which demonstrates the best SoH performance shows a slightly larger increase in impedance than cell E, whose SoH performance is somewhat poorer. This demonstrates the importance of this analysis, as it shows that SoH and impedance are not necessarily well correlated.

As with SoH, the impedance results for method 3 (figure 6.9c & 6.9f) lie between the two extremes of the other methods. Cell C exhibits an impedance profile very similar to that of those for method 2, although the increase, whilst still broadly linear, is more pronounced. Cell F, on the other hand, shows a profile much like those of method 1, with the increase in impedance becoming greater as the test progresses. In this case, however, the increase is less than that seen in method 1.

These results further reinforce those from the SoH assessment, and show that method 1 is the most degrading to the cells, whilst method 2 is the least. Method 3 lies between these two extremes.

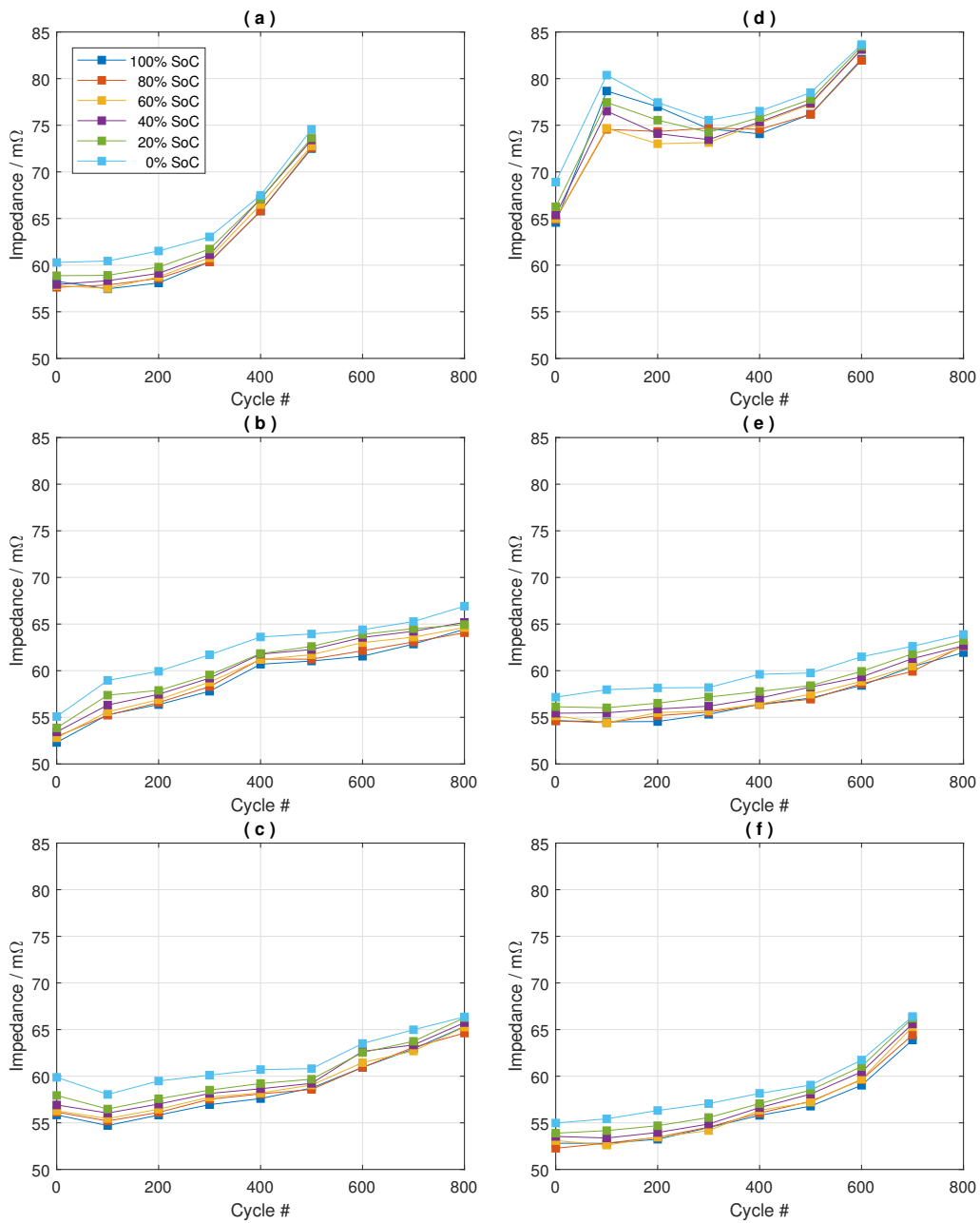


Figure 6.9: Cell Impedance at Various SoC Levels. (a) Cell A, (b) Cell B, (c) Cell C, (d) Cell D, (e) Cell E, (f) Cell F

6.3.5 Conclusions

The results of this study show that, in this application, attempting to maximise stored energy is not the optimal strategy, as whilst method 1 does deliver the largest amount of energy stored per cycle, it also suffers from the highest degradation of all the methods tested, this being two – four times higher than the other methods. When this is combined with the fact that alternative methods delivered 85 % of the energy of this approach, the total energy delivered over the life of the cell is the lowest in this instance. This method also has the largest increase in cell impedance, and hence reduction efficiency of all the methods investigated.

Of the remaining two methods, there was little to choose between them in terms of energy storage ability. Method 2 showed a clear advantage in terms of degradation with both cells so treated achieving 800 cycles with more than 70 % of their initial capacity remaining and little increase in impedance. Method 3, however had the advantage of increased charge speed, charging in around 75 % of the time taken by method 2. This advantage, however, comes at the cost of nearly twice the rate of degradation per cycle than method 2.

It would seem, therefore, that the optimal strategy is a balance between methods 2 & 3. It being desirable to charge using method 2 by default, but if demand for battery-packs were high, greater throughput could be achieved by switching to method 3 charging. As long as this was limited to reasonably short periods, demand could be satisfied more quickly without significantly impacting on cell lifetime or energy stored. Obviously, the decision on when precisely to make the switch will be driven by the economics of the situation.

Chapter 7

Conclusions & Further Work

This investigation has performed a comprehensive assessment of the issues associated with the testing and performance of lead-acid batteries in HEV applications. The results generated by this process have extended the current state of knowledge in this area and has prompted proposals for methods by which some of these issues may be overcome. Furthermore, some preliminary work has considered how the different charging methods can be applied to cells with lithium chemistries.

7.1 Chapter 2

This chapter undertook a detailed review of the literature surrounding the use of batteries in automotive applications, how this has changed in recent years and the issues which have arisen from this change. It also examined the current state of knowledge of the effects of ripple currents on battery performance.

This showed that the advancement in battery technology and changing environmental sensibilities had combined to make hybrid electric vehicles a practical and commercially viable proposition by the mid-2000's. For the typical duty cycles present in HEV applications, lead-acid remained a sensible choice of battery chemistry, despite other higher-performance options being available, due to its low initial cost and high availability of recycling

infrastructure. Despite this however, there were challenges to the use of lead-acid batteries in HEVs, particularly in respect of operation under HRPSoC conditions and their DCA performance.

As time passed, more work was performed and the main factors influencing DCA performance were isolated: SoC, operational history, rest periods and temperature. Test procedures began to be proposed to identify and characterise the DCA performance of batteries. Around this time automotive OEMs began to demand that batteries be designed to operate specifically under HRPSoC conditions and studies were undertaken to establish the best way to achieve this. By 2015, the work had culminated in the official adoption of a European Standard test procedure to determine the DCA performance of lead-acid batteries for automotive applications. This procedure, however, had some shortcomings and did not fully address all the factors which influence DCA performance.

In terms of the effects of high frequency ripple, the review found very little literature dealing with the subject, particularly at the higher frequencies likely to result from modern power converters. What little literature there was however appeared to form a consensus that there was no detrimental effect on batteries caused by ripple currents. No literature at all was found which described the influence of ripple on DCA performance.

Together, this gave a clear direction to both strands of the research: firstly, to investigate fully the effect of varying the test parameters and environmental conditions on the standard DCA test, and further to investigate the influence of ripple on DCA performance.

7.2 Chapter 3

This described a detailed investigation into the effects on DCA performance of varying the parameters and environmental conditions used in the standard DCA test procedure. Beginning with an analysis of the test procedure, this revealed the major shortcomings of the test itself: the currents used were far lower than those seen in practice, the effects of history were difficult to properly assess, and the procedure only examined performance across a

very narrow SoC band. Added to this were two additional parameters for investigation: the effect of varying rest period within the test procedure, and the influence of temperature on the results.

To remedy these defects a modified test procedure was proposed, which increased the charge currents to a more realistic level and considered a full range of SoC conditions, with consistency between charge and discharge history. This modified procedure was then performed on carbon-enhanced lead-acid cells, designed specifically for HEV use, using a range of rest periods and temperatures. The results of this testing showed that the DCA performance achieved was significantly better than that which would be predicted by the standard test, further it was shown that reducing the rest period within the test improves charge acceptance, as does the battery having discharge history. Again these traits were impossible to determine from the standard test methodology. Finally it was shown that increasing the temperature also increases charge acceptance.

The testing was then extended to consider the performance of standard lead-acid. This showed that the behaviour was broadly similar, with the exception that carbon enhancement improves charge acceptance over standard lead when the cell has discharge history. Finally the work investigated the effect of further increasing the charge current, which showed an upper limit of charge acceptance of around $8 \text{ A}\cdot\text{Ah}^{-1}$, and applying much longer microcycles, which showed a tendency for charge and discharge history performance to equalise after a long period of cycling.

The work described has advanced the state of scientific knowledge in this area, by demonstrating that the deficiencies of the standard test do have a real and significant impact on the difference between the performance suggested and that which may actually be achievable. Whilst the modified test procedure described is not proposed as a practical alternative to the European Standard method, it does offer an indication of what elements need to be accounted for if the current standard is to be improved upon.

7.3 Chapter 4

This chapter builds upon the preceding one and considers the effect of cell degradation on DCA performance. The shorter cycle life of lead-acid cells is something which often gets an oblique reference in literature, but no work was found which had investigated whether this would be an issue for DCA performance, and if so, how serious it would be.

Analysing the mathematics underpinning the DCA calculation, the work showed that the fact the test procedure normalises to the measured capacity of the cell has the potential to skew the DCA results as a cell degrades. A degraded cell will have a lesser capacity, and therefore the currents applied by the DCA test will be lower, thereby resulting in an easier test and artificially limiting the maximum potential charge acceptance.

A batch of lead-acid cells were subjected to 200 charge–discharge cycles, with their DCA performance being analysed every 25 cycles. For one set of cells this analysis used the standard, variable, DCA normalisation method, whilst the others were normalised using the, static, nominal capacity of the cell.

The results of this showed that the standard normalisation did indeed mask the true DCA performance, making it appear as if charge acceptance fell in unison with capacity. The alternative method, however, showed that in reality capacity is a poor indicator of charge acceptance, and no loss in performance was observed until the cells had lost around 30 % of their initial capacity, by which point they would likely be reaching the end of their useful life.

This is a very important piece of work, and is the first time such a result has been reported in literature. From a practical perspective, it suggests that the batteries in HEVs may have a longer life than would normally be predicted, and that for applications where charge acceptance is a primary concern an alternative measure, other than capacity, is needed to determine the end of life point for the battery.

7.4 Chapter 5

Up until this point, the investigations had been passive, determining the factors which influence charge acceptance and how they may be better assessed, Chapter 5 begins to consider methods to actively improve DCA performance. It had been previously identified in Chapter 3 that by reducing the rest period within the test, charge acceptance could be improved. This would be deeply impractical in real-life, but it did suggest that there may be potential to increase charge acceptance with purely electrical means.

Moving from individual cells, to a more representative battery, a detailed characterisation was performed using EIS techniques to determine the frequency-dependant behaviour of the battery. This was used to produce an electrical model of the battery, derived from the traditional Randles circuit combined with a high-frequency model proposed in literature. From this model analyses were performed to determine the best frequency for affecting the battery performance, which was shown to be around 700 Hz. A bespoke test rig was constructed to allow ac ripple currents to be applied to the battery simultaneously with a dc bias current, and to ensure all relevant parameters were measured.

A DCA test, using the knowledge gained from the previous chapters, was applied to the battery, both with and without a 1.6 A_{rms} ripple current present. This showed that the ripple current did increase the charge acceptance performance of the battery, particularly when it had charge history. This was significant as the DCA performance was significantly poorer with charge history, so the ripple current was seen to begin to compensate for the difference between charge and discharge history.

The work was then extended to consider higher frequencies of 4.5 kHz, 30 kHz and 180 kHz. This showed that increasing the frequency of the ripple further increased DCA performance, with improvements over the baseline of more than 50 % being observed. This performance increase was not linear however, with most improvement being seen by around 30 kHz. Again this is significant, as the losses in the battery begin to rise dramatically above 30 kHz, due to the battery performance becoming inductive at very high

frequencies.

Whilst the above work had shown that an applied ripple current could improve DCA performance, it was important to determine if the ripple was in any way damaging to the battery. A further series of tests was thus performed, comparing the SoC, SoH and cell imbalance performance between batteries with and without ripple current. In all cases, it was found that the presence of ripple currents had no measurable effect on any of these metrics.

Again, this is the first report in literature of the use of ripple currents to improve DCA performance, and whilst the methodology described is not likely to be practical in a real-world system, it does show that it is possible, and thus may lead to practical methods by which this may be achieved. This also adds to the existing body of evidence that ripple currents are not damaging to batteries.

7.5 Chapter 6

Chapter 6 represents a departure from the previous work, as it describes an expansion of the investigation to consider lithium-based cells. The work contained within covers two separate, but related areas.

Firstly, the work undertaken in Chapter 3 is extended and applied to lithium cell. Using an identical testing methodology, albeit with different voltage limits, the DCA performance of a LFP cell is determined. The results of this show that the trends in performance identified previously also exist in lithium chemistries, cell performance is broadly similar to that of standard lead, with little variation due to operational history and only a moderate influence from the rest period. The main difference is that charge acceptance is very consistent across all SoC, with far less variation than previously seen.

This work shows that the test methodology developed is valid across a range of chemistries, as are the factors which have been shown to influence DCA performance in lead-acid batteries. The result also shows that whilst the performance of lithium may be more consistent, it is unable to achieve the same magnitude of charge acceptance as carbon-enhanced lead-acid.

The second area of investigation considered the optimal charging method

for lithium cells when charged at a high rate. Three test procedures were developed, one standard, one in which the charge voltage was reduced, to limit voltage stress and the final one with an increased charge current termination, to limit the time the cell spent at the peak voltage. In all cases the cells were to be charged and discharged at a rate of $1 C_{nom}$ A, with 1 hour rest periods between charging and discharging.

Six Li-ion cells were subjected to these procedures, two for each test. The results showed that by reducing the charge voltage cycle life is improved significantly, with a typical degradation of around one-third that of the baseline. Increasing the charge termination current also produced a increase in cycle life, albeit not as great, however, it did allow for charging to be completed more quickly than either of the other methods.

This work showed that high-rate charging is possible, without causing significant degradation or loss of energy stored, simply by a small reduction in the voltage window used, and benefits can also be achieved without sacrificing charge speed. This could have significant benefits in many applications where the fast-charging of lithium cells is desired.

7.6 Further Work

The work described above has produced useful results and extended the current state of knowledge, it does however point to some areas which may benefit from further investigation:

DCA Test Procedure

Chapters 3 & 4 have identified the limitations of the current DCA test standard, using the work described above it is proposed to develop an alternative test procedure which better accounts for the issues identified.

DCA Improvement

Chapters 5 has demonstrated that it is possible to improve DCA performance using ripple currents. It is proposed that this work should be extended to develop a practical method of implementation, perhaps by

using the converter fitted within the vehicle to generate the necessary ripple.

Other Chemistries

This work has focussed heavily on lead-acid cells, however Chapter 6 has shown that some of the traits identified are also present in other cell chemistries. It is proposed that elements of this work are extended to consider how other chemistries behave under similar conditions.

References

- [1] Compiled from UK Office of National Statistics ‘*Monthly feed-in tariff commissioned installations by month*’ data.
- [2] Compiled from the Society of Motor Manufacturers and Traders ‘*EV and AFV Registrations*’ (2011 & 12) and ‘*EV Registrations*’ (2012 – 2018) data.
- [3] E. Karden, P. Shinn, P. Bostock, J. Cunningham, E. Schoultz, and D. Kok, “Requirements for future automotive batteries—a snapshot,” *Journal of Power Sources*, vol. 144, no. 2, pp. 505–512, 2005.
- [4] E. Karden, S. Ploumen, B. Fricke, T. Miller, and K. Snyder, “Energy storage devices for future hybrid electric vehicles,” *Journal of Power Sources*, vol. 168, no. 1, pp. 2–11, 2007.
- [5] D. U. Sauer, E. Karden, B. Fricke, H. Blanke, M. Thele, O. Bohlen, J. Schiffer, J. B. Gerschler, and R. Kaiser, “Charging performance of automotive batteries—An underestimated factor influencing lifetime and reliable battery operation,” *Journal of Power Sources*, vol. 168, no. 1, pp. 22–30, 2007.
- [6] P. T. Moseley and D. A. Rand, “Partial state-of-charge duty: A challenge but not a show-stopper for lead-acid batteries!,” *ECS Transactions*, vol. 41, no. 13, pp. 3–16, 2012.
- [7] M. Thele, J. Schiffer, E. Karden, E. Surewaard, and D. Sauer, “Modeling of the charge acceptance of lead–acid batteries,” *Journal of Power Sources*, vol. 168, no. 1, pp. 31–39, 2007.

- [8] J. Kowal, D. Schulte, D. U. Sauer, and E. Karden, "Simulation of the current distribution in lead-acid batteries to investigate the dynamic charge acceptance in flooded SLI batteries," *Journal of Power Sources*, vol. 191, no. 1, pp. 42–50, 2009.
- [9] S. Schaeck, A. Stoermer, and E. Hockgeiger, "Micro-hybrid electric vehicle application of valve-regulated lead–acid batteries in absorbent glass mat technology: Testing a partial-state-of-charge operation strategy," *Journal of Power Sources*, vol. 190, no. 1, pp. 173–183, 2009.
- [10] S. Schaeck, A. Stoermer, F. Kaiser, L. Koehler, J. Albers, and H. Kabza, "Lead-acid batteries in micro-hybrid applications. Part I. Selected key parameters," *Journal of Power Sources*, vol. 196, no. 3, pp. 1541–1554, 2011.
- [11] S. Schaeck, A. Stoermer, J. Albers, D. Weirather-Koestner, and H. Kabza, "Lead-acid batteries in micro-hybrid applications. Part II. Test proposal," *Journal of Power Sources*, vol. 196, no. 3, pp. 1555–1560, 2011.
- [12] H. Budde-Meiwes, D. Schulte, J. Kowal, D. U. Sauer, R. Hecke, and E. Karden, "Dynamic charge acceptance of lead–acid batteries: Comparison of methods for conditioning and testing," *Journal of Power Sources*, vol. 207, pp. 30–36, 2012.
- [13] P. T. Moseley, D. A. Rand, and B. Monahov, "Designing lead–acid batteries to meet energy and power requirements of future automobiles," *Journal of Power Sources*, vol. 219, pp. 75–79, 2012.
- [14] European Committee for Electrotechnical Standardisation, "EN 50342-6:2015. Lead-acid starter batteries - Part 6: Batteries for micro-cycle applications," November 2015.
- [15] F. Lacressonniere, B. Cassoret, and J.-F. Brudny, "Influence of a charging current with a sinusoidal perturbation on the performance of a lead-acid battery," *Electric Power Applications, IEE Proceedings -*, vol. 152, pp. 1365–1370, Sept 2005.

- [16] T.-H. Kim, J.-B. Jeong, B.-H. Lee, D.-H. Shin, H.-S. Song, B.-H. Kim, and H.-J. Kim, “Analytical study on low-frequency ripple effect of battery charging,” in *Vehicle Power and Propulsion Conference (VPPC), 2012 IEEE*, pp. 809–811, Oct 2012.
- [17] S. Bala, T. Tengner, P. Rosenfeld, and F. Delince, “The effect of low frequency current ripple on the performance of a Lithium Iron Phosphate (LFP) battery energy storage system,” in *Energy Conversion Congress and Exposition (ECCE), 2012 IEEE*, pp. 3485–3492, Sept 2012.
- [18] Emerson Network Power, “Effects of ac ripple current on VRLA battery life.” Technical report. [Online]. Available: <http://bit.ly/2PLkmL0>.
- [19] S. Okazaki, S. Higuchi, O. Nakamura, and S. Takahashi, “Influence of superimposed alternating current on capacity and cycle life for lead-acid batteries,” *Journal of Applied Electrochemistry*, vol. 16, no. 6, pp. 894–898, 1986.
- [20] S. De Breucker, K. Engelen, R. D’Hulst, and J. Driesen, “Impact of current ripple on Li-ion battery ageing,” in *Electric Vehicle Symposium and Exhibition (EVS27), 2013 World*, pp. 1–9, Nov 2013.
- [21] J. Wang, K. Zou, C. Chen, and L. Chen, “A high frequency battery model for current ripple analysis,” in *Applied Power Electronics Conference and Exposition (APEC), 2010 Twenty-Fifth Annual IEEE*, pp. 676–680, IEEE, 2010.
- [22] L.-R. Chen, S.-L. Wu, D.-T. Shieh, and T.-R. Chen, “Sinusoidal-ripple-current charging strategy and optimal charging frequency study for Li-ion batteries,” *IEEE Transactions on Industrial Electronics*, vol. 60, no. 1, pp. 88–97, 2013.
- [23] L. Chen and C. Wu, “Sinusoidal ripple current charging system with PLL function,” in *Industrial Electronics (ISIE), 2014 IEEE 23rd International Symposium on*, pp. 1836–1841, IEEE, 2014.

- [24] Y.-D. Lee and S.-Y. Park, “Electrochemical state-based sinusoidal ripple current charging control,” *IEEE Transactions on Power Electronics*, vol. 30, no. 8, pp. 4232–4243, 2015.
- [25] A. Bessman, R. Soares, S. Vadivelu, O. Wallmark, P. Svens, H. Ekström, and G. Lindbergh, “Challenging sinusoidal ripple-current charging of lithium-ion batteries,” *IEEE Transactions on Industrial Electronics*, vol. 65, no. 6, pp. 4750–4757, 2018.
- [26] S. Yang, A. Bryant, P. Mawby, D. Xiang, L. Ran, and P. Tavner, “An industry-based survey of reliability in power electronic converters,” *Industry Applications, IEEE Transactions on*, vol. 47, no. 3, pp. 1441–1451, 2011.
- [27] A. Ruddell, A. Dutton, H. Wenzl, C. Ropeter, D. Sauer, J. Merten, C. Orfanogiannis, J. Twidell, and P. Vezin, “Analysis of battery current microcycles in autonomous renewable energy systems,” *Journal of Power Sources*, vol. 112, no. 2, pp. 531–546, 2002.
- [28] L. Lu, X. Han, J. Li, J. Hua, and M. Ouyang, “A review on the key issues for lithium-ion battery management in electric vehicles,” *Journal of Power Sources*, vol. 226, pp. 272–288, 2013.
- [29] D. Gladwin, C. Gould, D. Stone, and M. Foster, “Viability of ‘second-life’ use of electric and hybridelectric vehicle battery packs,” in *Industrial Electronics Society, IECON 2013-39th Annual Conference of the IEEE*, pp. 1922–1927, IEEE, 2013.
- [30] M. Ehsani, Y. Gao, and J. M. Miller, “Hybrid electric vehicles: Architecture and motor drives,” *Proceedings of the IEEE*, vol. 95, no. 4, pp. 719–728, 2007.
- [31] J. Albers, E. Meissner, and S. Shirazi, “Lead-acid batteries in micro-hybrid vehicles,” *Journal of Power Sources*, vol. 196, no. 8, pp. 3993–4002, 2011.

- [32] Advanced Lead-Acid Battery Consortium, “The Mild-Hybrid, Lead-Acid Advantage for Lower Cost and Extra Environmental Protection,” 2012 (accessed September 20, 2018). [Online] <http://www.alabc.org/publications/mild-hybrid-lead-acid-advantage>.
- [33] C. Chumchal and D. Kurzweil, “Lead–acid battery operation in micro-hybrid and electrified vehicles,” in *Lead-Acid Batteries for Future Automobiles*, pp. 395–414, Elsevier, 2017.
- [34] ISOLAB 3a, “Development and testing of VRLA cells with optimised grid designs for mild hybrid applications: Accelerated programme to provide batteries for vehicle trials in a Honda Insight (ALABC Project 1012KD).” Progress Report, May 2013.
- [35] K. Vetter, *Elektrochemische Kinetik. (German) [Electrochemical Kinetics]*. Springer, Berlin, 1961.
- [36] C. R. Gould, C. M. Bingham, D. A. Stone, and P. Bentley, “New battery model and state-of-health determination through subspace parameter estimation and state-observer techniques,” *Vehicular Technology, IEEE Transactions on*, vol. 58, no. 8, pp. 3905–3916, 2009.
- [37] A. Fairweather, M. Foster, and D. Stone, “Modelling of VRLA batteries over operational temperature range using Pseudo Random Binary Sequences,” *Journal of Power Sources*, vol. 207, pp. 56–59, 2012.
- [38] S. Arrhenius, “Über die Dissociationswärme und den Einfluss der Temperatur auf den Dissociationsgrad der Elektrolyte. (German) [On the dissociation heat and the influence of temperature on the degree of dissociation of the electrolytes],” *Zeitschrift für Physikalische Chemie. (German) [Journal of Physical Chemistry]*, vol. 4, no. 1, pp. 96–116, 1889.
- [39] K. J. Laidler, “The development of the Arrhenius equation,” *Journal of Chemical Education*, vol. 61, no. 6, p. 494, 1984.
- [40] L. Pauling, *General Chemistry*. Courier Corporation, 1988.

- [41] T. Sharpe and R. Conell, “Low-temperature charging behaviour of lead-acid cells,” *Journal of Applied Electrochemistry*, vol. 17, no. 4, pp. 789–799, 1987.
- [42] B. Dunn, H. Kamath, and J.-M. Tarascon, “Electrical energy storage for the grid: A battery of choices,” *Science*, vol. 334, no. 6058, pp. 928–935, 2011.
- [43] P. Ruetschi, “Aging mechanisms and service life of lead–acid batteries,” *Journal of Power Sources*, vol. 127, no. 1, pp. 33–44, 2004.
- [44] A. Barré, B. Deguilhem, S. Grolleau, M. Gérard, F. Suard, and D. Riu, “A review on lithium-ion battery ageing mechanisms and estimations for automotive applications,” *Journal of Power Sources*, vol. 241, pp. 680–689, 2013.
- [45] K.-S. Ng, Y.-F. Huang, C.-S. Moo, and Y.-C. Hsieh, “An enhanced coulomb counting method for estimating state-of-charge and state-of-health of lead-acid batteries,” in *Telecommunications Energy Conference, 2009. INTELEC 2009. 31st International*, pp. 1–5, IEEE, 2009.
- [46] A. Widodo, M.-C. Shim, W. Caesarendra, and B.-S. Yang, “Intelligent prognostics for battery health monitoring based on sample entropy,” *Expert Systems with Applications*, vol. 38, no. 9, pp. 11763–11769, 2011.
- [47] Y. Xing, N. Williard, K.-L. Tsui, and M. Pecht, “A comparative review of prognostics-based reliability methods for lithium batteries,” in *Prognostics and System Health Management Conference (PHM-Shenzhen), 2011*, pp. 1–6, IEEE, 2011.
- [48] W. Peukert, “Über die Abhängigkeit der Kapazität von der Entladestromstärke bei Bleiakкумуляtoren. (German) [*On the dependence of the capacity on the discharge current in lead-acid batteries*],” *Elektrotechnische Zeitschrift. (German) [Electrotechnical Journal]*, vol. 20, pp. 20–21, 1897.

- [49] D. Doerffel and S. A. Sharkh, “A critical review of using the Peukert equation for determining the remaining capacity of lead-acid and lithium-ion batteries,” *Journal of Power Sources*, vol. 155, no. 2, pp. 395–400, 2006.
- [50] B. M. Gundogdu, S. Nejad, D. T. Gladwin, M. Foster, and D. Stone, “A battery energy management strategy for UK Enhanced Frequency Response and Triad avoidance,” *IEEE Transactions on Industrial Electronics*, 2018.
- [51] S. Buller, M. Thele, R. W. De Doncker, and E. Karden, “Impedance-based simulation models of Supercapacitors and Li-ion batteries for power electronic applications,” in *Industry Applications Conference, 2003. 38th IAS Annual Meeting. Conference Record of the*, vol. 3, pp. 1596–1600, IEEE, 2003.
- [52] D. A. Howey, P. D. Mitcheson, V. Yufit, G. J. Offer, and N. P. Brandon, “Online measurement of battery impedance using motor controller excitation,” *IEEE transactions on vehicular technology*, vol. 63, no. 6, pp. 2557–2566, 2014.
- [53] D. Howey, V. Yufit, P. Mitcheson, G. Offer, and N. Brandon, “Impedance measurement for advanced battery management systems,” in *Electric Vehicle Symposium and Exhibition (EVS27), 2013 World*, pp. 1–7, IEEE, 2013.
- [54] J. Kim, J. Shin, C. Chun, and B. Cho, “Stable configuration of a Li-ion series battery pack based on a screening process for improved voltage / SOC balancing,” *IEEE Transactions on Power Electronics*, vol. 27, no. 1, pp. 411–424, 2012.
- [55] J. R. Belt, C. D. Ho, T. J. Miller, M. A. Habib, and T. Q. Duong, “The effect of temperature on capacity and power in cycled lithium ion batteries,” *Journal of Power Sources*, vol. 142, no. 1-2, pp. 354–360, 2005.

- [56] J. Qi and D. D.-C. Lu, “Review of battery cell balancing techniques,” in *Power Engineering Conference (AUPEC), 2014 Australasian Universities*, pp. 1–6, IEEE, 2014.
- [57] J. Cao, N. Schofield, and A. Emadi, “Battery balancing methods: A comprehensive review,” in *Vehicle Power and Propulsion Conference, 2008. VPPC’08. IEEE*, pp. 1–6, IEEE, 2008.
- [58] F. Baronti, R. Roncella, and R. Saletti, “Performance comparison of active balancing techniques for lithium-ion batteries,” *Journal of Power Sources*, vol. 267, pp. 603–609, 2014.
- [59] International Energy Agency *et al.*, “World energy outlook 2011,” *Int. Energy Agency*, p. 666, 2011.
- [60] S. Mandelli, J. Barbieri, R. Mereu, and E. Colombo, “Off-grid systems for rural electrification in developing countries: Definitions, classification and a comprehensive literature review,” *Renewable and Sustainable Energy Reviews*, vol. 58, pp. 1621–1646, 2016.
- [61] T. Urmee, D. Harries, and A. Schlapfer, “Issues related to rural electrification using renewable energy in developing countries of Asia and Pacific,” *Renewable Energy*, vol. 34, no. 2, pp. 354–357, 2009.
- [62] W. Waag, S. Käbitz, and D. U. Sauer, “Experimental investigation of the lithium-ion battery impedance characteristic at various conditions and aging states and its influence on the application,” *Applied Energy*, vol. 102, pp. 885–897, 2013.

Appendix: High Frequency Test Rig Schematics

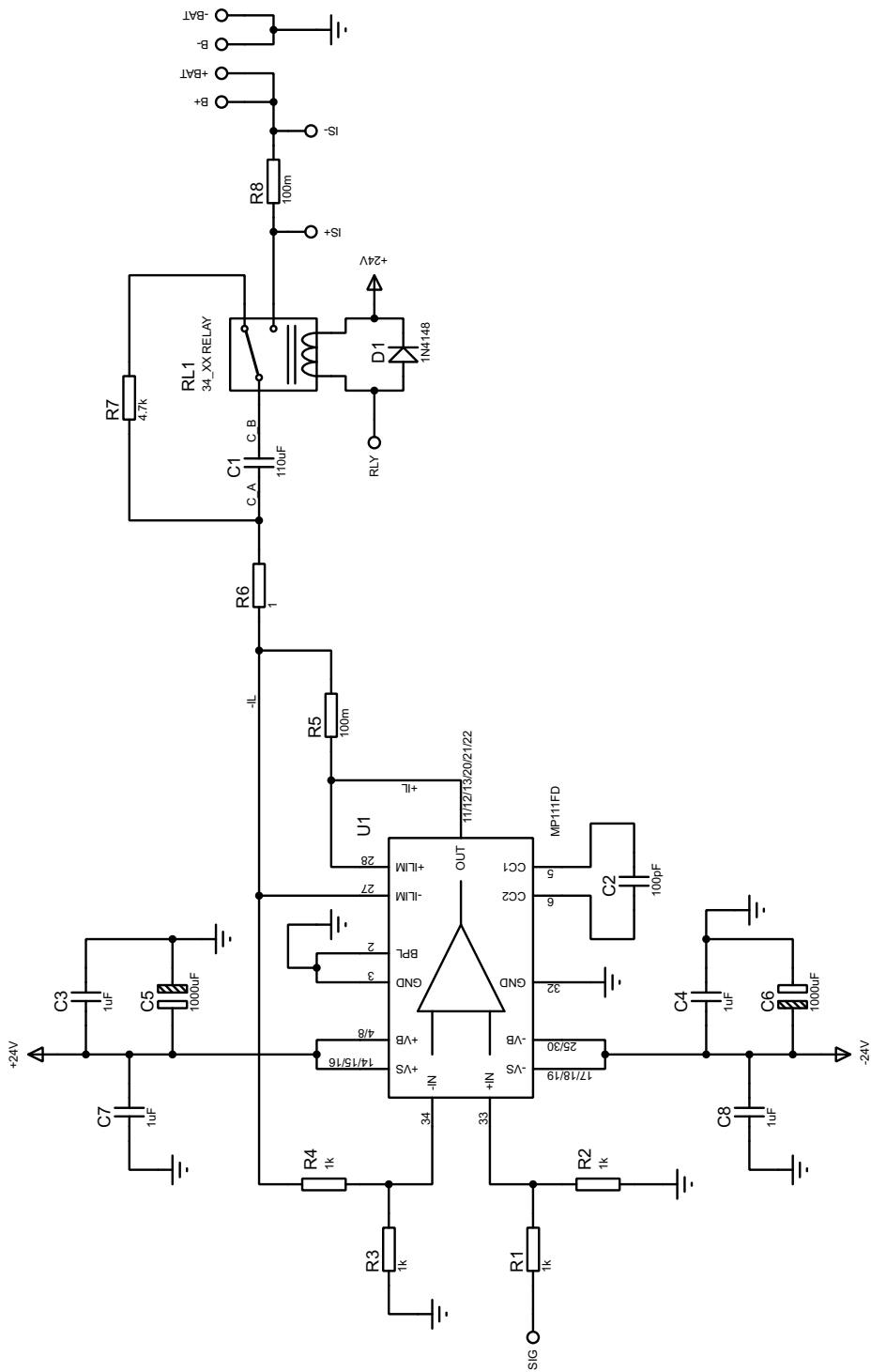


Figure A1: MP111FD Amplifier and Ancillaries

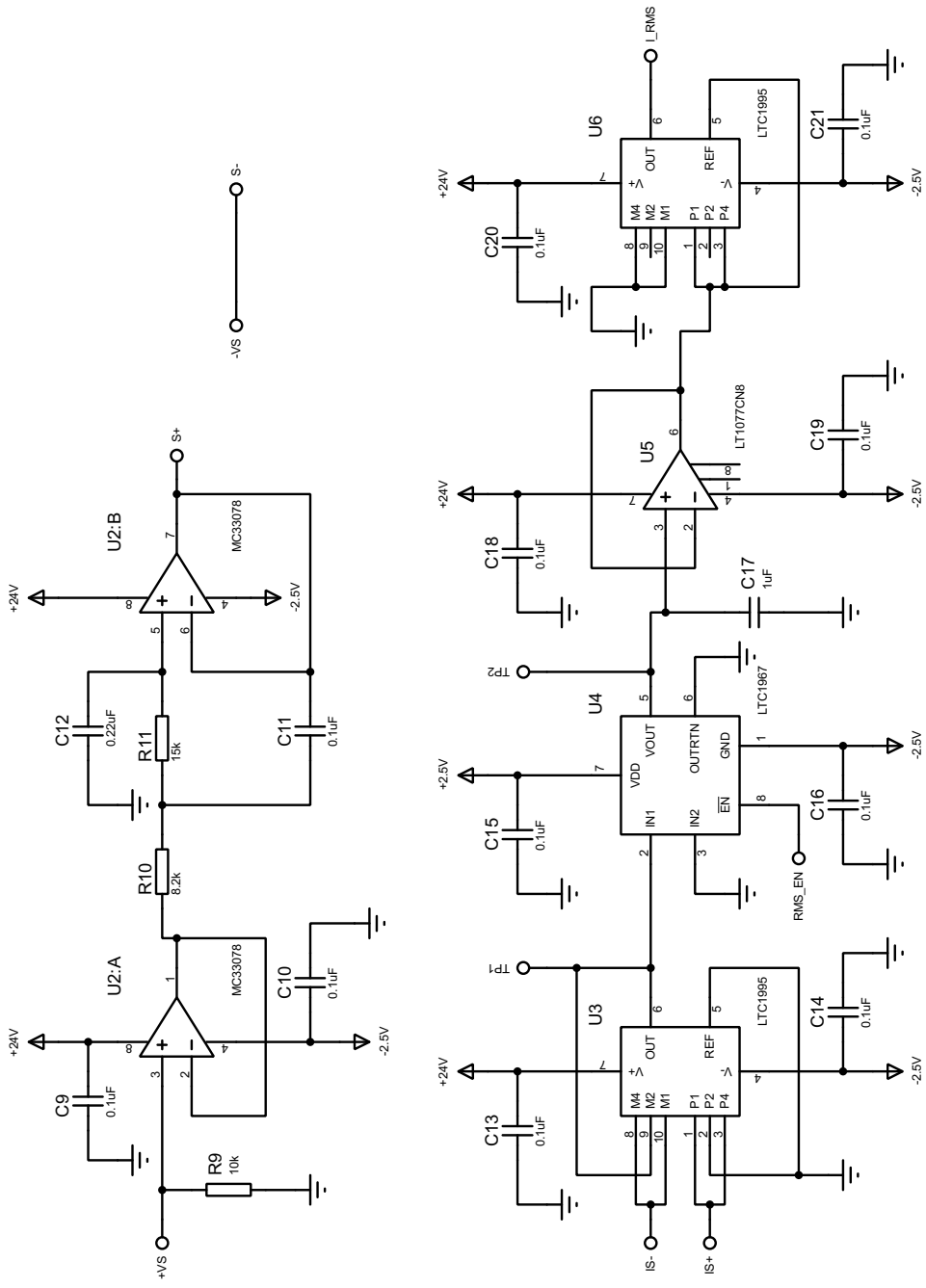


Figure A2: Signal Processing

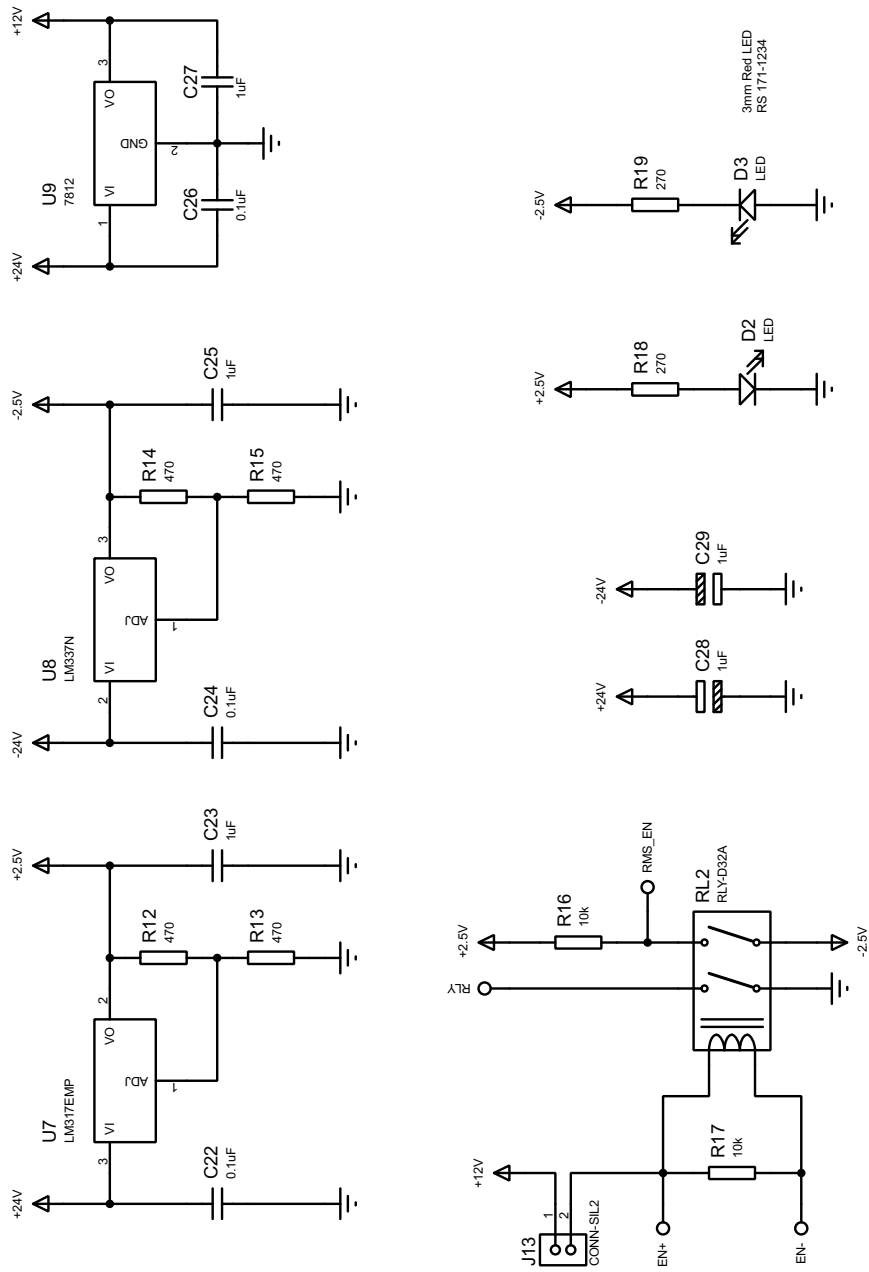


Figure A3: Power Supplies

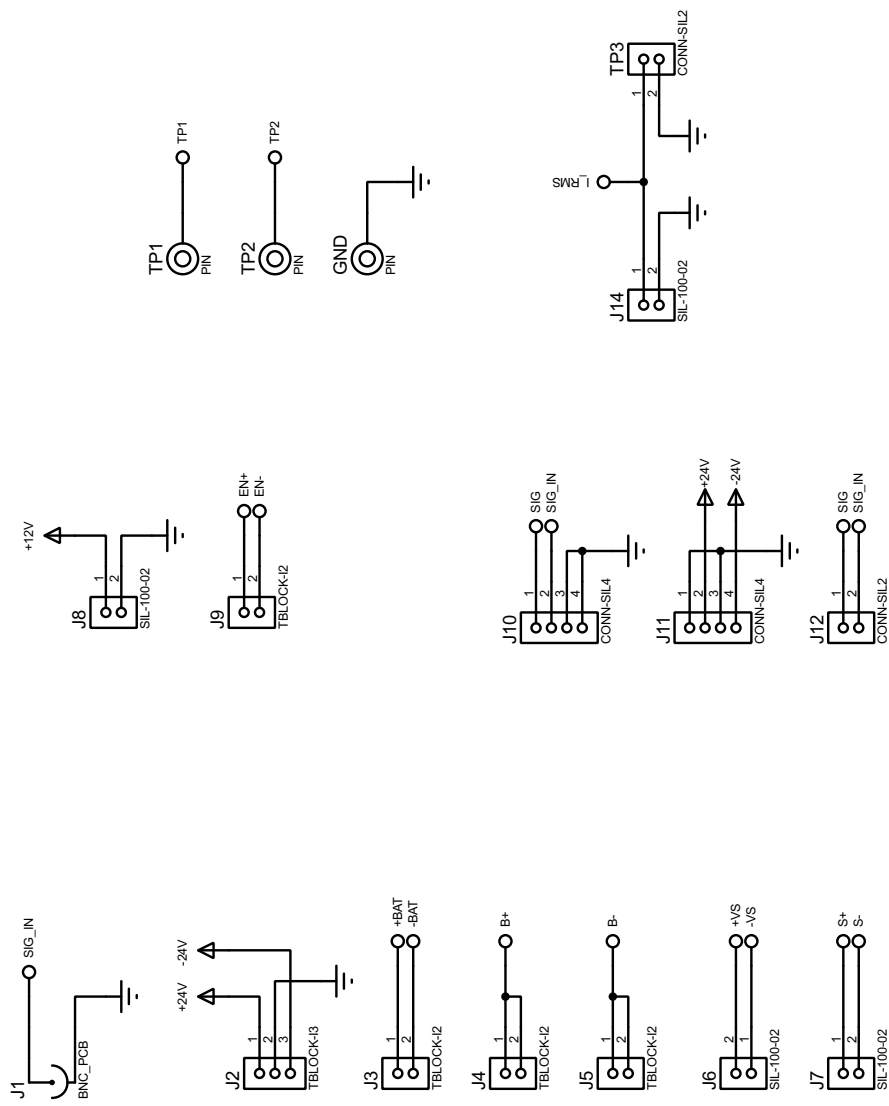


Figure A4: IO Connections